The First Step in Catalysis of the Radical S-Adenosylmethionine Methylthiotransferase MiaB Yields an Intermediate with a [3Fe-4S]⁰-like Auxiliary Cluster

Bo Zhang,^{1,†} Arthur J. Arcinas,^{2,§} Matthew I. Radle,¹ Alexey Silakov,¹ Squire J. Booker,^{1,2,3,*} and Carsten Krebs^{1,2,*}

¹Department of Chemistry, ²Department of Biochemistry and Molecular Biology, and ³Howard Hughes Medical Institute, The Pennsylvania State University, University Park, Pennsylvania 16802, United States

ABSTRACT

The enzyme MiaB catalyzes the attachment of a methylthio (-SCH₃) group at the C2 position of N^6 -(isopentenyl)adenosine (i⁶A) in the final step of the biosynthesis of the hypermodified tRNA nucleotide 2-methythio-N⁶-(isopentenyl)adenosine (ms²i⁶A). MiaB belongs to the expanding subgroup of enzymes of the radical S-adenosylmethionine (SAM) superfamily that harbor one or more auxiliary [4Fe-4S] clusters in addition to the [4Fe-4S] cluster that all family members require for the reductive cleavage of SAM to afford the common 5'-deoxyadenosyl 5'-radical (5'-dA•) intermediate. While the role of the radical SAM cluster in generating the 5'-dA• is well understood, the detailed role of the auxiliary cluster, which is essential for MiaB catalysis, remains unclear. It has been proposed that the auxiliary cluster may either serve as a coordination site for exogenously derived sulfur destined for attachment to the substrate, or that the cluster itself provides the sulfur atom and is sacrificed during turnover. In this work, we report spectroscopic and biochemical evidence that the auxiliary [4Fe-4S]²⁺ cluster in Bacteroides thetaiotaomicron (Bt) MiaB is converted to a [3Fe-4S]⁰-like cluster during the methylation step of catalysis. Mössbauer characterization of the MiaB [3Fe-4S]⁰-like cluster revealed unusual spectroscopic properties compared to those of other wellcharacterized cuboidal [3Fe-4S]⁰ clusters. Specifically, the Fe sites of the mixed-valent moiety do not have identical Mössbauer parameters. Our results support a mechanism where the auxiliary [4Fe-4S] cluster is the direct sulfur source during catalysis.

INTRODUCTION

The radical *S*-adenosylmethionine (SAM) (RS) superfamily of enzymes catalyze a wide variety of reactions using a 5'-deoxyadenosyl 5'-radical (5'-dA•) intermediate, a potent oxidant derived from the reductive cleavage of SAM. The 5'-dA• typically functions to initiate radical-based catalysis by abstracting a hydrogen atom (H•) from a noncovalently bound substrate. In all instances studied to date, the reductive cleavage of SAM requires a redox-active [4Fe–4S]^{2+/1+} cluster, termed the RS cluster, that is ligated by three cysteinyl residues found in an almost universally conserved CxxxCxxC motif. The unique (non-cysteinyl ligated) Fe ion of the RS cluster can be coordinated by SAM via SAM's amino and carboxylate groups. The reduced RS [4Fe-4S]⁺ cluster initiates the reductive cleavage of SAM, yielding methionine, 5'-dA•, and the oxidized RS [4Fe-4S]²⁺ cluster. Recent work has provided evidence for the 5'-dA• intermediate, 12,13 which has been shown to be stored as an organometallic species with a C5'-Fe bond. And the oxidized RS [4Fe-4S]²⁺ beautiful to the stored as an organometallic species with a C5'-Fe bond.

Methylthiotransferases (MTTases) are a subfamily of RS enzymes that install a methylthio (–SCH₃) group on their substrates. The RS MTTase MiaB, the subject of this study, catalyzes the methylthiolation of N^6 -isopentenyl adenosine (i⁶A) nucleotides found at position 37 in tRNAs that decode mRNA codons containing a leading uridine, giving rise to a C2-methylthio- N^6 -isopentenyl adenosine (ms²i⁶A) product (**Scheme 1**).¹⁵ The ms²i⁶A modification imparts enhanced base-pairing interactions between mRNA codons and the cognate tRNA, decreasing slippage and maintaining the ribosomal reading frame during translation.¹⁶⁻²⁰ The reaction catalyzed by MiaB requires the dimethylallyl modification of N^6 of the target adenosine, A37, which in *Escherichia coli* is installed by the enzyme MiaA using dimethylallyl pyrophosphate as a substrate.²¹⁻²³ Additionally,

methylthiolation by CDKAL1, the human ortholog of the MTTase MtaB, which methylthiolates N^6 -threonylcarbamoyladenosine (t^6A) in tRNAs, has been implicated in insulin maturation and the development of type II diabetes. Furthermore, methylthiolation catalyzed by the human MiaB ortholog CDK5RAP1 has been linked to the development of neurodegenerative diseases via an undetermined mechanism. Lastly, the MTTase RimO methylthiolates the β carbon of aspartate 89 of the ribosomal S12 protein, a strictly conserved residue near the functional center of the ribosome. This reaction involves the stereoselective abstraction of the 3 *pro-S* H• of aspartate 89 with subsequent transfer of a methylthio group with inversion of configuration to give (3R)-methylthioaspartate.

In addition to the RS MTTases, there are two well-studied RS enzymes that install sulfur onto unactivated carbon centers. These include biotin synthase (BioB), which installs one sulfur atom between C6 and C9 of dethiobiotin, creating the thiophane ring of the molecule,³⁴ and lipoyl synthase (LipA), which installs two sulfhydryl groups, at C6 and C8, on an octanoyllysyl chain of a lipoyl carrier protein to create the lipoyl cofactor.³⁵ BioB, LipA, and the MTTases (MiaB and RimO) have in common that they require two distinct Fe/S clusters in catalysis.⁶ The first cluster is the RS [4Fe-4S] cluster, which is used for generation of the 5'-dA•, while the second cluster is termed the auxiliary (Aux) cluster. BioB harbors an Aux [2Fe-2S] cluster,^{36,37} while LipA, RimO, and MiaB contain an Aux [4Fe-4S] cluster.^{32,38,39} In recent years, it was shown that the Aux [2Fe-2S] cluster in BioB and the Aux [4Fe-4S] cluster in LipA are the immediate sources of sulfur to be incorporated into the product.⁴⁰⁻⁴⁴ However, for the MTTases, the functional role of the Aux cluster remains less well defined.

Catalysis by MiaB appears to take place in two distinct half-reactions (Scheme 1). 45,46 In the first stage, which does not require a low-potential reductant, a methyl group is transferred from a SAM molecule to a protein-associated sulfur species via a polar nucleophilic attack to generate a methylthio intermediate.^{6,45-47} This intermediate is labile in the presence of acid and base and is vulnerable to chaotropic agents, suggesting that the methyl acceptor is an Fe/S cluster in nature rather than a side chain of an amino acid residue. 45 Consistent with this assignment, treatment of the methylated protein with acid results in formation of methanethiol. When the intermediate is formed using S-adenosyl-[methyl- ${}^{2}H_{3}$]-methionine (d_{3} -SAM) and then isolated and added to a reaction containing a low-potential reductant and unlabeled SAM, a burst of deuterium-containing product is observed before slower formation of unlabeled product.⁴⁵ Similarly, when methanethiol or methaneselenol is included in the MiaB or RimO reactions, a methylthio or methylseleno group derived from these compounds is incorporated intact into ms²i⁶A (mse²i⁶A) of tRNA or aspartate 89 of a synthetic peptide substrate. 45,48 Electrochemical characterization of Bt MiaB and Tm RimO suggests that the Aux [4Fe-4S] cluster is transformed to a state with an unusually low reduction potential for a [4Fe-4S]^{2+/1+} redox pair as a direct result of methylation.⁴⁶

The auxiliary cluster in the MTTases is ligated by three cysteine residues, raising the possibility that the unique non-cysteine ligated Fe could serve as a coordination site for exogenously derived sulfur destined for insertion into the substrate.^{39,48,49} The crystal structure of holo *Tm* RimO, obtained in the absence of SAM and its polypeptide substrate, revealed a pentasulfide bridge connecting the unique Fe ions of the RS and Aux clusters.⁴⁸ While the presence of the pentasulfide bridge is likely an artifact resulting

from chemical reconstitution of the Fe/S clusters, given that it occupies the expected binding site for SAM and the polypeptide substrate, its observation suggests the propensity of the unique Fe site of the Aux cluster to bind exogenous (poly)sulfide. Subsequently, a mechanism was proposed involving a (poly)sulfide species bound exogenously to the auxiliary clusters of MiaB and RimO that could be capped by a methyl group transferred from SAM and incorporated into the methylated product. 45,48

Recent crystallographic and spectroscopic investigation into the mechanism of the sulfur-inserting enzyme LipA revealed another possible mechanism for the MTTases, in which the Aux cluster is sacrificed as the ultimate sulfur source for the lipoyl product. Mechanistic studies of LipA provided structural and spectroscopic evidence for the disassembly of the Aux cluster during catalysis. In LipA's first half reaction, a substrate-Fe/S cluster cross-linked intermediate species is generated. Analysis of this species by Mössbauer spectroscopy revealed the presence of a [3Fe-4S]⁰-like cluster, which contains 3 iron ions, 3 sulfide ions, and one C6-mercaptooctanoyl ligand, formally affording a [3Fe-3S-1SR]⁻¹ species.⁴² The cross-linked species and the [3Fe-4S]⁰-like cluster were subsequently confirmed by X-ray crystallography.⁵⁰

In this work, we present the Mössbauer-spectroscopic characterization of *Bacteroides thetaiotaomicron (Bt)* MiaB during the steps leading to the formation of the methylated intermediate. The results reveal conversion of the Aux [4Fe–4S]²⁺ cluster to a [3Fe-4S]⁰–like cluster in the absence of a low-potential reductant. The [4Fe-4S]²⁺ to [3Fe-4S]⁰–like cluster transformation occurs on the same time scale as that of SAH formation and is only observed under conditions that promote the methylation reaction. Furthermore, the [3Fe-4S]⁰–like intermediate is chemically and kinetically competent to

proceed to product ms²i⁶A tRNA. The electronic structure of the MiaB [3Fe-4S]⁰–like cluster is different from that of other spectroscopically characterized cuboidal [3Fe-4S]⁰ clusters. A potential sacrificial role for the auxiliary [4Fe-4S]²⁺ cluster as the direct sulfur source will be discussed in light of the observed unusual electronic structure of the [3Fe-4S]⁰–like cluster. Although the [3Fe-4S]⁰–like clusters in MiaB and LipA are likely generated by different mechanisms (polar and radical, respectively), its observation in two mechanistically different radical SAM enzymes suggests a potential role for this type of Fe/S cluster as a common intermediate in radical SAM enzymes that catalyze sulfur insertion and that contain auxiliary [4Fe-4S]²⁺ clusters.

RESULTS

Assessment of the time scale of the methylation reaction by Bt MiaB. To facilitate the preparation of Bt MiaB samples for characterization by Mössbauer spectroscopy, the time scale of the MiaB-catalyzed methylation step was determined by liquid chromatography coupled to analysis by mass spectrometry (LC/MS), as previously described.⁴⁵ Upon incubating Bt MiaB with i⁶A-containing tRNA and SAM, the formation of SAH was observed to reach a plateau (88 μM, ~0.5 equivalents) within 20 min with an initial rate for SAH formation of 86 μM min⁻¹ (Figure 1A). No 5'-dAH or ms²i⁶A was formed under these reaction conditions, consistent with the requirement for a low-potential reductant and tRNA substrate to initiate the reductive cleavage of SAM.⁴⁵ This state, herein referred to as the methylated intermediate, is chemically and kinetically competent, because addition of sodium dithionite after a 20-min incubation with SAM

led to the formation of ms^2i^6A and 5'-dAH with rates of 28 μ M min⁻¹ and 36 μ M min⁻¹, respectively, without any lag phase (**Figure 1B**).

Mössbauer-spectroscopic evidence for a [3Fe-4S]⁰-like cluster in the methylated intermediate of MiaB. The 4.2-K/zero-field Mössbauer spectrum of a Bt MiaB sample prior to addition of SAM is shown in Figure 2A (black vertical bars). Analysis of the sample indicates a stoichiometry of 7.6 ± 0.1 Fe per protein. Facilitated by the Mössbauer characterization of variants lacking either the RS or the Aux cluster (Figure S2 and associated text in Supporting Information), the spectrum of Bt MiaB prior to addition of SAM can be adequately simulated as a superposition of ~0.85 RS [4Fe-4S]²⁺ and ~0.80 auxiliary [4Fe-4S]²⁺ clusters per MiaB monomer. The typical features of a [2Fe-2S]²⁺ cluster (~0.45 cluster per MiaB monomer, ~12% of total ⁵⁷Fe) and of a cuboidal [3Fe-4S]⁺ cluster (less than 0.04 cluster per MiaB monomer, ~1.5% of total ⁵⁷Fe) are also observed by Mössbauer and EPR spectroscopies, respectively (Figures S1 and S2). However, their presence in the sample likely results from degradation of [4Fe-4S]²⁺ clusters. 51,52 Other common EPR-active Fe/S clusters with a half-integer spin ground state (e.g. [2Fe-2S]⁺, [4Fe-4S]⁺, or [4Fe-4S]³⁺) are not observed. As expected for a sample containing almost exclusively Fe/S clusters with a diamagnetic ground state, the spectrum of Bt MiaB recorded in a weak, externally applied magnetic field of 53 mT is identical to that recorded in the absence of an applied magnetic field (Figure 2A, red line; the small fraction of [3Fe-4S]⁺ clusters is beyond the detection limit of Mössbauer spectroscopy).

For the characterization of the methylated intermediate, a sample intended for Mössbauer spectroscopy was prepared by incubating 165 μ M Bt MiaB with 330 μ M i^6 A

tRNA and 600 µM SAM for 20 min. The conditions were chosen to allow maximum accumulation of SAH, based on LC/MS analysis of a sample prepared under identical conditions (Figure 1A). The 4.2-K/zero-field Mössbauer spectrum of this sample (Figure 2B, black vertical bars) reveals three distinct differences from that of reconstituted MiaB alone: (1) the prominent high-energy line of the quadrupole doublet associated with the $[4\text{Fe-}4\text{S}]^{2+}$ clusters at a position of ~ 1.0 mm/s is reduced in intensity; (2) the intensity between the two most prominent lines at ~0.6 mm/s increases (Figure 2B, black arrow); and (3) a new absorption feature is observed at ~ 2.7 mm/s, a position typical for the high-energy line of a quadrupole doublet of high-spin (HS) Fe^{II} (blue arrow). The analysis of this spectrum (see below and Figure S3) reveals that this component has an isomer shift (δ) of ~ 1.3 mm/s and a quadrupole splitting parameter ($\Delta E_{\rm O}$) of ~ 2.8 mm/s, which are typical for N/O-coordinated HS Fe^{II} ions.⁵³ Interestingly, the spectrum collected in an applied field of 53 mT (Figure 2B, red line) reveals that a fraction of the Fe exhibits unresolved magnetically split features extending from approximately -1.0 mm/s to +2 mm/s (**Figure 2B**, green arrows). This field-strength dependence is typical of a species with a paramagnetic, integer-spin ground state. The fact that treatment of MiaB with SAM results in a reduction of the intensity associated with [4Fe-4S]²⁺ clusters and yields a HS Fe^{II} species along with a new paramagnetic species in an ~1:3 ratio (vide infra) suggests that one [4Fe-4S]²⁺ cluster is converted to a 3Fe cluster with a paramagnetic integer spin ground state plus an Fe^{II} ion.

The spectral features associated with the 3Fe cluster are more easily discernable in the [0-53mT] difference spectrum (**Figure 3A**, vertical bars), wherein its features in a 53-mT field (broad and featureless, magnetically split absorption extending from -1 to +2

mm/s; see arrows) point upwards, while its features in zero applied field (overlapping quadrupole doublets of the three Fe sites of the cluster) point downwards. Importantly, the other cluster remains in the $[4\text{Fe-4S}]^{2+}$ configuration, which does not exhibit any field-strength dependence, due to its diamagnetic ground state. The [0-53mT] difference spectrum of the 20-min sample qualitatively resembles that of the cuboidal $[3\text{Fe-4S}]^0$ -like auxiliary cluster in the *E.coli* LipA monothiolated intermediate with $S_{\text{tot}} = 2$ (**Figure S4**),⁴² although the MiaB difference spectrum does not display the unique 2:1 intensity ratio of the quadrupole doublets associated with the valence-delocalized Fe₂^{2.5+} pair and the Fe^{III} site without applied field.⁵⁴

In order to determine the values of δ and ΔE_Q of the three Fe sites of the intermediate, the zero-field reference spectrum of the MiaB [3Fe-4S]⁰-like cluster (Figure 3B, vertical bars) was generated by adding back a spin-Hamiltonian simulation (*vide infra*) of the [3Fe-4S]⁰-like cluster in a 53-mT magnetic field (Figure 3A, black line) to the difference spectrum (Figure 3A, vertical bars). We note that due to the broadness of the 53-mT spectrum, the relative amount of the simulation to be added back to generate the zero-field reference spectrum cannot be determined accurately. We have therefore generated several reference spectra by adding back varying amounts (21-36% of total ⁵⁷Fe absorption in 3% increments) of the simulation of the 53-mT spectrum. Analyses of these spectra and spectra collected in large externally applied fields suggest that the subspectra associated with the [3Fe-4S]⁰-like cluster contribute 27 \pm 6% of the total ⁵⁷Fe absorption. The resulting zero-field reference spectra are qualitatively similar and suggest that the MiaB [3Fe-4S]⁰-like cluster can be modeled with three symmetrical quadruple doublets having equal intensity. This model yields 15 mathematically

equivalent solutions, of which only six yield physically reasonable parameters (**Table 1**). Of those, we prefer solutions 1 (Figure 3B) and 2 (Figure S6), because Fe site 1 has parameters very similar to those of the HS Fe^{III} site of cuboidal [3Fe-4S]⁰ clusters. The other two Fe sites are associated with the mixed-valent (MV) (Fe₂)⁵⁺ site. In regular [3Fe-4S]⁰ clusters, the MV unit is fully valence-delocalized and the two Fe sites have indistinguishable Mössbauer parameters, which are the average of typical parameters for Fe^{II} and Fe^{III} in a distorted tetrahedral S₄ coordination environment, thus establishing formally the oxidation state of +2.5 for both Fe sites.⁵⁴ In the [3Fe-4S]⁰-like cluster of MiaB, the two Fe sites of the MV unit have distinct parameters. In solution 1, sites 2 and 3 have virtually identical quadrupole splittings, but rather different isomer shifts (0.35) mm/s and 0.61 mm/s), which are typical of S₄-coordinated Fe^{III} and Fe^{II} sites and suggest a valence-localized MV unit. By contrast, in solution 2, sites 2 and 3 have different quadrupole splittings, but virtually identical isomer shifts (0.47 mm/s and 0.48 mm/s), suggesting a valence-delocalized MV unit, wherein both sites have a formal +2.5 oxidation state, but distinct coordination environments leading to different quadrupole splittings. Possible geometric structures of this cluster are presented in the *Discussion*. Importantly, the parameters obtained from the above analysis of other zero-field reference spectra (obtained by adding back varying amounts of the simulated 53-mT spectrum) do not vary significantly (Figure S5). Taken together, the entire 4.2-K/zerofield spectrum of Bt MiaB after incubation with SAM and i⁶A tRNA substrate in the absence of reductant can be analyzed as a superposition of a [3Fe-4S]⁰-like cluster, a [4Fe-4S]²⁺ cluster and a small amount of [2Fe-2S]²⁺ cluster (**Figure S3**).

Exploring the requirements for generating the [3Fe-4S]⁰-like cluster in MiaB. Although the [0-53mT]-difference spectrum is rather broad and difficult to quantify, it is nevertheless a diagnostic feature for the presence of the MiaB [3Fe-4S]⁰-like cluster. An analysis of the amplitudes of the [0-53mT]-difference spectra of samples treated for varying amounts of time with SAM in the absence of reductant reveals that the amplitudes, and therefore the amount of the [3Fe-4S]⁰-like cluster, mirror the trend in the amount of SAH generated in the reaction (Figures 1A and S7). When Bt MiaB is treated with SAM, even in the absence of the tRNA substrate, the [3Fe-4S]⁰-like cluster is also formed, consistent with the generation of SAH in parallel LC/MS experiments (Figure S8). Incubation of MiaB variants—wherein either the three cysteine residues coordinating the RS cluster (\(^{\Delta RS}\)MiaB) or the three cysteines coordinating the Aux cluster (\(^{\text{Aux}}\)MiaB) are changed to alanines—with SAM and the tRNA substrate does not lead to formation of the [3Fe-4S]⁰-like cluster and does not yield SAH as a product (**Figures S9** and S10). Likewise, the characteristic difference spectrum is not observed for a sample of MiaB in the absence of SAM, but in the presence of the tRNA substrate (Figure S11). Taken together, these results reveal that the [3Fe-4S]⁰-like cluster is only observed under conditions that lead to generation of SAH and the methylated intermediate that was previously shown to be chemically and kinetically competent for ms²i⁶A formation. Because the RS [4Fe-4S] cluster is required in the second step of catalysis for generating the 5'-dA• intermediate, we conclude that it is the Aux [4Fe-4S]²⁺ cluster that is converted to the [3Fe-4S]⁰-like cluster.

Finally, we also evaluated whether treatment of Bt MiaB with methanethiol, which was reported to result in a methanethiol-derived ms²i⁶A product, ^{45,48} would result

in generation of the [3Fe-4S]⁰-like cluster. Evaluation of the Mössbauer spectra suggests that a small amount of the [3Fe-4S]⁰-like cluster is formed (at most half of the amount observed in the sample where MiaB is treated with SAM in the presence of tRNA substrate), along with a small amount (at most ~4% of total ⁵⁷Fe) of N/O-coordinated Fe^{II} (**Figure S12**). We note that the amounts of both species are at the detection limit of the method. However, the formation of the [3Fe-4S]⁰-like cluster by exposure of MiaB to methanethiol would invariably involve a mechanism different from that for generating the methylated intermediate upon reacting MiaB with SAM, because the S-C_{methyl} bond is already formed in this substrate analog (see *Discussion*).

Characterization of the [3Fe-4S]⁰-like cluster of the methylated Bt MiaB intermediate by variable-field Mössbauer spectroscopy. The variable-field magnetic Mössbauer spectra of the MiaB [3Fe-4S]⁰-like cluster were analyzed with the assumption that the cluster has an $S_{tot} = 2$ ground state (the validity of this assumption is proved below) using the values of δ and ΔE_Q obtained from analysis of the zero-field spectrum (solution 1), and published spin Hamiltonian parameters of the cuboidal [3Fe-4S]⁰ cluster from D. gigas ferredoxin as a starting point.⁵⁴ Because these simulations depend on up to ~50 parameters with each of the three Fe sites contributing only ~10% of the total intensity to the spectrum, it is impossible to determine the spin Hamiltonian parameters unambiguously. Fortuitously, the initial simulations yielded reasonable agreement, and we then refined the parameters to improve the quality of the simulations (**Figures 4** and **S13** and **Table 2**). Simulations using the values of of δ and ΔE_Q from solution 2 of Table

1 and slightly different spin Hamiltonian parameters fit the experimental data comparably well. In the following section, we present salient features of this analysis.

All [3Fe-4S]⁰ clusters reported to date have an $S_{\text{tot}} = 2$ ground state with an axial zero field splitting (ZFS) parameter, $D_{S=2}$, ranging from -2 to -4 cm⁻¹, and a rhombicity, $(E/D)_{S=2}$, of ~ 0.2 .^{42,54,55} These ZFS parameters give rise to a large, uniaxial spin expectation value in the z-direction, $\langle S_z \rangle$, for moderate external fields of up to ~ 1 T that is particularly sensitive to the values of D and E/D (Figure S14). The sizable magnetic hyperfine splitting induced by an applied field as weak as 53 mT indicates that the Bt MiaB [3Fe-4S]⁰-like cluster has a $S_{\text{tot}} = 2$ ground state (*vide infra* for consideration of other possible spin states). With the assumption that the [3Fe-4S]⁰-like cluster has an $S_{\text{tot}} = 2$ ground state, the analysis of the field-dependent spectra yield $D_{S=2} \sim -3.0 \pm 1.0$ cm⁻¹ and $(E/D)_{S=2}$ between 0.2 and 0.3. Because the observed splitting depends on the product of the spin expectation value in the z-direction and the magnitude of the hyperfine tensor in the z-direction, i.e. $\langle S_z \rangle - A_z$, the A_z values can be determined with reasonable accuracy.

In the spectra recorded in strong externally applied magnetic fields of 4, 6, and 8 T, the features of the [3Fe-4S]⁰-like cluster are dominated by strong internal magnetic fields and are better resolved from the features of the [4Fe-4S]²⁺ cluster, which has a diamagnetic ground state and no internal field; analysis of these spectra suggests that the [3Fe-4S]⁰-like cluster contributes ~30% of total intensity, consistent with the analysis from the [0-53mT] difference spectrum (*vide supra*). Two subcomponents of an antiferromagnetically (AF) coupled cluster can be readily distinguished in these spectra. One subcomponent, which accounts for ~10% of the total ⁵⁷Fe absorption, exhibits *increased* splitting with *increasing* field strength (green lines in **Figure 4** and **Figure**

S13B). This component is associated with an Fe site that has a *positive* A-tensor with respect to the total spin and hence a *negative* spin projection factor.⁵³ It is assigned to the HS Fe^{III} site with S = 5/2. Conversely, the other component (~20% total ⁵⁷Fe absorption, thus accounting for two Fe sites) exhibits *decreasing* splitting with *increasing* external field (red and blue lines in **Figure 4** and **Figure S13B**). This component is associated with the two Fe sites that have a *negative* A-tensor with respect to the total spin and a *positive* spin projection factor.⁵³ This component is assigned to the subspectra arising from sites 2 and 3. They exhibit similar splittings and are no longer resolved experimentally, because the magnetic hyperfine features are large compared to the small difference in δ and ΔE_Q of sites 2 and 3. Importantly, this observation further suggests that Fe sites 2 and 3 have similar spin projection factors (with the assumption that they have the similar intrinsic a-tensors). These two sites are assigned to the MV dimeric unit with $S_{mv} = 9/2$.

Taken together, the variable-field magnetic Mössbauer spectra of the MiaB [3Fe-4S]⁰–like cluster can be analyzed using the values of isomer shift and quadruple splitting obtained from the zero-field reference spectrum, the assumption that the cluster has an $S_{\text{tot}} = 2$ spin ground state, and the parameters given in **Table 2**. The fact that the spin Hamiltonian parameters are similar to those observed for other cuboidal [3Fe-4S]⁰ clusters supports the notion that the electronic structure is adequately described by invoking AF coupling between a HS Fe^{III} center (S = 5/2) and the MV unit ($S_{\text{mv}} = 9/2$), yielding a $S_{\text{tot}} = 2$ ground state.

Evaluation of possible electron spin ground states of the [3Fe-4S]⁰-like cluster. Although the variable-field Mössbauer spectra can be satisfactorily simulated with parameters typical of [3Fe-4S] 0 clusters, the fact that the δ and ΔE_Q values of the two Fe sites of the MV unit are different reveals the presence of either a valence-localized MV unit (solution 1) or a valence-delocalized unit with different coordination environments (solution 2), thus posing the question, whether the ground state of the [3Fe-4S]⁰-like cluster in MiaB is still the $|9/2, 2\rangle$ state (spin states are designated as $|S_{mv}, S_{tot}\rangle$), as in all other [3Fe-4S]⁰ clusters. We therefore explored the possibility that other spin states could be the ground state using a spin-coupling model adopted from that introduced by Münck and coworkers.⁵⁴ The Münck model takes into account both the spin-dependent delocalization (viz double exchange) of the MV (Fe₂)⁵⁺ unit, parameterized by the double exchange parameter, $B_{\rm mv}$, and further assumes three identical AF superexchange interactions between any two Fe centers (J). Because methylation could potentially occur at one of the µ₂-sulfido ligands of a cuboidal [3Fe-4S]⁰-like cluster, which would be expected to result in a decrease of the exchange coupling constant between the two Fe ions bridged by the methanethiolate ligand, in analogy to the well-established reduction of the exchange coupling of oxo-bridged clusters upon protonation or alkylation, 56-58 we expanded the Münck model to explore the effect of one J value being smaller. The case that the exchange coupling within the MV unit, $J_{\rm mv}$, is different from the other two exchange coupling constants, J, can be easily solved analytically (see Supplemental Material for details on the model).⁵⁹ Because methanethiolate is a weaker ligand than sulfide, it is expected to bind preferentially to the Fe^{II} or Fe^{2.5} sites, rather than the Fe^{III} site; i.e., it is expected to bridge the two Fe centers of the MV unit, thus validating the above assumption. The evaluation of possible spin ground states as a function of J_{mv}/J and B_{mv}/J , shown in **Figure 5**, reveals that five states can be the ground state (for $J_{\text{mv}}/J > 0$) and $B_{\text{mv}}/J > 0$). The specific case explored by Münck and coworkers ($J_{\text{mv}}/J = 1$) is indicated by the dashed horizontal line in **Figure 5**; it can yield $|9/2, 2\rangle$, $|7/2, 1\rangle$, and $|5/2, 0\rangle$ ground states. The $|9/2, 2\rangle$ ground state established for the previously characterized $[3\text{Fe-4S}]^0$ clusters requires $B_{\text{mv}}/J > 2$ with the assumption $J_{\text{mv}} = J$, consistent with the observation of a fully valence-delocalized MV (Fe₂)⁺⁵ unit.⁵⁴ For values of $J_{\text{mv}}/J > 1$, the $|1/2, 2\rangle$ and $|3/2, 1\rangle$ states can also be the ground state. However, the latter two states are disfavored because the bridging methanethiolate ligand is expected to decrease J_{mv} compared to J, i.e. $J_{\text{mv}}/J < 1$.

Of these five possible spin ground states, the $|5/2, 0\rangle$ state can be easily ruled out, because the experimental data unequivocally show that the ground state is paramagnetic. The two states with $S_{tot} = 1$, $|7/2, 1\rangle$ and $|3/2, 1\rangle$, can also be ruled out, because the smaller limiting value of $\langle S \rangle = 1$ would then require ~2-fold larger average A-values (compared to the A-values with respect to a $S_{tot} = 2$ ground state described in the previous section) to reproduce the experimentally observed splitting of the spectra. Calculation of the intrinsic a-values using spin projection techniques (see **Table 3** for spin projection coefficients)⁶⁰ yields a-values that are significantly larger than typical intrinsic a-values of Fe/S clusters.⁶¹ Lastly, the $|1/2, 2\rangle$ ground state can be ruled out because the spin projection factor of the Fe sites of the MV unit are much smaller than those associated with the $|9/2, 2\rangle$ state (see **Table 3**), resulting in intrinsic a-values that are 2-fold smaller than typical intrinsic a-values of Fe/S clusters.⁶¹ We therefore conclude that the $[3\text{Fe-4S}]^0$ -like cluster in MiaB has a $|9/2, 2\rangle$ ground state.

DISCUSSION

Previous work has shown that treatment of the RS MTTase MiaB with the cosubstrate, SAM, in the absence of a low-potential reductant leads to an intermediate with an acid-labile methylthio group and the co-product SAH.45 In this work, we used Mössbauer spectroscopy to monitor the fate of the two [4Fe-4S]²⁺ clusters of MiaB upon generating the methylated intermediate. Our results show that one [4Fe-4S]²⁺ cluster remains intact, while the other is converted to a [3Fe-4S]⁰-like cluster and HS N/Ocoordinated Fe^{II}. We assign the [4Fe-4S]²⁺ cluster to the RS cluster, because this cluster is needed for the reductive cleavage of SAM to generate the 5'-dA• oxidant in a subsequent step of the MiaB-catalyzed reaction. Consequently, we assign the [3Fe-4S]⁰-like cluster to the Aux cluster. The combination of Mössbauer spectroscopy and LC/MS showed that the kinetics of formation of the [3Fe-4S]⁰-like cluster match those of SAH formation. Furthermore, taking into consideration the previous observation that incubation of the methylated intermediate of MiaB with the tRNA substrate, sodium dithionite (required low-potential reductant), and d₃-SAM leads to formation of unlabeled ms²i⁶A before formation of labeled ms²i⁶A, the results presented herein indicate that the methylated intermediate is catalytically important.

In contrast to all other characterized [3Fe-4S]⁰ clusters, which contain a fully valence-delocalized MV unit, of which the two Fe sites have identical Mössbauer parameters,⁵⁴ the two Fe sites of the MV unit of the MiaB intermediate have different Mössbauer isomer shifts and quadrupole splittings. Of the two solutions we identified, the first has almost identical quadrupole splittings for the two Fe sites of the MV unit (1.02)

mm/s and 1.04 mm/s), but different isomer shifts (0.35 mm/s and 0.61 mm/s). These parameters would suggest valence localization within the MV unit, because these isomer shifts are typical of those of Fe^{III} and Fe^{II} sites, respectively, in [4Fe-4S] clusters.^{54,62} The second solution has more different quadrupole splittings (0.78 mm/s and 1.28 mm/s), but essentially identical isomer shifts (0.47 mm/s and 0.48 mm/s). These parameters would in turn indicate valence delocalization within the MV unit, but with different coordination environments of the two Fe sites, resulting in different quadrupole splittings.

The electronic structure of the ground state of MV clusters with two or more paramagnetic sites, such as Fe/S clusters, depends delicately on (1) the strength of the exchange coupling between the paramagnetic centers, (2) the strength of double exchange interaction between the two paramagnetic centers, and (3) the magnitude of the vibronic coupling of the two sites.⁶³ In particular, the relative magnitude of the double exchange interaction (which favors valence delocalization) and of the vibronic coupling (which favors valence localization) determines whether the ground state is valence localized or valence delocalized. Only subtle structural perturbations, such as the degree of saturation of a bridging ligand, ⁶⁴ are required to change the ground state from valence-localized to valence-delocalized. Borshch, et al. developed a model for [3Fe-4S]⁰ cluster of D. gigas, which takes into account the above three interactions. Importantly, this model rationalizes the experimental observation that the excess electron is delocalized over two Fe sites.⁶⁵ Subsequently, work by Solomon and co-workers employed ligand K-edge X-ray spectroscopy to measure the average covalency of the Fe-S bonds of various Fe/S clusters with MV units. 66-68 These experiments provided further insight into the electronic structures of Fe/S clusters with MV units, because the covalency of the Fe-S bonds affects the strength of the exchange coupling and the double exchange interactions (increased covalency results in stronger AF coupling via the bridging sulfides and decreases the double exchange interaction via the direct overlap of Fe-based orbitals).

Variable-field Mössbauer spectroscopy revealed that the MiaB [3Fe-4S]⁰-like cluster has an $|9/2, 2\rangle$ electronic ground state resulting from AF coupling between the high-spin Fe^{III} site (S = 5/2) and the MV pair ($S_{mv} = 9/2$). Münck and co-workers have shown that for the [3Fe-4S]⁰ cluster, the $|9/2, 2\rangle$ state is only observed for $B_{mv}/J > 2$ (see dashed line and red-shaded area in **Figure 5**). In the absence of the double exchange interaction ($B_{mv}/J = 0$) and for $J_{mv} = J$, the ground state would be the $|5/2, 0\rangle$ state, due to spin frustration caused by three equally strong AF couplings between the three Fe sites. Closer inspection of **Figure 5** reveals that the $|9/2, 2\rangle$ state can be the ground state for $J_{mv}/J < 1$. For $J_{mv}/J \le 0.555$ (5/9), the $|9/2, 2\rangle$ state is the ground state even in the absence of the double exchange interaction ($B_{mv}/J = 0$) (y-axis of **Figure 5**). This behavior can be understood by the loss of spin frustration in the trinuclear cluster. The stronger AF exchange couplings between the HS Fe^{III} site and the two Fe ions of the MV unit therefore result in parallel alignment of the spins of the MV unit to yield $S_{mv} = 9/2$.

A plausible geometric structure of the MiaB [3Fe-4S]⁰-like cluster that is in accordance with the electronic structure described by parameters of solution 1 invokes a methanethiolate ligand bridging the two Fe sites of the MV unit asymmetrically, with a stronger interaction with Fe_B than with Fe_A (**Figure 6A**). We assign Fe_B to the Fe^{III} site, because the reduced donor strength of the methanethiolate ligand (compared to that of sulfide) for stabilization of the Fe^{III} site would be compensated for by the asymmetric

binding mode with a stronger interaction with Fe_B. The $|9/2, 2\rangle$ ground state can be rationalized by the (presumably) less efficient exchange coupling pathway via the μ_2 -methanethiolate ligand (compared to that involving the μ_2 -sulfide ligands), thus reducing the AF coupling. For $J_{\text{mv}}/J < 0.555$, the $|9/2, 2\rangle$ will be the ground state (**Figure 5**), even in the absence of valence delocalization ($B_{\text{mv}} = 0$).

Plausible geometric structures of the [3Fe-4S]⁰-like cluster of MiaB that are in accordance with the electronic structure with the parameters of solution 2 are shown in Figure 6B and 6C. They both feature a symmetric [2Fe-2S] core geometry of the MV unit that would provide an efficient delocalization pathway involving the through-space overlap of the orbitals on Fe_A and Fe_B. In structure **B**, with the methanethiolate ligand bridging the Fe ions of the MV unit, the difference in quadrupole splitting could be attributed to distinct coordination geometries for Fe_A and Fe_B (e.g. a distorted Fe_B-µ₂-S- Fe^{III} fragment and/or distorted Cys coordination to FeB). In structure C, the $\mu_2\text{-}$ methanethiolate is depicted as bridging Fe_B and Fe^{III} asymmetrically, with a stronger interaction to Fe^{III} in order to compensate for the weaker donor strength of methanethiolate compared to that of sulfide. This in turn would render the coordination environments of Fe_A and Fe_B different, which could rationalize their different quadrupole splittings. For both structures, the $|9/2, 2\rangle$ ground state can be rationalized by the a strong double exchange interaction, favoring $S_{mv} = 9/2$ and AF coupling to Fe^{III} via at least one strong AF coupling pathway. We recognize that the asymmetry in structures $\mathbf{A} - \mathbf{C}$ could be stabilized by the protein scaffold and that other structures not depicted here can account for the experimentally observed site inequivalence of the MV unit.

Finally, the Aux [3Fe-4S]⁰-like cluster of the LipA cross-linked intermediate, which has a fully valence-delocalized MV unit, of which both Fe sites have indistinguishable parameters⁴² and which is known to have a μ_2 -6-mercapto-octanoyl bridging ligand,⁵⁰ could be described by the symmetric core structure shown in **Figure 6D**.

Recent electrochemical studies on Bt MiaB revealed unusual time-dependent redox properties of one of the $[4\text{Fe-4S}]^{2+}$ clusters upon treatment with SAM. Hills both $[4\text{Fe-4S}]^{2+}$ clusters in Bt MiaB exhibit typical reduction potentials (-390 mV for the Aux cluster and -450 mV for the RS cluster), incubation with SAM in the absence of the tRNA substrate significantly shifts the potential of the auxiliary cluster to -600 mV on a time scale that is consistent with the generation of the methylated intermediate. The authors rationalized the unusual low-potential state as a consequence of methylation of the Aux cluster without change of its chemical nature as a [4Fe-4S] cluster, while pointing out that such a low reduction potential is indeed rare for a $[4\text{Fe-4S}]^{2+/+}$ redox couple. In light of our work, we reason that the low reduction potential corresponds to that of the $[3\text{Fe-4S}]^{0/-1}$ -like Aux cluster of the methylated intermediate.

There are four known oxidation states of the cubane-type [3Fe-4S] clusters. The [3Fe-4S]^{+/0} couple is the most physiologically relevant redox pair in biological systems, with reported potentials spanning approximately 550 mV (- 460 mV to + 90 mV).⁶⁹ To the best of our knowledge, [3Fe-4S] clusters in the –1 core oxidation state have not been observed in a discrete form in any biological system. However, a [3Fe-4S]⁻ moiety has been deduced from studies on heterometallic cuboidal [M-3Fe-4S] clusters where M is a

redox-inert, divalent metal, such as Zn²⁺ or Cd²⁺.⁷⁰ The potentials reported for the [M-3Fe-4S]^{2+/+} redox couple, where the Fe/S fragment formally corresponds to a [3Fe-4S]^{0/-} unit, are – 492 mV for [Zn-3Fe-4S]^{2+/+} and – 569 mV for [Cd-3Fe-4S]^{2+/+}.⁷⁰ It has been demonstrated that [3Fe-4S]⁰ clusters can be reduced electrochemically in the region of ~ –700 mV to a [3Fe-4S]²⁻ state in a process that involves a cooperative proton-coupled two-electron reduction and thus by-passes the [3Fe-4S]⁻ state.⁷¹ It has been postulated that a discrete [3Fe-4S]⁻ state is not accessible under physiological conditions without binding to a positively charged moiety, such as divalent metal ions or protons.^{70,71} Similarly, replacement of a dianionic sulfido ligand (S²⁻) with a monoanionic methanethiolato ligand is expected to increase the reduction potential of the [3Fe-4S]^{0/-} couple in the MiaB [3Fe-4S]⁰-like cluster, perhaps to an extent that the [3Fe-4S]⁻ state becomes accessible under physiologically relevant conditions. In this instance, the one-electron reduction event at –600 mV detected electrochemically in the study by Maiocco, *et al.* might correspond to the [3Fe-4S]^{0/-} redox couple.⁴⁶

Previously, the proposed structures for the methylated intermediate of the MTTases MiaB and RimO were depicted as having a terminal methanethiolato ligand to the unique, non-cysteinyl coordinated Fe ion of the Aux [4Fe-4S] cluster based primarily on two experimental observations by Atta and co-workers. 45,48,72 The first was the X-ray crystal structure of RimO, which showed that the unique Fe sites of the Aux and RS clusters are connected by a pentasulfide bridge. 48 While the pentasulfide ligand detected in the X-ray structure is almost certainly an artifact of the crystallization conditions, given that the unique Fe site of the RS cluster binds SAM, this result nevertheless

underscores the ability of the unique Fe site of the Aux cluster to be coordinated by a terminal (hydro)sulfido ligand. Second, hyperfine sublevel correlation (HYSCORE) spectroscopy was used to demonstrate that exogenously supplied methanethiolate or methaneselenolate can bind as a terminal ligand to the unique Fe site of the Aux [4Fe-4S]⁺ cluster. 48 Thus, it was proposed that MiaB has a terminal sulfide ligand on the unique Fe site of its [4Fe-4S]²⁺ Aux cluster, which can attack the methyl carbon of SAM to generate the coproduct, SAH, and yield a terminal methanethiolato ligand (Scheme 2A). It is expected that the Aux cluster of the methylated intermediate would be a stable [4Fe-4S]²⁺ cluster, given that it would be coordinated by four thiolate ligands (three cysteines from the protein and the methanethiolate). However, this structure of the methylated intermediate is in contrast with our observation of a [3Fe-4S]⁰-like Aux cluster, the formation of which would require an unstable Aux cluster capable of losing the unique Fe site together with its terminal methanethiolate ligand. We disfavor this scenario, because (1) the Mössbauer parameters of the Fe^{II} observed in the sample containing the methylated intermediate are typical of HS N/O-coordinated Fe^{II 53} and do not support coordination by sulfur (in this case the isomer shift would be expected to decrease to ~1.1 mm/s, ⁷³ which is not supported by our data) (2) the remaining cluster would be expected to be a regular cuboidal [3Fe-4S]⁰ cluster with a fully valencedelocalized MV unit, which is not observed, and (3) there is thus far no evidence for a binding site for a Fe^{II}-SMe fragment on MiaB.

An alternative sulfur source to be methylated would be one of the μ_3 -sulfido ligands of the Aux [4Fe-4S]²⁺ cluster (**Scheme 2B**). Nucleophilic attack of the μ_3 -sulfido ligand on C_{methyl} of SAM would yield SAH and a [4Fe-4S]²⁺-like cluster, wherein one μ_3 -

sulfido ligand has been converted to a μ_3 -methanethiolato ligand. Loss of the unique iron ion as Fe^{II} would then yield the [3Fe-4S]⁰-like cluster, which we assume is effected by a weakening of the Fe_{unique}–SMe bond. We note that the order of these two steps could also be reversed, i.e. loss of Fe^{II} to make a [3Fe-4S]⁰ cluster, followed by attack of one of the μ_2 -sulfides on the methyl group of SAM. This mechanism is consistent with the results obtained in this work by Mössbauer spectroscopy, namely observation of Fe^{II} in solution and a [3Fe-4S]⁰-like cluster with an unusual electronic structure, which is attributed to the fact that one of sulfides is converted to a methanethiolate.

At face value the results from previous work using HYSCORE spectroscopy. Spectroscopy contradict our results from Mössbauer spectroscopy. We speculate that the discrepancy arises from the way the samples were prepared. In our study, wild-type *Bt* MiaB was used under conditions that lead to generation of the methylated intermediate by a nucleophilic substitution on the co-substrate, SAM, which is known to be chemically competent to make the methylthiolated product. By contrast, the HYSCORE study was carried out on a sample of a MiaB variant that lacks the RS cluster. More importantly, the sample was generated by treatment with methanethiol, a reagent wherein the S-C_{methyl} bond is already formed. We speculate that the formation of the experimentally observed Aux [4Fe-4S]⁺ cluster featuring a terminal methanethiolato/selenolato ligand involves a ligand substitution, wherein the methanethiolato/selenolato replaces the ligand (perhaps a water or buffer molecule) to the unique Fe of the Aux [4Fe-4S] cluster. Thus, the unequivocal experimental observation that a methanethiolato/selenolato ligand can serve as exogenous ligand to one Fe site (likely the unique Fe site) of the [4Fe-4S] Aux cluster is nevertheless

no proof that this state is an intermediate on the pathway and hence not in contrast to our observation of a [3Fe-4S]⁰-like Aux cluster.

The formation of a related [3Fe-4S]⁰-like cluster has recently been demonstrated in the catalytically competent intermediate on the Aux cluster of the RS enzyme LipA, 42 which features a μ_2 -6-mercapto-octanoyl ligand. Although the reactions of LipA and MiaB feature the conversion of a [4Fe-4S]²⁺ Aux cluster to a [3Fe-4S]⁰-like Aux cluster, the mechanisms of this conversion in the two enzymes are fundamentally different. In the LipA-catalyzed reaction, the formation of the new C-S bond is initiated by attack of the C6 octanoyl radical—generated by abstraction of the C6 *proR* hydrogen by the 5'-dA•—on one of the μ_3 -sulfido ligands of the Aux [4Fe-4S]²⁺ cluster. Formally, in this reaction the new C-S bond is formed by one electron from the substrate radical and the other from the lone pair on the sulfide ligand. The remaining electron of the sulfido lone pair then formally reduces the cluster by one electron, yielding a [4Fe-4S]⁺-like intermediate, which is not observed in the native LipA reaction. Loss of one Fe^{II} and an additional electron then yields the experimentally observed [3Fe-4S]⁰-like cluster (**Scheme 2C**).

Previous studies indicated that MiaB and RimO may share a similar mechanism for the first step of their reactions: generation of the methylated intermediate.⁴⁵ Considering the biochemical and electrochemical similarities between the proposed methylated intermediates in MiaB and RimO, it will be interesting to explore if a [3Fe-4S]⁰-like intermediate is also observed in RimO. A recent study by Molle, *et al.* on *Tm* RimO reported observation of HS Fe^{II} species and unspecified paramagnetic species by

Mössbauer spectroscopy following incubation of samples of Tm RimO containing predominantly [4Fe-4S]²⁺ clusters with SAM.⁷² In the study by Molle, et al., the Mössbauer spectra were recorded in an applied field of 60 mT and the remaining spectral features were modeled as a superposition of valence-delocalized [4Fe-4S]²⁺, site-differentiated [4Fe-4S]²⁺, and [2Fe-2S]²⁺ clusters. We acknowledge the complexity associated with spectral simulation of multiple Fe-containing species with heavily overlapping features. However, it will be interesting to see if the observed spectral changes in Tm RimO could also be rationalized by invoking conversion of a [4Fe-4S]²⁺ cluster to a potential [3Fe-4S]⁰-like cluster.

The reaction mechanisms of the second step of the reactions of RimO and MiaB, the conversion of the methylated intermediate to the respective products, wherein SAM functions as the source of the 5'-dA• intermediate, are likely different. In RimO, the second phase of the reaction is initiated by abstraction of the aliphatic 3-*pro-S* hydrogen of the substrate by the 5'-dA• intermediate, followed by transfer of the methylthio group to the C3 substrate radical.³³ While the mechanism of the latter radical coupling reaction resulting in generation of the C3-S bond remains to be elucidated, there is precedent for such a reaction in the related RS enzyme BioB.^{41,43} In the second step of the BioB reaction, the substrate is 9-mercapto-dethiobiotin, which is generated during the first step of the reaction and involves attack of the C9 dethiobiotinyl radical (generated by abstraction of hydrogen from C9 by 5'-dA•) on one of the μ_2 -sulfido ligands of the Aux [2Fe-2S]²⁺ cluster, which gets reduced to the [2Fe-2S]⁺ form in the process. A second equivalent of 5'-dA• abstracts the 6-*pro-S* hydrogen from the substrate, followed by

attack of the ensuing radical on the sulfur of the coordinated thiolate of the substrate, yielding the thiophane ring of biotin.^{5,41,43} Again, this radical coupling step results in further reduction of the Aux [2Fe-2S] cluster by one electron. The second part of the RimO reaction has been proposed to proceed according to that mechanism, namely attack of the C3 radical from the substrate on the coordinated methanethiolate, yielding a one-electron reduced Aux cluster.^{33,72}

The second step of the MiaB reaction, installment of the methylthio moiety on C2 of the substrate, is likely different, because the homolytic bond dissociation energy (BDE) of the C2-H bond of the substrate (estimated to be ~105 kcal/mol)⁷⁴ is expected to be too high for the hydrogen to be abstracted by the 5'-dA• oxidant. Recent work by Arcinas, et al. demonstrated that nevertheless, the hydrogen atom from C2 is removed by the 5'-dA•. The proposed mechanism for the second part of the MiaB reaction (Scheme 3) is initiated by nucleophilic attack by the coordinated methanethiolate on C2 of the substrate, which would decrease the BDE of the C2-H bond due to rehybridization of C2 from sp^2 to sp^3 . In the next step, the 5'-dA• is proposed to abstract the hydrogen from C2, followed by loss of an electron from the substrate to generate the 2-methylthiolated product. Importantly, in this mechanism, formation of the new C-S bond occurs before hydrogen abstraction, while in RimO (and all other RS enzymes that catalyze C-S bond formation via radical-based mechanisms involving the 5'-dA• radical, like BioB, LipA, and RimO) formation of the new C-S bond is known or proposed to occur after hydrogen atom abstraction.

Our proposal that a methylated [3Fe-4S]⁰-like cluster being the immediate source of sulfide to be incorporated into the final product is also consistent with two previous

observations. It has been previously demonstrated that Tm MiaB containing [4Fe-4Se]²⁺ instead of [4Fe-4S]²⁺ clusters, is able to catalyze formation of mse²i⁶A.⁷⁶ Furthermore, in E. coli, a decrease in MiaB activity in vivo has been associated with the inactivation of the ygfZ gene. 77,78 E. coli ygfZ and its yeast homolog Iba57 have recently been recognized as playing prominent roles in the biogenesis of Fe/S clusters. 78,79 In particular, although yeast Iba57 is not required for the de novo assembly of Fe/S clusters, it is required for the in vivo functions of both BioB and LipA.79 Taken together, these observations are consistent with the MiaB auxiliary [4Fe-4S]²⁺ cluster as the most likely ultimate source of the sulfide to be incorporated into the final ms²i⁶A product. Due to the importance of tRNA methylthiolation, a sacrificial role of the MiaB auxiliary cluster was considered unfavorable due to concerns that inclusion of cluster generation during catalysis may not be able to sustain the cellular demand of the MiaB reaction product.⁴⁸ Recently, it has been demonstrated that the E.coli Fe/S cluster carrier protein NfuA is able to efficiently restore the Aux [4Fe-4S] cluster in LipA during catalysis in a process that is not rate limiting.⁴⁴ Intriguingly, studies on Fe/S cluster trafficking in *E.coli* have demonstrated that NfuA is able to physically interact with MiaB and to deliver a [4Fe-4S]²⁺ cluster to both RS and auxiliary cluster domains in MiaB.80 Therefore, it is tempting to speculate that NfuA might play a role in restoration of the Aux cluster in MiaB, like it does in LipA.

ASSOCIATED CONTENT

Supporting Information

Materials and Methods and Figures S1-S15 (PDF).

AUTHOR INFORMATION

Corresponding Author

*Carsten Krebs (ckrebs@psu.edu)

*Squire J. Booker (squire@psu.edu)

Present Addresses

† Present Address: Genomatica, 4757 Nexus Center Dr., San Diego, California 92121

§ Present Address: Department of Biochemistry, Albert Einstein College of Medicine,

Bronx, New York 10461

Funding Sources

This work has been supported by the National Institutes of Health (awards GM-122595-to S.J.B. and GM-127079 to C.K.), the National Science Foundation (MCB-1716686 to S.J.B.), and the Eberly Family Distinguished Chair in Science (S.J.B). S.J.B is an Investigator of the Howard Hughes Medical Institute.

Notes

The authors declare no competing financial interest.

ACKNOWLEDGEMENT

We thank Reviewer 1 for helpful discussion concerning plausible geometric structures of the [3Fe-4S]⁰-like cluster in MiaB.

ABBREVIATIONS

RS, radical SAM; SAM, S-adenosylmethionine; d_3 -SAM, S-adenosyl-[methyl- 2 H₃]-methionine; Aux cluster, auxiliary cluster; RC, reconstituted; AI, as isolated; WT, wild

type; 5'-dAH, 5'-deoxyadenosine; 5'-dA•, 5'-deoxyadenosyl radical; SAH, S-adenosylhomocysteine; i⁶A, N⁶-(isopentenyl)adenosine; ms²i⁶A, 2-methythio-N⁶-(isopentenyl)adenosine; Tm, Thermotoga maritima; Bt, Bacteroides thetaiotaomicron; MTTase, methylthiotransferase; AF, antiferromagnetic; LC/MS, liquid chromatography coupled to mass spectrometry; MV, mixed-valent.

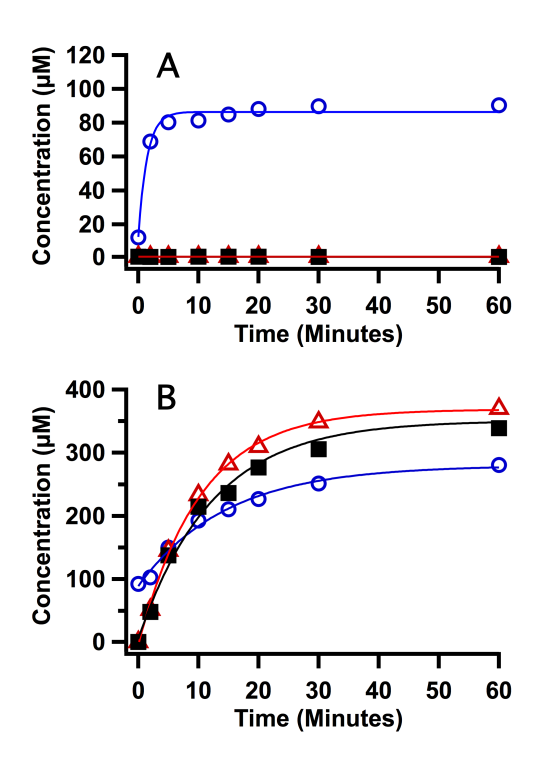


Figure 1. LC/MS analysis of the progress of the *Bt* MiaB reaction. (**A**) Reconstituted *Bt* MiaB (165 μM) was incubated with SAM (600 μM) and tRNA substrate i^6A (330 μM) for varying reaction times. (**B**) Reconstituted MiaB (165 μM) was incubated with SAM (600 μM) and tRNA substrate i^6A (330 μM) for 20 min and then reacted with sodium dithionite for varying reaction times. The reaction was monitored by formation of the products SAH (blue circles), 5'-dAH (red triangles), and ms^2i^6A (black squares). The solid lines are fits to a first-order exponential using parameters mentioned in the text.

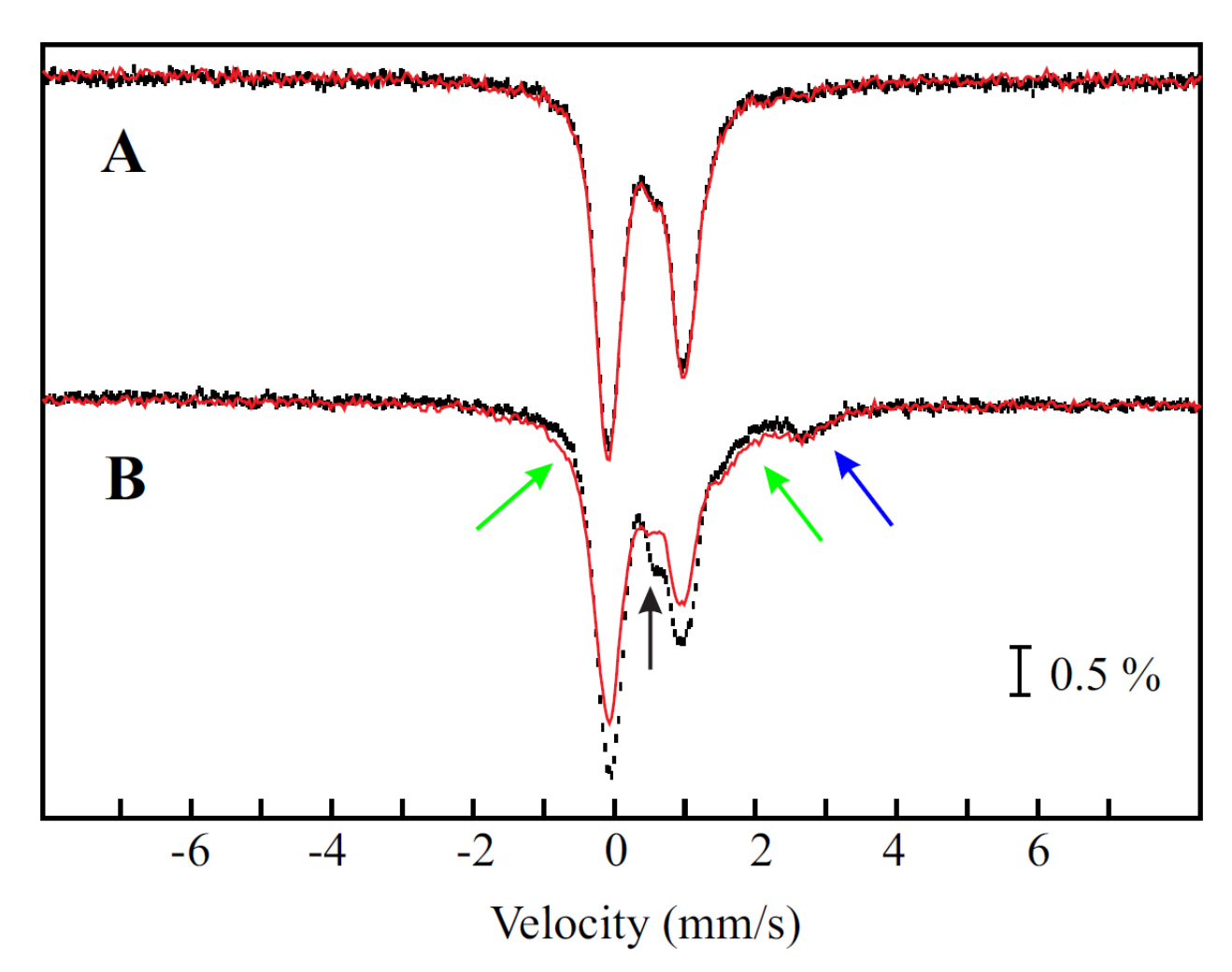


Figure 2. Comparison of Mössbauer spectra of reconstituted Bt MiaB collected at 4.2 K with either no applied magnetic field (black vertical bars) or in a 53-mT magnetic field oriented parallel to the γ beam (red lines) before (**A**) and after (**B**) incubation with SAM for 20 min. The black arrow indicates the increased absorption at ~ 0.6 mm/s. The blue arrow indicates the high-energy line of high-spin Fe^{II}. The green arrows indicate the broad unspecific absorption of the component with paramagnetic integer-spin ground state in the 53-mT spectrum.

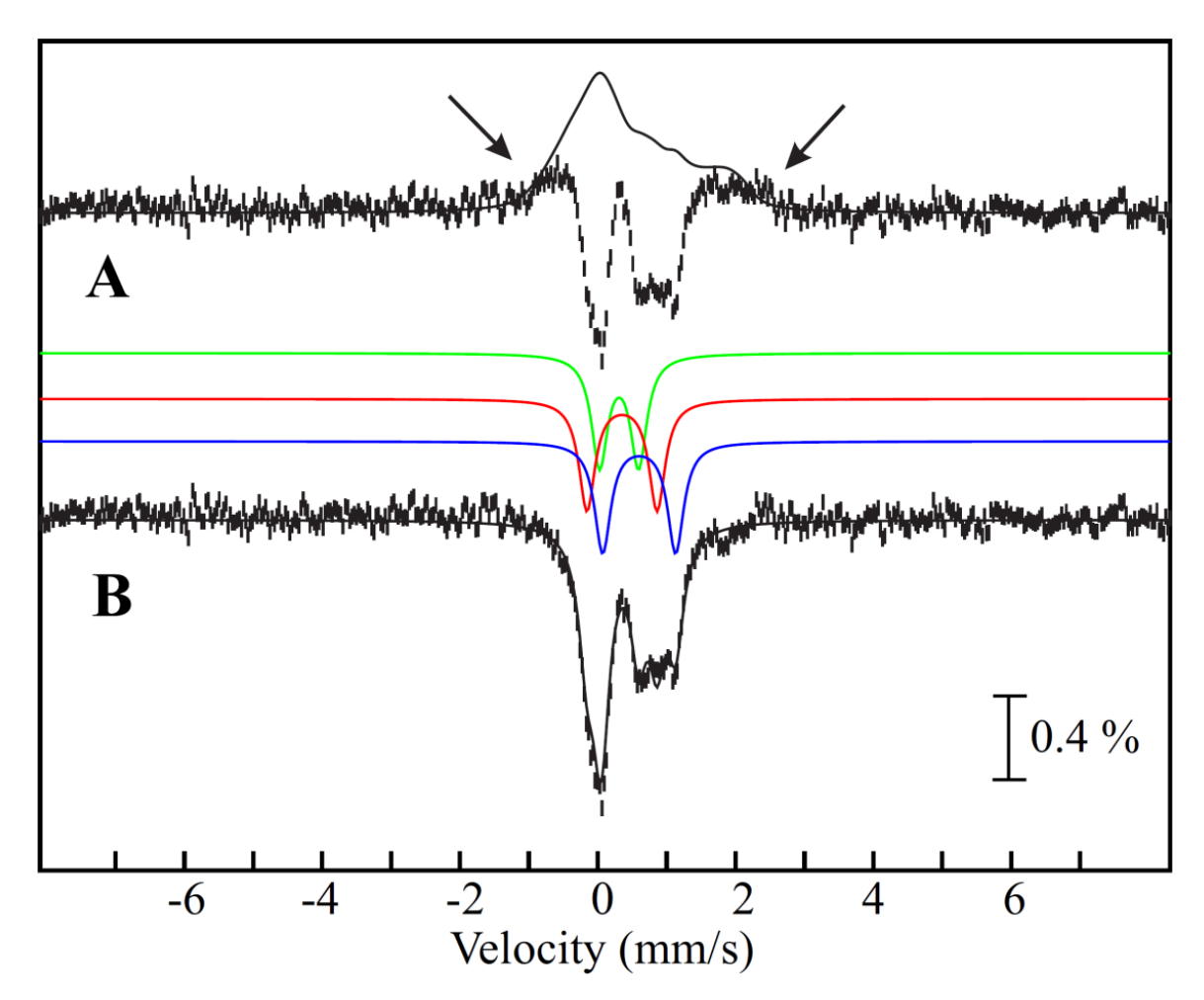


Figure 3. Analysis of the zero-field and 53 mT Mössbauer spectra of reconstituted *Bt* MiaB after incubation with tRNA and SAM for 20 min. (**A**) [0-53mT] difference spectrum (vertical bars) and a simulation of the MiaB [3Fe-4S]⁰–like cluster in 53 mT using the parameters listed in Table 2 and scaled to –27% of total ⁵⁷Fe absorption (black line). The arrows indicate the onset of the broad absorption features arising from the magnetic hyperfine splitting of the MiaB [3Fe-4S]⁰–like cluster. (**B**) The zero-field reference spectrum of the MiaB [3Fe-4S]⁰–like cluster (vertical bars). The black line is the simulation of the MiaB [3Fe-4S]⁰–like cluster in zero-field with parameters from Table 1, solution 1 (30 % of total intensity). Individual contributions from the three sites are shown above the zero-field reference spectrum (site **1** (green), site **2** (red), site **3** (blue); 10 % of total intensity each).

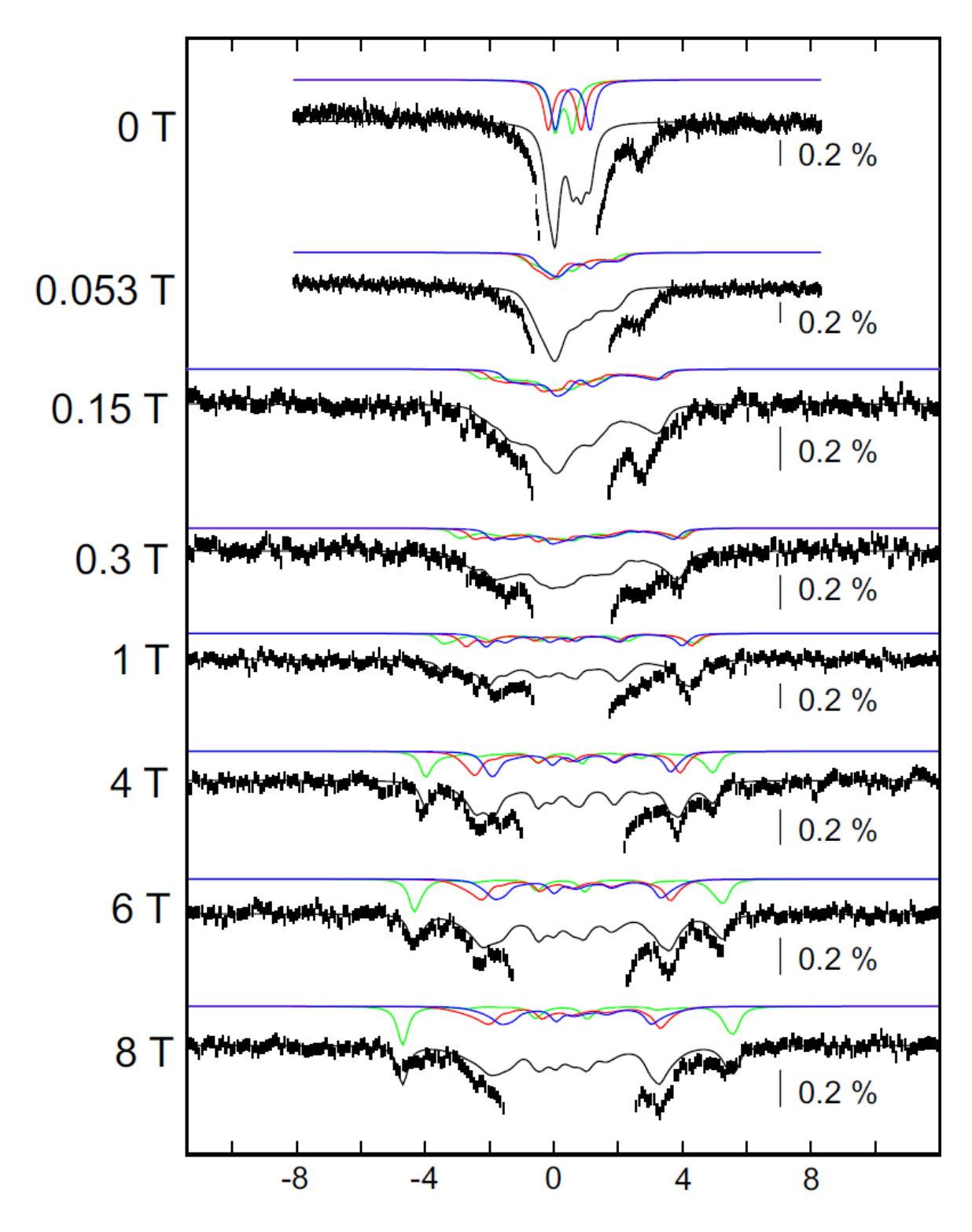


Figure 4. 4.2-K/variable-field Mössbauer spectra of a sample of reconstituted Bt MiaB incubated with SAM and tRNA substrate for 20 min. Experimental spectra are shown as vertical bars. The strength of the external magnetic field applied parallel to the γ beam is indicated for each spectrum. In all spectra, the experimental data are shown as black

vertical bars. The central region of the spectra is dominated by the features of the [4Fe-4S]²⁺ clusters and is cut off in order to amplify the weaker, magnetically split features associated with the [3Fe-4S]⁰-like cluster. The total simulations of the [3Fe-4S]⁰-like cluster are shown as black lines using the spin Hamiltonian parameters quoted in Table 2 (27 % total intensity). The solid green, red, and blue lines are spin Hamiltonian simulations using the parameters in Table 2 of the unique Fe^{III} site (site 1, 9 % of total intensity, green lines), the "Fe^{III}-like" site of the MV unit (site 2, 9 % of total intensity, red lines), and the "Fe^{II}-like" site of the MV unit (site 3, 9 % of total intensity, blue lines). The full spectra are shown in **Figure S13A**.

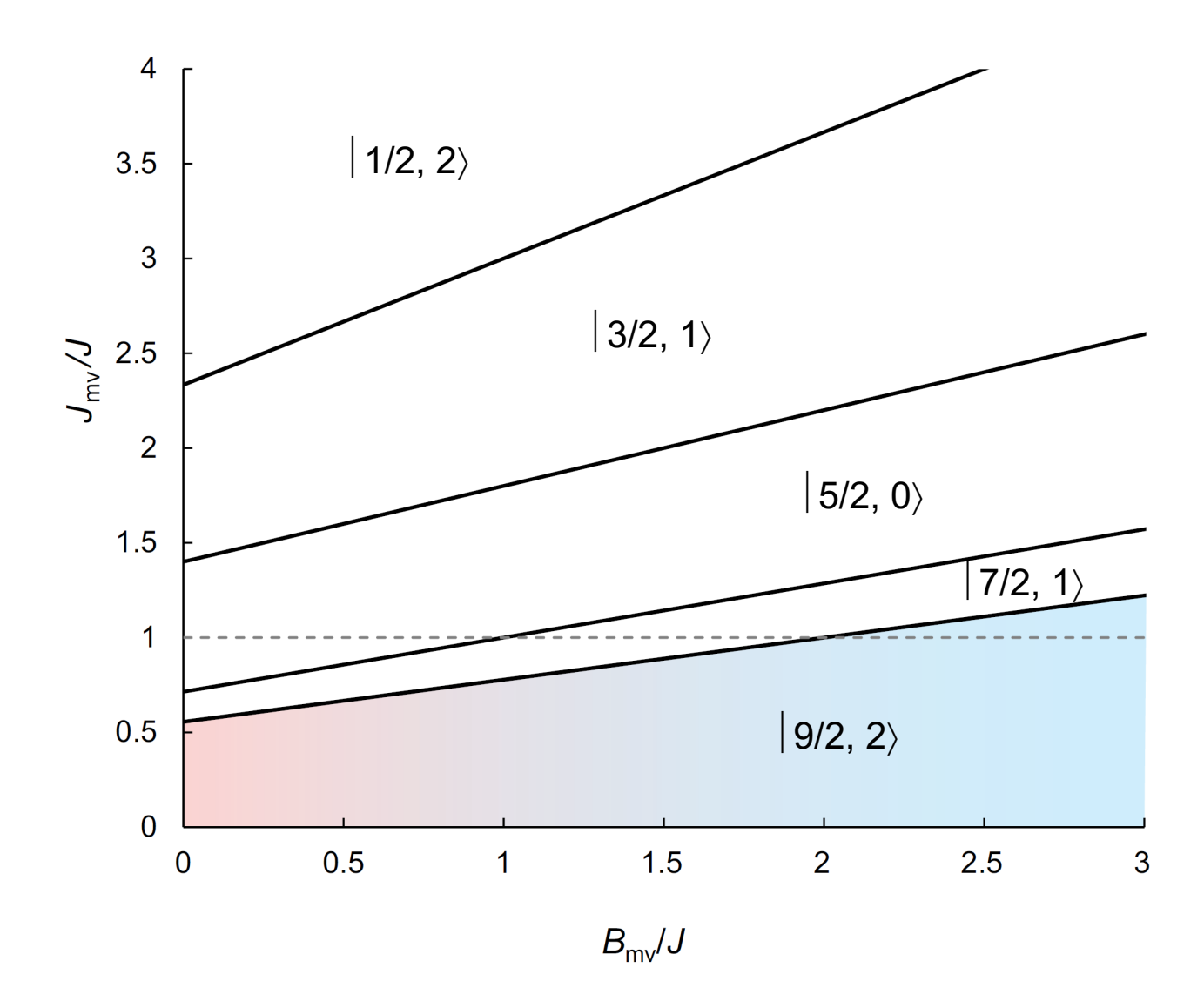


Figure 5. Possible total spin ground states of the [3Fe-4S]⁰-like cluster as a function of $J_{\rm mv}/J$ and $B_{\rm mv}/J$. Spin states are labeled as $|S_{\rm mv}, S_{\rm tot}\rangle$. The parameter space containing values of $J_{\rm mv}/J$ and $B_{\rm mv}/J$ yielding the experimentally observed $|9/2, 2\rangle$ ground state is shown colored. The dashed line indicates $J_{\rm mv} = J$.

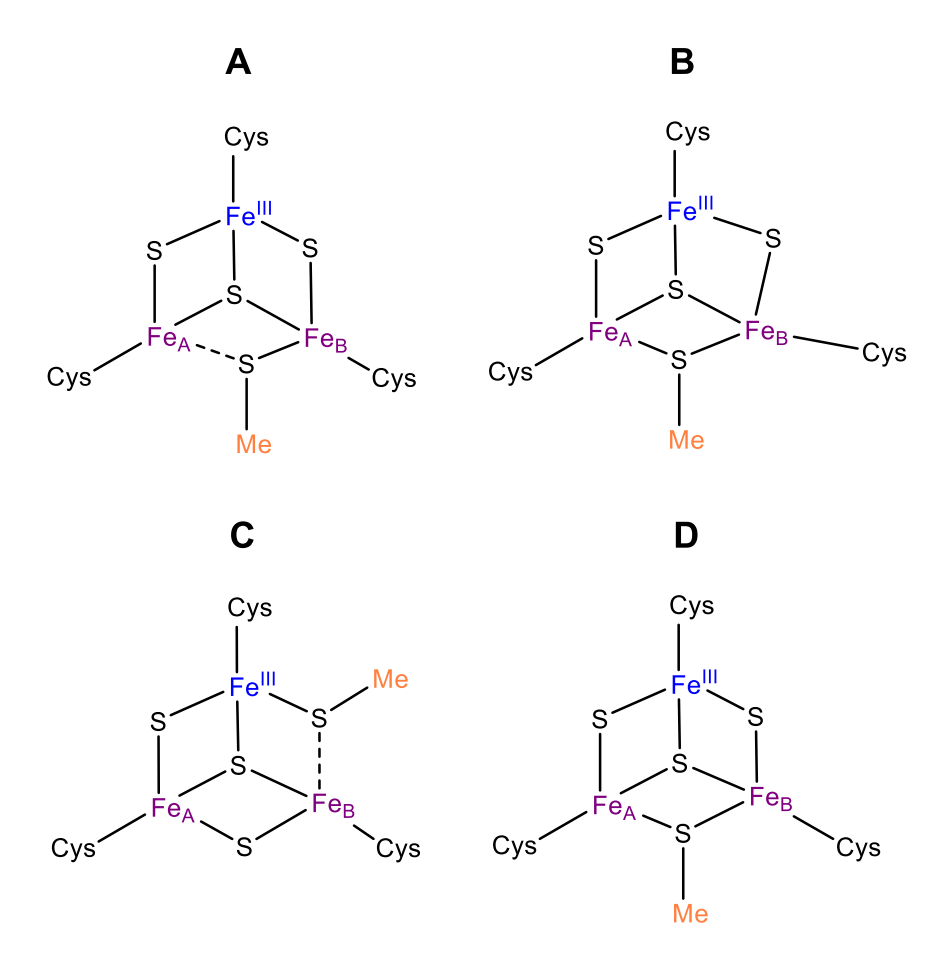
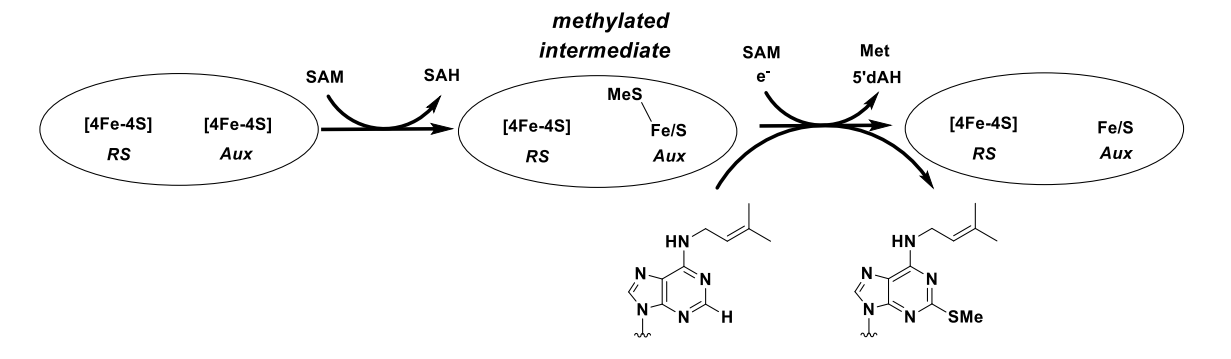


Figure 6. Possible structures of the [3Fe-4S]⁰-like Aux cluster in MiaB with a valence-localized MV unit (**A**), or with a valence-delocalized MV unit (**B** and **C**), and of the [3Fe-4S]⁰-like Aux cluster of LipA (**D**).



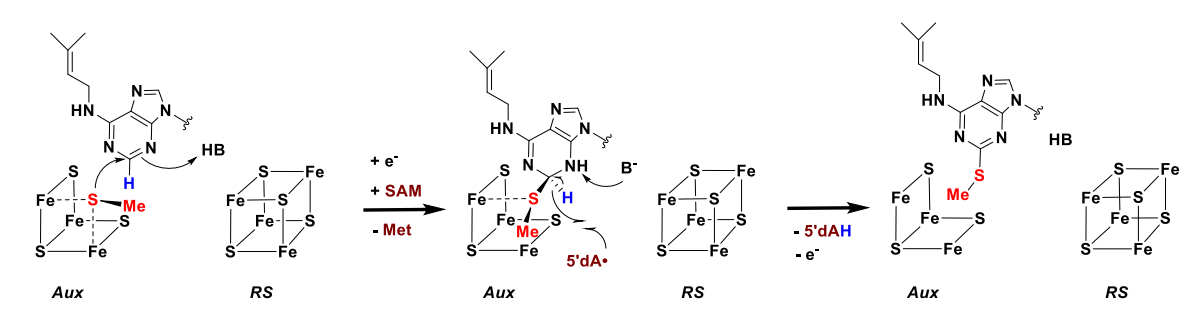
Scheme 1. Reaction catalyzed by MiaB.

Scheme 2. Two possible mechanisms for formation of the $[3\text{Fe-4S}]^0$ -like auxiliary cluster in MiaB by nucleophilic attack of either a terminal sulfide on the unique Fe site (**A**) or μ_3 -bridging sulfide (**B**) from the $[4\text{Fe-4S}]^{2^+}$ cluster on the methyl group of SAM and the mechanism for generation of the $[3\text{Fe-4S}]^0$ -like cluster by a radical mechanism in LipA (**C**). The sulfur atom and the methyl group forming the methylthio moiety of the intermediate are emphasized in bold red.

[4Fe-4S]⁺-like

[4Fe-4S]²⁺

[3Fe-4S]⁰-like



Scheme 3. Proposed mechanism for the second part of the MiaB reaction, *viz* the transfer of the methylthio group from the Aux Fe/S cluster to C2 of A37 of the tRNA substrate.

Table 1: Different sets of Mössbauer parameters for simulation of the zero-field reference spectrum of the [3Fe-4S]⁰-like cluster.

site	Solution 1		Solution 2		Solution 3		Solution 4		Solution 5		Solution 6	
	δ	ΔE_Q	δ	ΔE_Q	δ	ΔE_Q	δ	ΔE_Q	δ	ΔE_Q	δ	ΔE_Q
	(mm/s)	(mm/s)										
1	0.31	0.58	0.31	0.58	0.34	0.51	0.34	0.51	0.22	0.75	0.22	0.75
2	0.35	1.02	0.47	1.28	0.35	1.02	0.44	1.28	0.44	0.84	0.47	1.11
3	0.61	1.04	0.48	0.78	0.57	1.11	0.48	0.84	0.61	1.04	0.57	0.78

Table 2. Spin Hamiltonian parameters for simulation of Mössbauer spectra of [3Fe-4S]⁰ clusters.

Species	ZFS parameters		δ (mm/s)	$\Delta E_{\rm Q}$ (mm/s)	η	β (deg) ^a	$A/g_{\rm n}\beta_{\rm n}$ (T)	ref
		site 1 , sol. 1	0.31	0.58	2	0	(+12.3, +12.3, +12.3)	
	$D_{S=2} = -2.4 \text{ cm}^{-1}$ $(E/D)_{S=2} = 0.26$	sol. 2	0.31	0.58	2	0	(+12.3, +12.5, +12.3)	
Bt MiaB [3Fe-4S] ⁰ —		site 2 , sol. 1	0.35	1.02	1	0	(-11.7, -18.0, -11.6)	this
like cluster		sol. 2	0.47	1.28	2	0	(-11.2, -18.5, -11.4)	work
		site 3 , sol. 1	0.61	1.04	-2	0	(-10.0, -18.0, -10.0)	-
		sol. 2	0.48	0.78	0	0	(-10.0, -18.4, -10.3)	
Ec LipA [3Fe-4S] ⁰ —	$D_{S=2} = -4.0 \text{ cm}^{-1}$	Fe ^{III}	0.31	-0.55	-2	16	(+10.0, +11.8, +11.8)	42
like cluster	$(E/D)_{S=2} = 0.23$	$Fe_2^{2.5+}$	0.44	0.98	0.4	25	(-14.1, -14.1, -11.4)	
Dg ferredoxin [3Fe-	$D_{S=2} = -2.5 \text{ cm}^{-1}$	Fe ^{III}	0.32	-0.52	-2	16	(+10.0, +11.5, +12.6)	54
4S] ⁰ cluster	$(E/D)_{S=2} = 0.23$	$Fe_2^{2.5+}$	0.46	1.47	0.4	20	(-14.9, -14.9, -11.9)	
Av ferredoxin [3Fe-	$D_{S=2} = -2.5 \text{ cm}^{-1}$ $(E/D)_{S=2} = 0.23$	Fe ^{III}	0.29	-0.47	0.8	20	(+10.9, +10.2, +12.6)	- 55
4S] ⁰ cluster (pH 6)		Fe ₂ ^{2.5+}	0.47	1.41	1.1	24	(-15.2, -18.2, -10.4)	
			0.47	1.41	0.2	24	(-13.8, -16.0, -12.1)	
Av ferredoxin [3Fe-	$D_{S=2} = -2.5 \text{ cm}^{-1}$ $(E/D)_{S=2} = 0.23$	Fe ^{III}	0.29	-0.47	5	27	(+11.6, +10.2, +12.5)	- 55
4S] ⁰ cluster (pH 8.5)		$Fe_2^{2.5+}$	0.47	1.41	1	19	(-13.8, -19.6, -12.1)	33
		1 02	0.47	1.41	0	19	(-14.5, -16.0, -12.1)	

 $^{^{\}rm a}$ Euler angle β as defined in ref 24

Table 3. Spin projection factors for possible spin ground states of the [3Fe-4S]⁰-like cluster.

Spin state $ S_{mv}, S_{tot}\rangle$	Cferric-y,MV a	Cferrous-y,MV ^a	Cferric ^a
9/2, 2⟩	+1.019	+0.815	-0.833
	[+55/54]	[+22/27]	[-5/6]
1/2, 2⟩	-0.389	+0.222	+1.167
	[-7/18]	[+2/9]	[+7/6]
7/2, 1⟩	+1.321	+0.929	-1.25
	[+37/28]	[+13/14]	[-5/4]
3/2, 1⟩	-0.65	-0.1	+1.75
	[-13/20]	[-1/10]	[+7/4]
5/2, 0⟩ ^b	-	-	-

^a italicized values are expression as ratio of smallest integers

 $^{^{\}rm b}$ not defined due to $S_{\rm tot} = 0$ ground state

References

- (1) Frey, P. A.; Hegeman, A. D.; Ruzicka, F. J. The radical SAM superfamily, *Crit. Rev. Biochem. Mol. Biol.* **2008**, *43*, 63.
- (2) Atta, M.; Mulliez, E.; Arragain, S.; Forouhar, F.; Hunt, J. F.; Fontecave, M. S-Adenosylmethionine-dependent radical-based modification of biological macromolecules, *Curr. Opin. Struct. Biol.* **2010**, *20*, 684.
- (3) Vey, J. L.; Drennan, C. L. Structural Insights into Radical Generation by the Radical SAM Superfamily, *Chem. Rev.* **2011**, *111*, 2487.
- (4) Broderick, J. B.; Duffus, B. R.; Duschene, K. S.; Shepard, E. M. Radical *S*-Adenosylmethionine Enzymes, *Chem. Rev.* **2014**, *114*, 4229.
- (5) Jarrett, J. T. The Biosynthesis of Thiol- and Thioether-containing Cofactors and Secondary Metabolites Catalyzed by Radical S-Adenosylmethionine Enzymes, J. Biol. Chem. **2015**, 290, 3972.
- (6) Lanz, N. D.; Booker, S. J. Auxiliary iron-sulfur cofactors in radical SAM enzymes, *Biochim. Biophys. Acta Mol. Cell Res.* **2015**, *1853*, 1316.
- (7) Sofia, H. J.; Chen, G.; Hetzler, B. G.; Reyes-Spindola, J. F.; Miller, N. E. Radical SAM, a novel protein superfamily linking unresolved steps in familiar biosynthetic pathways with radical mechanisms: functional characterization using new analysis and information visualization methods, *Nucl. Acids Res.* **2001**, *29*, 1097.
- (8) Holliday, G. L.; Akiva, E.; Meng, E. C.; Brown, S. D.; Calhoun, S.; Pieper, U.; Sali, A.; Booker, S. J.; Babbitt, P. C. In *Radical Sam Enzymes*; Bandarian, V., Ed.; Elsevier Academic Press Inc: San Diego, 2018; Vol. 606, p 1.
- (9) Akiva, E.; Brown, S.; Almonacid, D. E.; Barber, A. E.; Custer, A. F.; Hicks, M. A.; Huang, C. C.; Lauck, F.; Mashiyama, S. T.; Meng, E. C.; Mischel, D.; Morris, J. H.; Ojha, S.; Schnoes, A. M.; Stryke, D.; Yunes, J. M.; Ferrin, T. E.; Holliday, G. L.; Babbitt, P. C. The Structure-Function Linkage Database, *Nucl. Acids Res.* **2014**, *42*, D521.
- (10) Krebs, C.; Broderick, W. E.; Henshaw, T. F.; Broderick, J. B.; Huynh, B. H. Coordination of Adenosylmethionine to a Unique Iron Site of the [4Fe-4S] of Pyruvate Formate-Lyase Activating Enzyme: A Mössbauer Spectroscopic Study, *J. Am. Chem. Soc.* **2002**, *124*, 912.

- (11) Walsby, C. J.; Hong, W.; Broderick, W. E.; Cheek, J.; Ortillo, D.; Broderick, J. B.; Hoffman, B. M. Electron-nuclear double resonance spectroscopic evidence that *S*-adenosylmethionine binds in contact with the catalytically active 4Fe-4S⁺ cluster of pyruvate formate-lyase activating enzyme, *J. Am. Chem. Soc.* **2002**, *124*, 3143.
- (12) Yang, H.; McDaniel, E. C.; Impano, S.; Byer, A. S.; Jodts, R.; Yokoyama, K.; Broderick, W. E.; Broderick, J. B.; Hoffman, B. M. The Elusive 5'-Deoxyadenosyl Radical: Captured and Characterized by EPR and ENDOR Spectroscopies, *J. Am. Chem. Soc.* **2019**, *141*, 12139.
- (13) Sayler, R. I.; Stich, T. A.; Joshi, S.; Cooper, N.; shaw, J. T.; Begley, T. P.; Tantillo, D. J.; Britt, R. D. Trapping and Electron Paramagnetic Resonance Characterization of the 5'dAdo• Radical in a Radical S-Adenosyl Methionine Enzyme Reaction with a Non-Native Substrate, *ACS Central Science* **2019**, DOI: 10.1021/acscentsci.9b00706.
- (14) Horitani, M.; Shisler, K.; Broderick, W. E.; Hutcheson, R. U.; Duschene, K. S.; Marts, A. R.; Hoffman, B. M.; Broderick, J. B. Radical SAM catalysis via an organometallic intermediate with an Fe- 5 '-C -deoxyadenosyl bond, *Science* **2016**, *352*, 822.
- (15) Atta, M.; Arragain, S.; Fontecave, M.; Mulliez, E.; Hunt, J. F.; Luff, J. D.; Forouhar, F. The methylthiolation reaction mediated by the Radical-SAM enzymes, *Biochim. Biophys. Acta Proteins and Proteomics* **2012**, *1824*, 1223.
- (16) Urbonavičius, J.; Qian, O.; Durand, J. M. B.; Hagervall, T. G.; Björk, G. R. Improvement of reading frame maintenance is a common function for several tRNA modifications, *EMBO Journal* **2001**, *20*, 4863.
- (17) Gustilo, E. M.; Franck, A. P. F.; Agris, P. F. tRNA's modifications bring order to gene expression, *Curr. Opin. Microbiol.* **2008**, *11*, 134.
- (18) Hagervall, T.; Ericson, J.; Esberg, K.; Li, J.; Björk, G. Role of transfer-RNA modification in translational fidelity, *Biochim. Biophys. Acta* **1990**, *1050*, 263.
- (19) Torres, A. G.; Batlle, E.; de Pouplana, L. R. Role of tRNA modifications in human diseases, *Trends in Molecular Medicine* **2014**, *20*, 306.
- (20) Durand, J. M. B.; Björk, G. R.; Kuwae, A.; Yoshikawa, M.; Sasakawa, C. The modified nucleoside 2-methylthio-N-6-isopentenyladenosine in tRNA of *Shigella flexneri* is required for expression of virulence genes, *J. Bact.* **1997**, *179*, 5777.

- (21) Bartz, J. K.; Kline, L. K.; Söll, D. N⁶-(Δ²-Isopentenyl)adenosine Biosynthesis in vitro in transfer RNA by an enzyme purified from *Escherichia coli*, *Biochem. Biophys. Res. Commun.* **1970**, *40*, 1481.
- (22) Caillet, J.; Droogmans, L. Molecular cloning of the *Escherichia coli miaA* gene involved in the formation of the Δ^2 -isopentenyl adenosine in transfer RNA, *J. Bact.* **1988**, *170*, 4147.
- (23) Rosenbaum, N.; Gefter, M. L. Δ^2 -Isopentenylpyrophosphate transfer ribonucleic acid Δ^2 -isopentenyltransferase from *Escherichia coli* Purification and properties of enzyme, *J. Biol. Chem.* **1972**, *247*, 5675.
- (24) Steinthorsdottir, V.; Thorleifsson, G.; Reynisdottir, I.; Benediktsson, R.; Jonsdottir, T.; Walters, G. B.; Styrkarsdottir, U.; Gretarsdottir, S.; Emilsson, V.; Ghosh, S.; Baker, A.; Snorradottir, S.; Bjarnason, H.; Ng, M. C. Y.; Hansen, T.; Bagger, Y.; Wilensky, R. L.; Reilly, M. P.; Adeyemo, A.; Chen, Y. X.; Zhou, J.; Gudnason, V.; Chen, G. J.; Huang, H. X.; Lashley, K.; Doumatey, A.; So, W.; Ma, R. C. Y.; Andersen, G.; Borch-Johnsen, K.; Jorgensen, T.; van Vliet-Ostaptchouk, J. V.; Hofker, M. H.; Wijmenga, C.; Christiansen, C.; Rader, D. J.; Rotimi, C.; Gurney, M.; Chan, J. C. N.; Pedersen, O.; Sigurdsson, G.; Gulcher, J. R.; Thorsteinsdottir, U.; Kong, A.; Stefansson, K. A variant in CDKAL1 influences insulin response and risk of type 2 diabetes, *Nature Genetics* **2007**, *39*, 770.
- (25) Ohara-Imaizumi, M.; Yoshida, M.; Aoyagi, K.; Saito, T.; Okamura, T.; Takenaka, H.; Akimoto, Y.; Nakamichi, Y.; Takanashi-Yanobu, R.; Nishiwaki, C.; Kawakami, H.; Kato, N.; Hisanaga, S.; Kakei, M.; Nagamatsu, S. Deletion of CDKAL1 Affects Mitochondrial ATP Generation and First-Phase Insulin Exocytosis, *PLoS One* **2010**, *5*.
- (26) Landgraf, B. J.; McCarthy, E. L.; Booker, S. J.; Kornberg, R. D. Radical *S*-Adenosylmethionine Enzymes in Human Health and Disease, *Annu. Rev. Biochem.* **2016**, *85*, 485.
- (27) Jessberger, S.; Gage, F. H.; Eisch, A. J.; Lagace, D. C. Making a neuron: Cdk5 in embryonic and adult neurogenesis, *Trends Neurosci.* **2009**, *32*, 575.
- (28) Liebl, J.; Fürst, R.; Vollmar, A. M.; Zahler, S. Twice switched at birth: Cell cycle-independent roles of the "neuron-specific" cyclin-dependent kinase 5 (Cdk5) in non-neuronal cells, *Cellular Signalling* **2011**, *23*, 1698.

- (29) Reiter, V.; Matschkal, D. M. S.; Wagner, M.; Globisch, D.; Kneuttinger, A. C.; Müller, M.; Carell, T. The CDK5 repressor CDK5RAP1 is a methylthiotransferase acting on nuclear and mitochondrial RNA, *Nucl. Acids Res.* **2012**, *40*, 6235.
- (30) Wei, F.; Zhou, B.; Suzuki, T.; Miyata, K.; Ujihara, Y.; Horiguchi, H.; Takahashi, N.; Xie, P.; Michiue, H.; Fujimura, A.; Kaitsuka, T.; Matsui, H.; Koga, Y.; Mohri, S.; Oike, Y.; Tomizawa, K. Cdk5rap1-Mediated 2-Methylthio Modification of Mitochondrial tRNAs Governs Protein Translation and Contributes to Myopathy in Mice and Humans, *Cell Metabolism* **2015**, *21*, 428.
- (31) Anton, B. P.; Saleh, L.; Benner, J. S.; Raleigh, E. A.; Kasif, S.; Roberts, R. J. RimO, a MiaB-like enzyme, methylthiolates the universally conserved Asp88 residue of ribosomal protein S12 in *Escherichia coli*, *Proc. Natl. Acad. Sci. USA* **2008**, *105*, 1826.
- (32) Lee, K. H.; Saleh, L.; Anton, B. P.; Madinger, C. L.; Benner, J. S.; Iwig, D. F.; Roberts, R. J.; Krebs, C.; Booker, S. J. Characterization of RimO, a New Member of the Methylthiotransferase Subclass of the Radical SAM Superfamily, *Biochemistry* **2009**, *48*, 10162.
- (33) Landgraf, B. J.; Booker, S. J. Stereochemical Course of the Reaction Catalyzed by RimO, a Radical SAM Methylthiotransferase, *J. Am. Chem. Soc.* **2016**, *138*, 2889.
- (34) Sanyal, I.; Cohen, G.; Flint, D. H. Biotin synthase purification, characterization as a [2Fe-2S] cluster protein, and *in vitro* activity of the *Escherichia coli bioB* gene product, *Biochemistry* **1994**, *33*, 3625.
- (35) Miller, J. R.; Busby, R. W.; Jordan, S. W.; Cheek, J.; Henshaw, T. F.; Ashley, G. W.; Broderick, J. B.; Cronan, J. E.; Marletta, M. A. *Escherichia coli* LipA is a lipoyl synthase: *In vitro* biosynthesis of lipoylated pyruvate dehydrogenase complex from octanoyl-acyl carrier protein, *Biochemistry* **2000**, *39*, 15166.
- (36) Ugulava, N. B.; Surerus, K. K.; Jarrett, J. T. Evidence from Mössbauer spectroscopy for distinct 2Fe-2S (2+) and 4Fe-4S (2+) cluster binding sites in biotin synthase from *Escherichia coli*, *J. Am. Chem. Soc.* **2002**, *124*, 9050.
- (37) Mader Cosper, M.; Jameson, G. N. L.; Hernández, H. L.; Krebs, C.; Huynh, B. H.; Johnson, M. K. Characterization of the Cofactor Composition of *Escherichia coli* Biotin Synthase, *Biochemistry* **2004**, *43*, 2007.

- (38) Cicchillo, R. M.; Lee, K. H.; Baleanu-Gogonea, C.; Nesbitt, N. M.; Krebs, C.; Booker, S. J. *Escherichia coli* lipoyl synthase binds two distinct [4Fe-4S] clusters per polypeptide, *Biochemistry* **2004**, *43*, 11770.
- (39) Hernández, H. L.; Pierrel, F.; Elleingand, E.; García-Serres, R.; Huynh, B. H.; Johnson, M. K.; Fontecave, M.; Atta, M. MiaB, a bifunctional radical-S-adenosylmethionine enzyme involved in the thiolation and methylation of tRNA, contains two essential [4Fe-4S] clusters, *Biochemistry* **2007**, *46*, 5140.
- (40) Ugulava, N. B.; Sacanell, C. J.; Jarrett, J. T. Spectroscopic changes during a single turnover of biotin synthase: Destruction of a 2Fe-2S cluster accompanies sulfur insertion, *Biochemistry* **2001**, *40*, 8352.
- (41) Jameson, G. N. L.; Mader Cosper, M.; Hernández, H. L.; Johnson, M. K.; Huynh, B. H. Role of the [2Fe-2S] Cluster in Recombinant *Escherichia coli* Biotin Synthase, *Biochemistry* **2004**, *43*, 2022.
- (42) Lanz, N. D.; Pandelia, M.-E.; Kakar, E. S.; Lee, K. H.; Krebs, C.; Booker, S. J. Evidence for a Catalytically and Kinetically Competent Enzyme-Substrate Cross-Linked Intermediate in Catalysis by Lipoyl Synthase, *Biochemistry* **2014**, *53*, 4557.
- (43) Tao, L. Z.; Stich, T. A.; Fugate, C. J.; Jarrett, J. T.; Britt, R. D. EPR-Derived Structure of a Paramagnetic Intermediate Generated by Biotin Synthase BioB, *J. Am. Chem. Soc.* **2018**, *140*, 12947.
- (44) McCarthy, E. L.; Booker, S. J. Destruction and reformation of an iron-sulfur cluster during catalysis by lipoyl synthase, *Science* **2017**, *358*, 373.
- (45) Landgraf, B. J.; Arcinas, A. J.; Lee, K. H.; Booker, S. J. Identification of an Intermediate Methyl Carrier in the Radical *S*-Adenosylmethionine Methylthiotransferases RimO and MiaB, *J. Am. Chem. Soc.* **2013**, *135*, 15404.
- (46) Maiocco, S. J.; Arcinas, A. J.; Landgraf, B. J.; Lee, K. H.; Booker, S. J.; Elliott, S. J. Transformations of the FeS Clusters of the Methylthiotransferases MiaB and RimO, Detected by Direct Electrochemistry, *Biochemistry* **2016**, *55*, 5531.
- (47) Mulliez, E.; Duarte, V.; Arragain, S.; Fontecave, M.; Atta, M. On the Role of Additional 4Fe-4S Clusters with a Free Coordination Site in Radical-SAM Enzymes, *Front. Chem.* **2017**, *5*.
- (48) Forouhar, F.; Arragain, S.; Atta, M.; Gambarelli, S.; Mouesca, J. M.; Hussain, M.; Xiao, R.; Kieffer-Jaquinod, S.; Seetharaman, J.; Acton, T. B.; Montelione, G. T.; Mulliez, E.; Hunt, J.

- F.; Fontecave, M. Two Fe-S clusters catalyze sulfur insertion by radical-SAM methylthiotransferases, *Nature Chem. Bio.* **2013**, *9*, 333.
- (49) Molle, T.; Clémancey, M.; Latour, J. M.; Kathirvelu, V.; Sicoli, G.; Forouhar, F.; Mulliez, E.; Gambarelli, S.; Atta, M. Unanticipated coordination of tris buffer to the Radical SAM cluster of the RimO methylthiotransferase, *J. Biol. Inorg. Chem.* **2016**, *21*, 549.
- (50) McLaughlin, M. I.; Lanz, N. D.; Goldman, P. J.; Lee, K. H.; Booker, S. J.; Drennan, C. L. Crystallographic snapshots of sulfur insertion by lipoyl synthase, *Proc. Natl. Acad. Sci. USA* **2016**, *113*, 9446.
- (51) Krebs, C.; Henshaw, T. F.; Cheek, J.; Huynh, B. H.; Broderick, J. B. Conversion of 3Fe-4S to 4Fe-4S clusters in native pyruvate formate-lyase activating enzyme: Mössbauer characterization and implications for mechanism, *J. Am. Chem. Soc.* **2000**, *122*, 12497.
- (52) Lanz, N. D.; Grove, T. L.; Gogonea, C. B.; Lee, K. H.; Krebs, C.; Booker, S. J.; Hopwood, D. A. RImN and AtsB as Models for the Overproduction and Characterization Radical SAM Proteins, *Natural Product Biosynthesis By Microorganisms and Plants, Pt B* **2012**, *516*, 125.
- (53) Münck, E. In *Physical Methods in Bioinorganic Chemistry*; Que, L., Jr., Ed.; University Science Books: Sausalito, CA, 2000, p 287.
- (54) Papaefthymiou, V.; Girerd, J. J.; Moura, I.; Moura, J. J. G.; Münck, E. Mössbauer study of *D. gigas* ferredoxin-II and spin-coupling model for the Fe₃S₄ cluster with valence delocalization, *J. Am. Chem. Soc.* **1987**, *109*, 4703.
- (55) Hu, Z. G.; Jollie, D.; Burgess, B. K.; Stephens, P. J.; Münck, E. Mössbauer and EPR studies of *Azotobacter vinelandii* ferredoxin-I, *Biochemistry* **1994**, *33*, 14475.
- (56) Gorun, S. M.; Lippard, S. J. Magnetostructural correlations in magnetically coupled (μ-oxo)diiron(III) complexes, *Inorg. Chem.* **1991**, *30*, 1625.
- (57) Baldwin, M. J.; Stemmler, T. L.; Riggs Gelasco, P. J.; Kirk, M. L.; Penner Hahn, J. E.; Pecoraro, V. L. Structural and magnetic effects of successive protonations of oxo bridges in high-valent manganese dimers, *J. Am. Chem. Soc.* **1994**, *116*, 11349.
- (58) Pantazis, D. A.; Krewald, V.; Orio, M.; Neese, F. Theoretical magnetochemistry of dinuclear manganese complexes: broken symmetry density functional theory investigation on the influence of bridging motifs on structure and magnetism, *Dalton Trans.* **2010**, *39*, 4959.

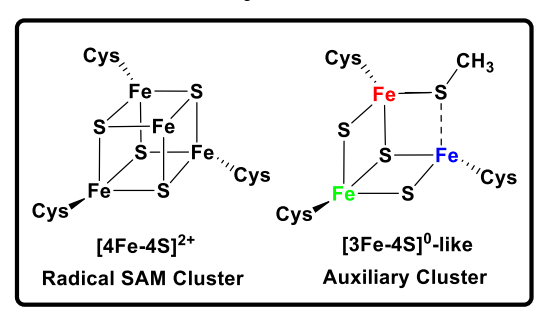
- (59) Kambe, K. On the paramagnetic susceptibilities of some polynuclear complex salts, *J. Phys. Soc. Japan* **1950**, *5*, 48.
- (60) Bencini, A.; Gatteschi, D. *EPR of Exchange Coupled Systems*; Springer-Verlag: Berlin, 1990.
- (61) Mouesca, J. M.; Noodleman, L.; Case, D. A.; Lamotte, B. Spin-densities and spin coupling in iron-sulfur clusters a new analysis of hyperfine coupling constants, *Inorg. Chem.* **1995**, *34*, 4347.
- (62) Pandelia, M.-E.; Lanz, N. D.; Booker, S. J.; Krebs, C. Mössbauer spectroscopy of Fe/S proteins, *Biochim. Biophys. Acta Molecular Cell Research* **2015**, *1853*, 1395.
- (63) Blondin, G.; Girerd, J. J. Interplay of electron exchange and electron transfer in metal polynuclear complexes in proteins or chemical models, *Chem. Rev.* **1990**, *90*, 1359.
- (64) Dutta, S. K.; Ensling, J.; Werner, R.; Flörke, U.; Haase, W.; Gütlich, P.; Nag, K. Valence-delocalized and valence-trapped Fe(II)Fe(III) complexes: Drastic influence of the ligands, *Angew. Chem.-Int. Ed.* **1997**, *36*, 152.
- (65) Borshch, S. A.; Bominaar, E. L.; Blondin, G.; Girerd, J. J. Double exchange and vibronic coupling in mixed-valent systems origin of the broken-symmetry ground state of Fe₃S₄⁰ cores in proteins and models, *J. Am. Chem. Soc.* **1993**, *115*, 5155.
- (66) Gamelin, D. R.; Bominaar, E. L.; Kirk, M. L.; Wieghardt, K.; Solomon, E. I. Excited-state contributions to ground-state properties of mixed-valence dimers: Spectral and electronic-structural studies of [Fe₂(OH)₃(tmtacn)₂]²⁺ related to the Fe₂S₂⁺ active sites of plant-type ferredoxins, *J. Am. Chem. Soc.* **1996**, *118*, 8085.
- (67) Glaser, T.; Rose, K.; Shadle, S. E.; Hedman, B.; Hodgson, K. O.; Solomon, E. I. S Kedge X-ray absorption studies of tetranuclear iron-sulfur clusters: μ-sulfide bonding and its contribution to electron delocalization, *J. Am. Chem. Soc.* **2001**, *123*, 442.
- (68) Dey, A.; Glaser, T.; Moura, J. J. G.; Holm, R. H.; Hedman, B.; Hodgson, K. O.; Solomon, E. I. Ligand K-edge X-ray absorption spectroscopy and DFT calculations on [Fe3S4]^{0,+} clusters: Delocalization, redox, and effect of the protein environment, *J. Am. Chem. Soc.* **2004**, *126*, 16868.
- (69) Johnson, M. K.; Smith, A. D. *Iron-sulfur proteins*; Second Edition ed.; John Wiley & Sons, 2005.

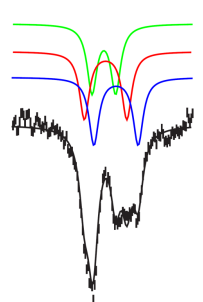
- (70) Butt, J. N.; Armstrong, F. A.; Breton, J.; George, S. J.; Thomson, A. J.; Hatchikian, E. C. Investigation of metalion uptake reactivities of [3Fe-4S] clusters in proteins voltammerty of coadsorbed ferredoxin aminocyclitol films at graphite electrodes and spectroscopic identification of transformed clusters, *J. Am. Chem. Soc.* **1991**, *113*, 6663.
- (71) Duff, J. L. C.; Breton, J. L. J.; Butt, J. N.; Armstrong, F. A.; Thomson, A. J. Novel redox chemistry of [3Fe-4S] clusters: Electrochemical characterization of the all-Fe(II) form of the [3Fe-4S] cluster generated reversibly in various proteins and its spectroscopic investigation in *Sulfolobus acidocaldarius* ferredoxin, *J. Am. Chem. Soc.* **1996**, *118*, 8593.
- (72) Molle, T.; Moreau, Y.; Clémancey, M.; Forouhar, F.; Ravanat, J. L.; Duraffourg, N.; Fourmond, V.; Latour, J. M.; Gambarelli, S.; Mulliez, E.; Atta, M. Redox Behavior of the *S*-Adenosylmethionine (SAM)-Binding Fe-S Cluster in Methylthiotransferase RimO, toward Understanding Dual SAM Activity, *Biochemistry* **2016**, *55*, 5798.
- (73) Tamanaha, E.; Zhang, B.; Guo, Y. S.; Chang, W.-c.; Barr, E. W.; Xing, G.; St Clair, J.; Ye, S. F.; Neese, F.; Bollinger, J. M., Jr.; Krebs, C. Spectroscopic Evidence for the Two C-H-Cleaving Intermediates of *Aspergillus nidulans* Isopenicillin *N* Synthase, *J. Am. Chem. Soc.* **2016**, *138*, 8862.
- (74) McMillen, D. F.; Golden, D. M. Hydrocarbon bond-dissociation energies, *Annu. Rev. Phys. Chem.* **1982**, *33*, 493.
- (75) Arcinas, A. J. Mechanistic Studies of the Radical S-Adenosylmethinine tRNA Methylthiotransferase MiaB, *Ph.D. Thesis, The Pennsylvania State University* **2016**.
- (76) Pierrel, F.; Douki, T.; Fontecave, M.; Atta, M. MiaB protein is a bifunctional radical-S-adenosylmethionine enzyme involved in thiolation and methylation of tRNA, *J. Biol. Chem.* **2004**, *279*, 47555.
- (77) Ote, T.; Hashimoto, M.; Ikeuchi, Y.; Su'etsugu, M.; Suzuki, T.; Katayama, T.; Kato, J. I. Involvement of the *Escherichia coli* folate-binding protein YgfZ in RNA modification and regulation of chromosomal replication initiation *Molecular Microbiology* **2006**, *60*, 252.
- (78) Waller, J.; Alvarez, S.; Naponelli, V.; Lara-Nuñez, A.; Blaby, I.; Da Silva, V.; Ziemak, M.; Vickers, T.; Beverley, S.; Edison, A.; Rocca, J.; Gregory, J.; de Crécy-Lagard, V.; Hanson, A. A role for tetrahydrofolates in the metabolism of iron-sulfur clusters in all domains of life, *Proc. Natl. Acad. Sci. USA* **2010**, *107*, 10412.

- (79) Gelling, C.; Dawes, I. W.; Richhardt, N.; Lill, R.; Mühlenhoff, U. Mitochondrial Iba57p is required for Fe/S cluster formation on aconitase and activation of radical SAM enzymes, *Molecular and Cellular Biology* **2008**, *28*, 1851.
- (80) Boutigny, S.; Saini, A.; Baidoo, E. E. K.; Yeung, N.; Keasling, J. D.; Butland, G. Physical and Functional Interactions of a Monothiol Glutaredoxin and an Iron Sulfur Cluster Carrier Protein with the Sulfur-donating Radical S-Adenosyl-L-methionine Enzyme MiaB, J. Biol. Chem. 2013, 288, 14200.

Table of Contents Figure

MiaB methylated intermediate





Supporting Information

The First Step in Catalysis of the Radical S-Adenosylmethionine Methylthiotransferase MiaB Yields an Intermediate with a [3Fe-4S]⁰-like Auxiliary Cluster

Bo Zhang,^{1,†} Arthur J. Arcinas,^{2,§} Matthew I. Radle,¹ Alexey Silakov,¹ Squire J. Booker,^{1,2,3,*} and Carsten Krebs^{1,2,*}

¹Department of Chemistry, ²Department of Biochemistry and Molecular Biology, and ³Howard Hughes Medical Institute, The Pennsylvania State University, University Park, Pennsylvania 16802, United States

Table of Contents

Materials and Methods	S3
Mössbauer-spectroscopic characterization of wt MiaB, $^{\Delta Aux}$ MiaB, and $^{\Delta RS}$ MiaB	S9
Evaluation of alternative spin states as ground state of the [3Fe-4S] ⁰ -like cluster	S11
Figures S1-S15	S14
References	S34

Materials and Methods

Materials

DNA-modifying enzymes and reagents were obtained from New England Biolabs (Ipswich, MA). FastAP alkaline phosphatase was obtained from ThermoScientific. P1 nuclease was obtained from US Biologicals (Salem, MA). Sodium methanethiolate and phosphodiesterase from *Crotalus adamanteus* were obtained from Sigma (St. Louis, MO). Egg white lysozyme and deoxyribonuclease were purchased from Alfa Aesar (Ward Hill, MA). Expression plasmids pET28a and pET26b were obtained from EMD Millipore, and DH5α and BL21(DE3) strains were obtained from Invitrogen (Carlsbad, CA). *Escherichia coli miaA*, used to generate the i⁶A tRNA substrate, was PCR amplified, expressed and purified as previously described.¹

Cloning and overexpressing of Bt MiaB and variants

The *Bacteroides thetaiotaomicron* (*Bt*) *miaB* gene (NCBI accession NP_812107.1) was amplified from a pSGC-His construct (obtained from Steve Almo (Albert Einstein University) of the Enzyme Function Initiative using the polymerase chain reaction (PCR). It was cloned into a pET28a expression vector, which was used to co-transform *Ec* BL21(DE3) along with pDB1282 for over production, as previously described.^{2,3} Plasmid pDB1282 encodes *Azotobacter vinelandii* proteins involved in Fe/S cluster assembly and trafficking, and enhances the over production of Fe/S proteins in a soluble form.

Site-directed mutagenesis was conducted using the QuikChange II system (Agilent, Santa Clara, CA) in conjunction with the *Bt* MiaB–pET28a construct as template and the mutagenesis primers described below. The *Bt* MiaB Cys to Ala variant to the RS cluster cysteinyl ligands (C170A, C174A, C177A) for the ΔRSMiaB variant was generated using the forward (5'- CC ATC ATG CGC GGA GCC AAT AAC TTC GCC ACC TAC GCT ATC GTG CCT TAT ACA CG-3') and reverse (5'- CG TGT ATA AGG CAC GAT AGC GTA GGT GGC GAA GTT ATT GGC TCC GCG CAT GAT GG -3') mutagenesis primers. The *Bt* MiaB Cys to Ala variants of the auxiliary cluster cysteinyl ligands (C26A, C62A, C96A) for the ΔAuxMiaB variant was generated sequentially. The C26A variant was generated using the forward (5'- C GAG ACT TAT GGC GCC CAG ATG AAC GTG G -3') and reverse (5'- C CAC GTT CAT CTG GGC GCC ATA AGT CTC G -3') primers. The C62A variant was generated using the forward (5'- GCA GTG TTT ATG AAT ACC GCC TCT ATC CGT GAC AAT GC -3') and reverse (5'- GC

ATT GTC ACG GAT AGA GGC GGT ATT CAT AAA CAC TGC -3') primers. The C96A variant was generated using the forward (5'- C GTA CTG GGC GCT ATG GCG GAA CG -3') and reverse (5'- CG TTC CGC CAT AGC GCC CAG TAC G -3') primers. After PCR mutagenesis, the resulting constructs were digested with DpnI for 3 h at 37 °C prior to transformation into DH5 using standard molecular biological techniques and subsequent nucleic acid sequence. The constructs bearing the correct sequence were co-transformed with the plasmid pDB1282 into the BL21(DE3) expression strain for overproduction.

Expression and Purification of Bt MiaB

The overproduction of Bt MiaB and variants was conducted in 16 L of M9 minimal media supplemented with 25 µM ⁵⁷FeCl₃ upon inoculation and shaken at 180 rpm at 37 °C. At an OD600 of 0.3, L-(+)-arabinose was added to a concentration of 0.2% (w/v) with 300µM Lcysteine and 50 µM ⁵⁷FeCl₃. At an OD600 of 0.6, the flasks were cooled prior to addition of 200 μM IPTG and incubation at 18 °C for 16 h. Afterwards, cell paste was collected by centrifugation at 6,000 × g for 15 min at 4 °C. Purification of Bt MiaB was conducted within an anaerobic chamber (Coy, Grass Lakes, MI) maintained in N2 and H2 (95%/5%) with less than 1 ppm O₂ using a palladium catalyst. Frozen cell paste was thawed in lysis buffer (50 mM HEPES pH 7.5, 300 mM KCl, 10 mM imidazole, 10 mM β-mercaptoethanol, 10 mM MgCl₂, 1 mg/ml lysozyme, 0.5 mg/ml DNase, 0.5 mg/ml PMSF). The cells were disrupted by sonication and the crude lysate was clarified by centrifugation at $40,000 \times g$ for 1.5 h at 4 °C. The clarified lysate was loaded onto Ni-NTA resin, washed with 150 mL of wash buffer (lysis buffer with 20 mM imidazole and without lysozyme, DNase and PMSF), then eluted with elution buffer (wash buffer with 250 mM imidazole). During elution, the dark brown fractions containing protein were pooled and buffer exchanged into gel filtration buffer (50 mM HEPES pH 7.5, 300 mM KCl, 1 mM DTT, 10 mM MgCl₂, 30 % (v/v) glycerol). The as-isolated Bt MiaB was subjected to FPLC size exclusion chromatography using a sephadex S200 16/60. Chemical reconstitution of the Bt MiaB Fe-S clusters was conducted as previously described for MiaB from Thermotoga maritima.1

Preparation of MiaB tRNA substrate

The full-length i⁶A tRNA Phe substrate was generated using in vitro run-off transcription with T7

RNA polymerase using a DNA template containing a T7 promoter region followed by the nucleic acid sequence corresponding to Tm tRNAPhe. To generate the template, a forward (5' -AAT TCC TGC AGT AAT ACG ACT CAC TAT AGG CCA GGT AGC TCA GTT GGT AGA GCA CTG G – 3') and reverse (5' – TmGG CCA GGG GCG GAA TCG AAC CGC CGA CAC CTG GAT TTT CAG TCC AGT GCT CTA CC - 3') primer containing a T7 promoter, a complementary sequence (underlined) and 2'-O-methyldeoxyguanosine (mG) were used in multiple PCR samples (10 × 100 μL) for primer overlap extension. The resulting product was purified by agarose gel electrophoresis, ethanol precipitated, and resuspended in water. The template was used at a final concentration of 2 µg/µL within in vitro transcription reactions containing 40 mM Tris-HCl pH 8, 10 mM DTT, 25 mM MgCl₂, 4 mM each of NTPs, and 10 % (v/v) of 51 μM T7 RNA polymerase. Transcription reactions were incubated at 37 °C for 3 h, centrifuged at 8,000 × g for 10 min, and the supernatant retained. Afterwards, 50 mM EDTA pH 8 was added, and the solution was concentrated to approximately 2.5 mL using an Amicon Ultra centrifugal filter with a 3 kDa NMWL cutoff. The RNA was extracted twice with (25:24:1) phenol:chloroform:isoamyl alcohol and the RNA was ethanol precipitated from the aqueous fraction overnight. The reaction was centrifuged, and the pellet was resuspended in sterile RNAse-free H₂O. The installation of the isopentenyl group at N6 of adenosine 37 in the tRNA was performed using E. coli MiaA according to previously published procedures¹.

Preparation of MiaB samples for Mössbauer, EPR and LC/MS analysis

Bt MiaB samples prepared for coupled Mössbauer, EPR and LC/MS analysis contained 165 μM (RC) WT Bt MiaB in buffer system (50 mM HEPES pH 7.5, 300 mM KCl and 10 mM MgCl₂) in a total volume of 505 μL, of which 150 μL was prepared for EPR analysis of non-reduced protein (**Figure S1A**), 150 μL was reduced with 2 mM dithionite for EPR analysis of reduced protein (**Figure S1B**), and 200 μL was prepared for Mössbauer analysis of non-reduced protein. Methylated Bt MiaB samples contained 165 μM WT enzyme and 330 μM i⁶A tRNA^{Phe} in buffer system as described above and initiated by addition of 600 μM SAM at 30 °C in a total volume of 455 μL. Of the total volume, 100 μL was utilized for LC/MS analysis during the course of the methylation reaction, during which 10 μL aliquots of the sample mixture was quenched in 0.2 M H₂SO₄, and prepared for LC/MS analysis as described above (**Figure 1A**). After 20 min of the methylation reaction, 150 μL of the reaction mixture was prepared for EPR analysis (**Figure S1C**), and 200 μL was prepared for Mössbauer analysis. Reaction conditions for Bt MiaB under turnover conditions were identical to the methylation conditions described

above and incubated for 20 min at 30 °C prior to reaction initiation with 2 mM dithionite in a total volume of 455 μ L. Of the total volume, 100 μ L was utilized for LC/MS analysis during the course of the reaction, during which 10 μ L aliquots of the methylation reaction was quenched in 0.2M H₂SO₄, and prepared for LC/MS analysis as described above (**Figure 1B**). After 15 min of reaction initiation, 150 μ L of the reaction mixture was prepared for EPR analysis (**Figure S1D**), and 200 μ L was prepared for Mössbauer analysis.

Bt MiaB samples prepared for coupled Mössbauer and LC/MS analysis contained either 200 μM enzyme (for MiaB WT), or 300 μM enzyme (for ΔRS MiaB and, ΔAux MiaB), prepared in the buffer system described above in a total volume of 450 μL. Samples incubated with substrate additionally contained either 200 μM i⁶A tRNA Phe (MiaB WT, ΔRS MiaB) or 320 μM i⁶A tRNA Phe (ΔAux MiaB) in a total volume of 450 μL and incubated for 15 min at 30 °C prior to Mössbauer analysis. Samples prepared under methylation conditions additionally contained either 500 μM SAM (MiaB WT, ΔRS MiaB) or 600 μM SAM (ΔAux MiaB), in a total volume of 550 μL and were incubated for 1 h at 30 °C prior to utilizing 100 μL for LC/MS monitoring and the remainder for Mössbauer analysis. Samples methylated under reducing conditions (MiaB WT) additionally contained 1 mM SAM and 1 mM dithionite in a total volume of 550 μL, and were incubated at 30 °C for 1 h prior to Mössbauer analysis. Assays incubated with methanethiol contained 200 μM of MiaB and 1 mM CH₃SH in a total volume of 550 μL and incubated for 30 min at 30 °C prior Mössbauer analysis.

⁵⁷Fe Mössbauer spectroscopy

The Mössbauer spectra were recorded at 4.2 K on constant acceleration spectrometers equipped with a Janis SVT-400 variable-temperature cryostat (zero and 53 mT) or 8TMOSS-OM-12SVT variable-temperature cryostat (up to 8 T). The external magnetic field was applied parallel to the γ beam. All isomer shifts quoted are relative to the centroid of the spectrum of α -iron metal at room temperature. Simulations were carried out using the WMOSS spectral analysis software from SEECO (www.wmoss.org; Edina, MN). Analyses of the MiaB [3Fe-4S]⁰-like cluster are based on spin-Hamiltonian formalism (Equation 1), in which the first three terms represent the electron Zeeman effect and zero field splitting (ZFS) of the electron-spin ground state, the fourth term represents the interaction between the electric field gradient and the nuclear quadrupole moment, the fifth term describes the magnetic hyperfine interactions of the electronic spin with the ⁵⁷Fe nucleus, and the last term represents the ⁵⁷Fe nuclear Zeeman interaction. The electronic spin S in the equation refer to the total spin of the [3Fe-4S]⁰-like cluster. Simulations were carried out with respect to the total electron spin of the [3Fe-4S]⁰-like cluster and in the slow relaxation limit. All symbols have their usual meanings.

$$\mathbf{H} = \beta \mathbf{S} \cdot \mathbf{g} \cdot \mathbf{B} + D \left(\mathbf{S}_{z}^{2} - \frac{S(S+1)}{3} \right) + E \left(\mathbf{S}_{x}^{2} - \mathbf{S}_{y}^{2} \right)$$

$$+ \sum_{i=1}^{3} \frac{eQV_{zz,i}}{4} \left[\mathbf{I}_{z,i}^{2} - \frac{I_{i}(I_{i}+1)}{3} + \frac{\eta}{3} \left(\mathbf{I}_{x,i}^{2} - \mathbf{I}_{y,i}^{2} \right) \right] + \sum_{i=1}^{3} \mathbf{S} \cdot \mathbf{A}_{i} \cdot \mathbf{I}_{i} - \sum_{i=1}^{3} \mathbf{g}_{n} \beta_{n} \mathbf{B} \cdot \mathbf{I}_{i}$$
(Equation 1)

The number of adjustable parameters for the spin Hamiltonian analysis is large. For each electronic spin ground state, in addition to the two zero-field splitting (ZFS) parameters (D and E/D), there are 14 parameters for each of the three individual Fe site (isomer shift; quadrupole splitting; the asymmetry parameter, η ; three Euler angles that correlate the electric field gradient (EFG) tensors and the frame of the ZFS tensors; three principle components of the magnetic hyperfine $\bf A$ tensor; three Euler angles that rotate the $\bf A$ and EFG tensors into the frame of the ZFS tensor; the line width; and absorption area). In order to simplify the Mössbauer analysis of the MiaB [3Fe-4S]⁰-like cluster to extract the most relevant spectroscopic information, the two sets of Euler angles were fixed to zero, and the line width and absorption area were constrained to be equal for the three sites.

EPR spectroscopy

Continuous wave X-band EPR spectra were obtained using a Bruker Elexsys E-560 spectrometer (Billerica, MA) equipped with a SuperX FT microwave bridge, an ITC503S temperature controller and ESR900 helium cryostat from Oxford Instruments (Concord, MA). Samples were analyzed at 10–15 K with 20 dB microwave power, 10 G modulation amplitude, 9.48 GHz microwave frequency and a receiver gain setting of 1x10⁵. Spin quantification of spectral features were determined by double integration and comparison of the signal area to that of a 200 μM Cu²⁺-EDTA standard solution, utilizing Kazan Viewer (Alexey Silakov, University Park, PA) and MatLab (Mathworks, Natick, MA) software for data analysis.

Mössbauer-spectroscopic characterization of wild-type Bt MiaB, and $^{\Delta Aux}$ MiaB and $^{\Delta RS}$ MiaB variants.

To facilitate the analysis of the Mössbauer spectra of wild-type (wt) Bt MiaB, spectra of variants lacking either auxiliary cluster ($^{\Delta Aux}$ MiaB) or radical SAM cluster ($^{\Delta RS}$ MiaB) were recorded.

The 4.2-K/53-mT spectrum of reconstituted $^{\Delta Aux}$ MiaB sample, which contains only the RS cluster, revealed an asymmetric doublet with a noticeably broader and partially resolved high-energy line (**Figure S2A**). The spectral features are reminiscent of those of the SAM-bound $[4\text{Fe-}4\text{S}]^{2^+}$ clusters, in which coordination of SAM to the non-cysteinyl-ligated Fe leads to increased site differentiation.^{4,5} Since no SAM was added during sample preparation, it is possible that the observed site-differentiation of the radical SAM cluster is caused by coordination of an exogenous molecule to the unique Fe-site.⁶ The spectrum can be adequately simulated as summation of three quadrupole doublets with the following parameters: $\delta = 0.45$ mm/s, $|\Delta E_Q| = 1.07$ mm/s and $\Gamma_{L,R} = 0.40$ mm/s for the valence-delocalized pair (50% of total ⁵⁷Fe absorption), $\delta = 0.67$ mm/s, $|\Delta E_Q| = 1.28$ mm/s, and $\Gamma_{L,R} = 0.31$ mm/s for the Fe²⁺ site of the partially valence-trapped pair (25% of total ⁵⁷Fe absorption), and $\delta = 0.36$ mm/s, $|\Delta E_Q| = 1.04$ mm/s, and $\Gamma_{L,R} = 0.28$ mm/s for the Fe³⁺ site of the partially valence-trapped pair (25% of total ⁵⁷Fe absorption).

The 4.2-K/53-mT spectrum (**Figure S2B**) associated with the Aux cluster from the $^{\Delta RS}$ MiaB sample can be analyzed as a broad, slightly asymmetric quadrupole doublet with parameters characteristic for [4Fe-4S]²⁺ clusters with two valence-delocalized pairs (δ = 0.45 mm/s, | ΔE_Q | = 1.10 mm/s, Γ_L = 0.32 mm/s and Γ_R = 0.35 mm/s (93% of total ⁵⁷Fe absorption). The spectrum also revealed the presence of a weak absorption at ~0.5 mm/s, which indicates a small amount of [2Fe-2S]²⁺ cluster in the sample (δ = 0.30 mm/s, | ΔE_Q | = 0.48 mm/s, and $\Gamma_{L,R}$ = 0.30 mm/s, accounting for 7 % of total ⁵⁷Fe absorption).

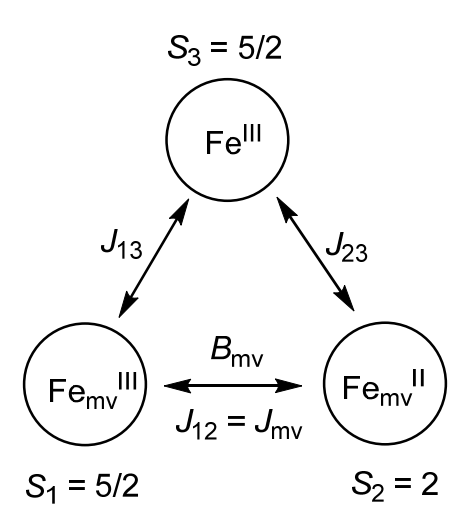
Subsequently, as shown in **Figure S2C**, the 4.2-K/53-mT spectrum of the wt *Bt* MiaB (165 μM enzyme, 7.56 Fe/MiaB) can be simulated as weighted superposition of the partially valence-trapped RS [4Fe-4S]²⁺ cluster (45% of total ⁵⁷Fe), the valence-delocalized Aux [4Fe-4S]²⁺ cluster (43% of total ⁵⁷Fe), and a small amount of [2Fe-2S]²⁺ cluster (12% of total ⁵⁷Fe). On the basis of Fe and protein quantification, the Mössbauer analysis revealed that the samples contain 0.85 RS [4Fe-4S]²⁺ cluster, 0.81 Aux [4Fe-4S]²⁺ cluster, 0.45 [2Fe-2S]²⁺ cluster. Additionally, EPR

characterization of an identical sample revealed the presence of trace amount of cuboidal [3Fe-4S]⁺ cluster (6.7 µM cluster, less than 0.04 cluster per MiaB monomer).

The 4.2-K/zero-field spectrum of wt Bt MiaB reacted with SAM (Figure S3) was analyzed as a superposition of the various components. Importantly, the spectrum reveals a pronounced shoulder at ~+1.6 mm/s, which does not emanate from the [3Fe-4S]⁰-like cluster. This shoulder is distinct from the shoulder at $\sim+1.3$ mm/s in the spectrum of $^{\Delta Aux}$ MiaB (Figure S2A). This shoulder is at a position typical of the high-energy line of the unique Fe site of the RS [4Fe-4S]²⁺ cluster that is coordinated by an exogenous molecule (e.g. SAM, TRIS buffer). We tentatively attribute it to coordination of S-adenosylhomocysteine to the unique Fe site. Because this shoulder accounts for 6-7% of total intensity, there is ~25% of total intensity attributable to this cluster. The various spectral components include those of the [3Fe-4S]⁰-like cluster (red line, simulated using parameters quoted in the main text, 30% total intensity); the high-spin Fe^{II} species (green line, $\delta = 1.32$ mm/s, $\Delta E_Q = 2.82$ mm/s, 12% total intensity); fully valencedelocalized [4Fe-4S]²⁺ cluster (orange line, $\delta = 0.44$ mm/s, $\Delta E_Q = 1.12$ mm/s, 22% total intensity); and site-differentiated [4Fe-4S]²⁺ cluster (blue line, $\delta_I = 0.44$ mm/s, $\Delta E_{QI} = 1.12$ mm/s, 13% total intensity; $\delta_2 = 0.37$ mm/s, $\Delta E_{O2} = 0.81$ mm/s, 6.5% total ⁵⁷Fe absorption; $\delta_3 =$ 0.73 mm/s, $\Delta E_{Q3} = 1.68$ mm/s, 6.5% total intensity); and [2Fe-2S]²⁺ cluster (purple line, $\delta = 0.29$ mm/s, $\Delta E_Q = 0.50$ mm/s, 4% total intensity).

Evaluation of alternative spin states as ground state of the [3Fe-4S]⁰-like cluster.

We start our exploration of possible spin ground states using the model introduced by Papaefthymiou, *et al.*, developed for the [3Fe-4S]⁰ cluster from *Desulfovibrio gigas* ferredoxin.⁷



This spin coupling model invokes in the first step the coupling of the spins of the formally highspin (HS) Fe^{III}, $S_1 = 5/2$, and HS Fe^{II} sites, $S_2 = 2$, comprising the mixed-valent (MV) unit, yielding S_{mv} [= S_{12}], and in the second step coupling of S_{mv} with the spin of the HS Fe^{III} site, $S_3 = 5/2$, to yield the total spin, S_{tot} . Spin states are denoted in the following as $|S_{mv}, S_{tot}\rangle$. This model requires three Heisenberg exchange coupling constants, J_{12} , J_{13} , and J_{23} . The simplest assumption invokes three identical J-values, which is justified by the approximately three-fold symmetry of the cluster. These interactions are described by the first term in equation S1. In addition, the model assumes the double exchange interaction, also known as spin-dependent delocalization, between the two Fe ions of the MV unit, which is parameterized by the second term in equation S1 with the double exchange parameter, B_{mv} . This term lifts the two-fold degeneracy of the spin states, which is due to the fact that in symmetric MV compounds, two isoenergetic resonance structures exist, $viz M_A^{n+} \cdots M_B^{(n+1)+}$ and $M_A^{(n+1)+} \cdots M_B^{n+}$.

$$E(S_{\text{tot}}, S_{\text{mv}}) = 1/2 J [S_{\text{tot}} \cdot (S_{\text{tot}} + 1)] \pm B_{\text{mv}} (S_{\text{mv}} + 1/2)$$
 (S1)

The dependence of the relative energies of the various spin states ($E(S_{tot}, S_{mv})/J$) as a function of B_{mv}/J (equation S2) can be plotted to determine the possible spin ground states (**Figure S15A**, also shown in **Figure 7** from Papaefthymiou, *et al.* ⁷).

$$E(S_{\text{tot}}, S_{\text{mv}})/J = 1/2 \left[S_{\text{tot}} \cdot (S_{\text{tot}} + 1) \right] \pm B_{\text{mv}}/J \left(S_{\text{mv}} + 1/2 \right)$$
 (S2)

The three possible ground states are $|5/2,0\rangle$ for B_{mv}/J between 0 and 1, $|7/2,1\rangle$ for B_{mv}/J between 1 and 2, and $|9/2,2\rangle$ for $B_{mv}/J > 2$. For the $[3\text{Fe-4S}]^0$ clusters, the $|9/2,2\rangle$ state is the ground state because the large value of B_{mv} favors the parallel alignment of the core spins of the MV unit to give $S_{mv} = 9/2$, which is antiferromagnetically (AF) coupled with the Fe^{III} site to give $S_{tot} = 2$.

In the next step we assumed that one *J*-value is different from the other two (equal) *J*-values. The first case we consider invokes that J_{mv} is different from $J_{13} = J_{23}$ [= *J*]. For such a system, the expression of the energies is given by equation S3 as:

$$E(S_{\text{tot}}, S_{\text{mv}}) = 1/2 J_{\text{mv}} [S_{\text{mv}} \cdot (S_{\text{mv}} + 1)] + 1/2 J [S_{\text{tot}} \cdot (S_{\text{tot}} + 1) - S_{\text{mv}} \cdot (S_{\text{mv}} + 1)]$$

$$\pm B_{\text{mv}} (S_{\text{mv}} + 1/2)$$
(S3)

The first two terms describe the contribution from the Heisenberg exchange, while the second term describes the double exchange interaction of the MV pair. Again, the dependence of $E(S_{\text{tot}}, S_{\text{mv}})/J$ as a function of B_{mv}/J (equation S4) can be plotted for for various ratios J_{mv}/J to evaluate the effect of non-identical J-values (**Figure S15B-E** for $J_{\text{mv}}/J = 0.75$, 0.5, 2, and 3, respectively).

$$E(S_{\text{tot}}, S_{\text{mv}})/J = 1/2 J_{\text{mv}}/J \left[S_{\text{mv}} \cdot (S_{\text{mv}} + 1) \right] + 1/2 \left[S_{\text{tot}} \cdot (S_{\text{tot}} + 1) - S_{\text{mv}} \cdot (S_{\text{mv}} + 1) \right]$$

$$\pm B_{\text{mv}}/J \left(S_{\text{mv}} + 1/2 \right)$$
(S4)

We show as **Figure 5** of the main manuscript the areas of the five possible ground states as a function of J_{mv}/J vs B_{mv}/J .

The case $J_{\text{mv}}/J < 1$ (i.e. $J_{\text{mv}} < J$) leads to progressive lowering of the relative energy of the $|9/2,2\rangle$ state. For $J_{\text{mv}}/J = 0.75$, this state is the ground state for $B_{\text{mv}}/J > 0.875$ (**Figure S15B**) and for $J_{\text{mv}}/J = 0.5$, this state is the ground state for any value of B_{mv}/J (**Figure S15C**). The behavior can be understood in terms of the forces that lead to stabilization of either the parallel or antiparallel alignment of the spins of the MV unit. AF coupling within the MV unit favors antiparallel alignment of the spins within the MV unit. By contrast, the AF couplings between the Fe^{III} site

and the two sites of the MV unit, as well as the double exchange interaction within the MV unit both will favor the parallel alignment of the spins within the MV unit. In the limiting case for $B_{\text{mv}}/J = 0$ (this is the y-axis of **Figure S15C**) and $J_{\text{mv}}/J \leq 0.555$ (5/9), the |9/2,2 \rangle state is the ground state, because the stronger AF interactions with the Fe^{III} site force the spins of the MV unit to be parallel.

Conversely, for $J_{\text{mv}}/J > 1$ the trend reverses, because now states with lower S_{mv} are lowered in energy. For $J_{\text{mv}}/J = 2$ (**Figure S15D**) the $|3/2,1\rangle$ state becomes the ground state for $B_{\text{mv}}/J < 1.5$ and for $J_{\text{mv}}/J = 3$ (**Figure S15E**) the $|1/2,2\rangle$ state even becomes the ground state for $B_{\text{mv}}/J < 1$.

The second case we consider invokes that one of the *J*-values between the ferric site and one of the Fe ions of the MV unit is different, while the other two *J*-values are the same, e.g. $J_{23} \neq J_{12} = J_{13}$. This case is more difficult to evaluate, because there is no simple analytical solution for the energies of the various spin states, if the same spin coupling model is used ($\mathbf{S}_1 + \mathbf{S}_2 = \mathbf{S}_{mv}$; $\mathbf{S}_{mv} + \mathbf{S}_3 = \mathbf{S}_{tot}$). Therefore, we treat this case qualitatively. Compared to the case with three identical *J*-values, the increase (decrease) of the J_{23} leads to a stabilization (destabilization) of states with parallel alignment of \mathbf{S}_1 and \mathbf{S}_2 to $\mathbf{S}_{mv} = 9/2$, because of the stronger (weaker) AF coupling between sites 2 and 3. Thus, the effect of changing the ratio J_{23}/J is opposite to that of changing J_{mv}/J (see above).

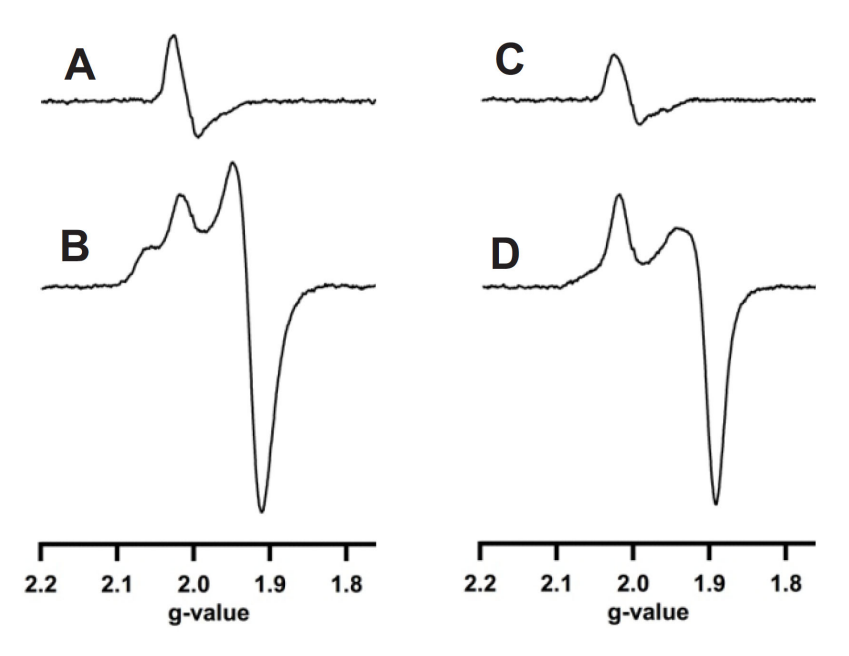


Figure S1. EPR analysis of various samples of reconstituted, wild-type Bt MiaB. Spectra were obtained at 15 K, with 0.2 mW microwave power, 9.623 GHz microwave frequency, 0.1 mT modulation amplitude, and 39 ms conversion time. (**A**) The spectrum obtained from a sample of 165 μM MiaB in the absence of reductant indicates the presence of an EPR active $[3Fe-4S]^{1+}$ cluster in RCN MiaB. (**B**) After reduction with dithionite (400 μM), reduced $[4Fe-4S]^{1+}$ clusters with parameters g = 2.08 and 2.02 were observed in MiaB WT, with the feature at g = 2.08 corresponding to the Aux cluster of the enzyme. (**C**) After incubation of MiaB with two equivalents (330 μM) of i^6 A tRNA and excess SAM (600 μM) for 20 min in the absence of reductant, an EPR signal consistent with a $[3Fe-4S]^{1+}$ cluster was observed. (**D**) Under turnover conditions in the presence of i^6 A tRNA (330 μM), excess SAM (600 μM) and dithionite (2 mM), the Aux cluster feature (g = 2.08) is less visible in comparison to the reduced enzyme alone.

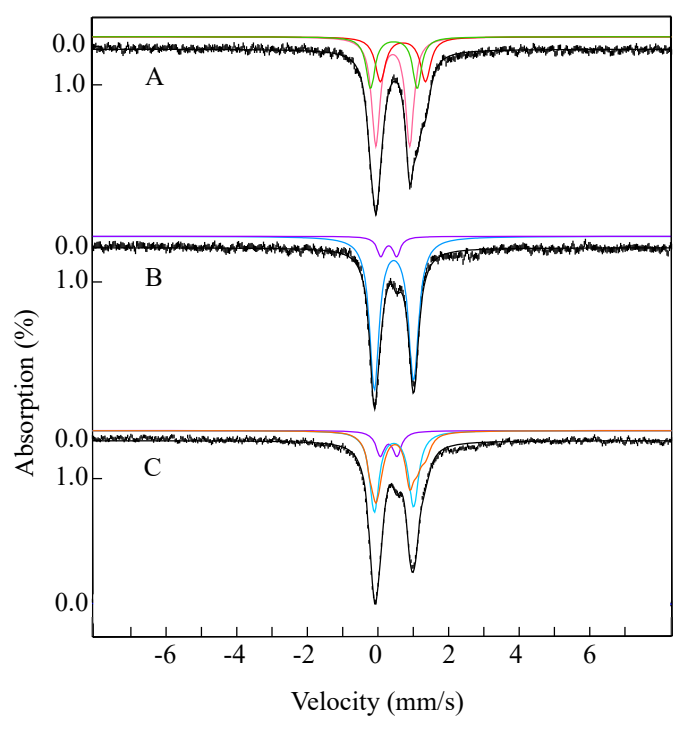


Figure S2. 4.2 K Mössbauer spectra of ^{AAux}MiaB (A), ^{ARS}MiaB (B) and wt Bt MiaB (C&D). Unless otherwise specified, all spectra were recorded in an external magnetic field of 53 mT applied parallel to the γ beam. (A) The spectrum of $^{\Delta Aux}MiaB$ is shown as vertical bars. The spectrum can be simulated with the following parameters: $\delta = 0.45$ mm/s, $\Delta E_Q = 1.07$ mm/s and $\Gamma_{L,R} = 0.40$ mm/s for the valence-delocalized pair (50% of total absorption, magenta line), $\delta =$ 0.67 mm/s, $\Delta E_Q = 1.28$ mm/s, and $\Gamma_{L,R} = 0.31$ mm/s for the Fe^{II} site of the partially valencetrapped pair (25% of total Fe absorption, red line), and $\delta = 0.36$ mm/s, $|\Delta E_Q| = 1.04$ mm/s, and $\Gamma_{L,R} = 0.28$ mm/s for the Fe^{III} site of the partially valence-trapped pair (25% of total absorption, green line). The added contribution is shown as black line. (B) The spectrum of ^ARSMiaB is shown as vertical bars. The light blue and purple lines are quadrupole doublet simulations of the Aux [4Fe-4S]²⁺ cluster (δ = 0.45 mm/s, ΔE_Q = 1.10 mm/s, Γ_L = 0.32 mm/s and Γ_R = 0.35 mm/s, 93% of total absorption) and the [2Fe-2S]²⁺ cluster (δ = 0.30 mm/s, ΔE_Q = 0.48 mm/s, and $\Gamma_{L,R}$ = 0.30 mm/s, 7 % of total absorption), respectively. The added contribution is shown as black line. (C) The spectrum of wt Bt MiaB (vertical bars). The orange, light blue, and purple lines mark the spectral contributions from the RS [4Fe-4S]²⁺ cluster with the above parameters (45% of total intensity) the Aux [4Fe-4S]²⁺ cluster with the above parameters (43% of total intensity), and the [2Fe-2S]²⁺ cluster with the above parameters (12% of total intensity), respectively. The added contribution is shown as black line.

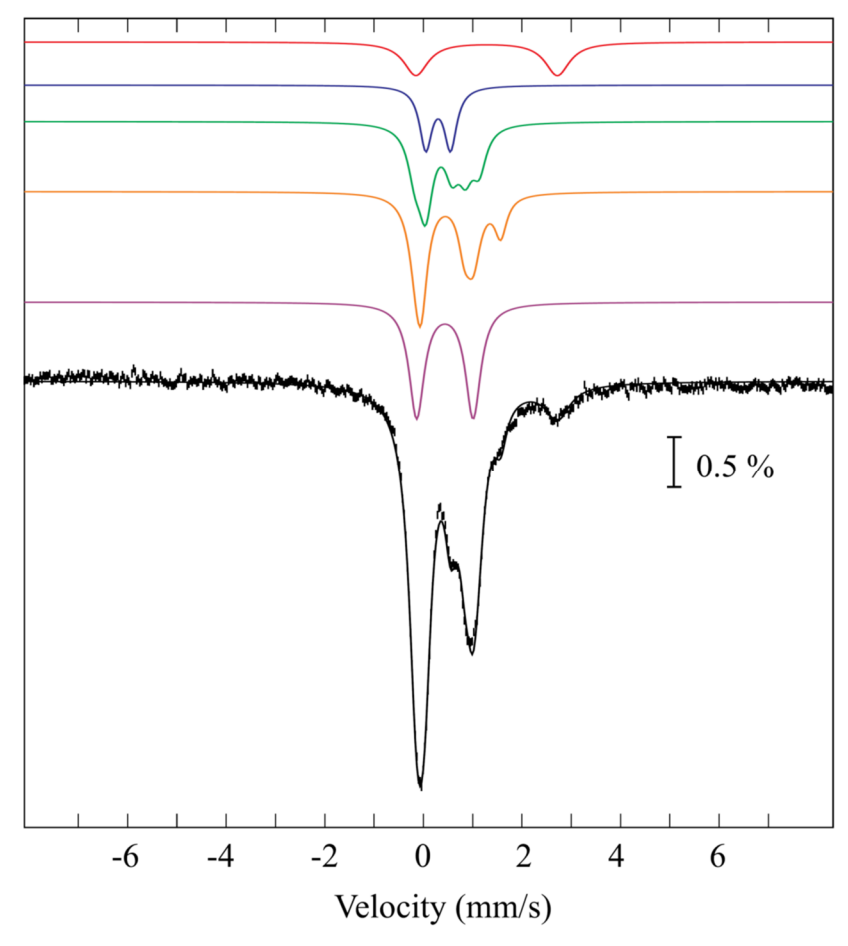


Figure S3. Analysis of the 4.2 K/zero-field Mössbauer spectrum of *Bt* MiaB after incubation with tRNA and SAM for 20 min. The spectrum is the same as the one presented in main text Figure 2B. The experimental data is shown as vertical bars and the simulation is shown as black line. The simulated spectral contributions from individual components are as the following: the high-spin Fe^{II} species (red line, $\delta = 1.28$ mm/s, $\Delta E_Q = 2.87$ mm/s, 12% total intensity); [2Fe-2S]²⁺ cluster (blue line, $\delta = 0.30$ mm/s, $\Delta E_Q = 0.50$ mm/s, 12% total intensity); [3Fe-4S]⁰-like cluster (green line, $\delta = 0.31$ mm/s, $\Delta E_Q = 0.58$ mm/s, $\delta = 0.35$ mm/s, $\Delta E_Q = 1.02$ mm/s, $\delta = 0.61$ mm/s, $\Delta E_Q = 1.04$ mm/s, 9% each of total intensity); site-differentiated [4Fe-4S]²⁺ cluster (orange line, $\delta_I = 0.43$ mm/s, $\Delta E_{QI} = 1.14$ mm/s, 13% total intensity; $\delta_2 = 0.38$ mm/s, $\Delta E_{Q2} = 0.87$ mm/s, 6.5% total ⁵⁷Fe absorption; $\delta_J = 0.77$ mm/s, $\Delta E_{QJ} = 1.61$ mm/s, 6.5% total intensity); and fully valence-delocalized [4Fe-4S]²⁺ cluster (purple line, $\delta = 0.43$ mm/s, $\Delta E_Q = 1.14$ mm/s, 27% total intensity).

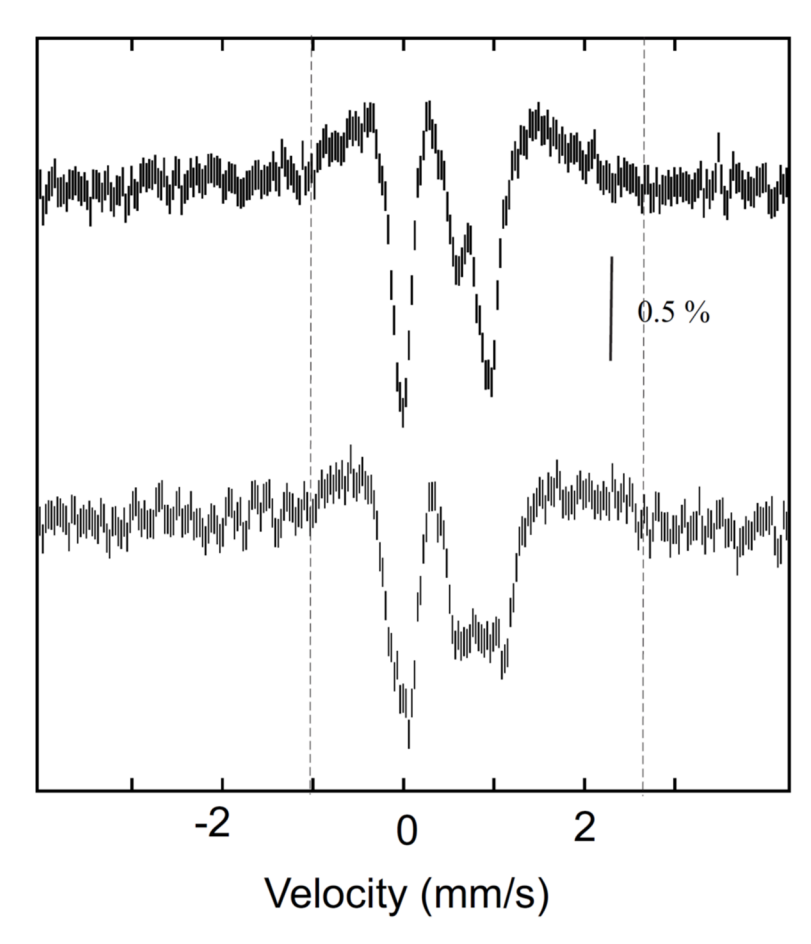
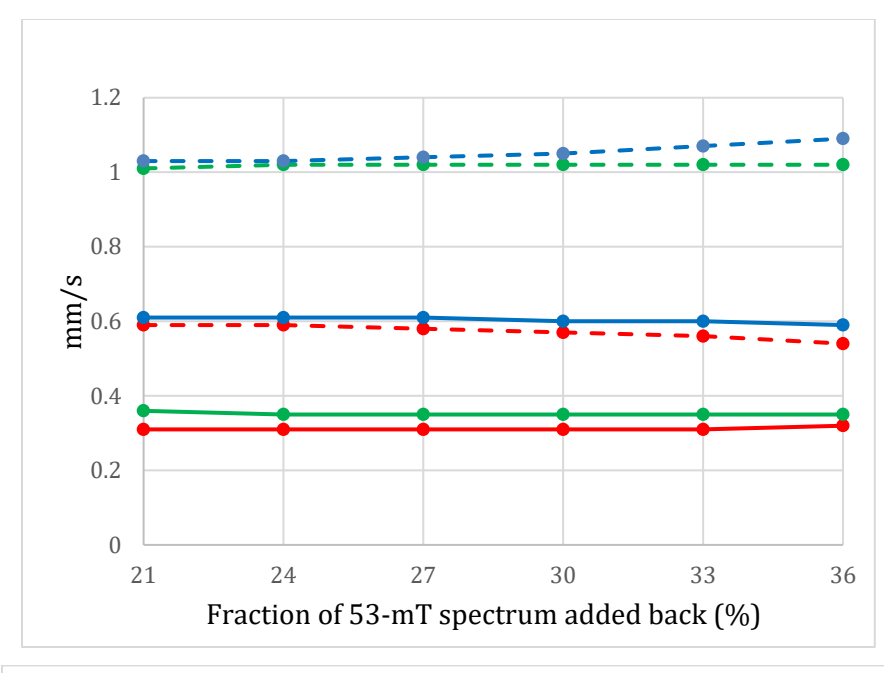


Figure S4. Comparison of [0-53mT] difference spectra of samples containing the [3Fe-4S]⁰-like clusters in *Escherichia coli* lipoyl synthase⁵ (top) and MiaB (bottom). The vertical dashed lines indicate the width of the magnetically split spectrum.



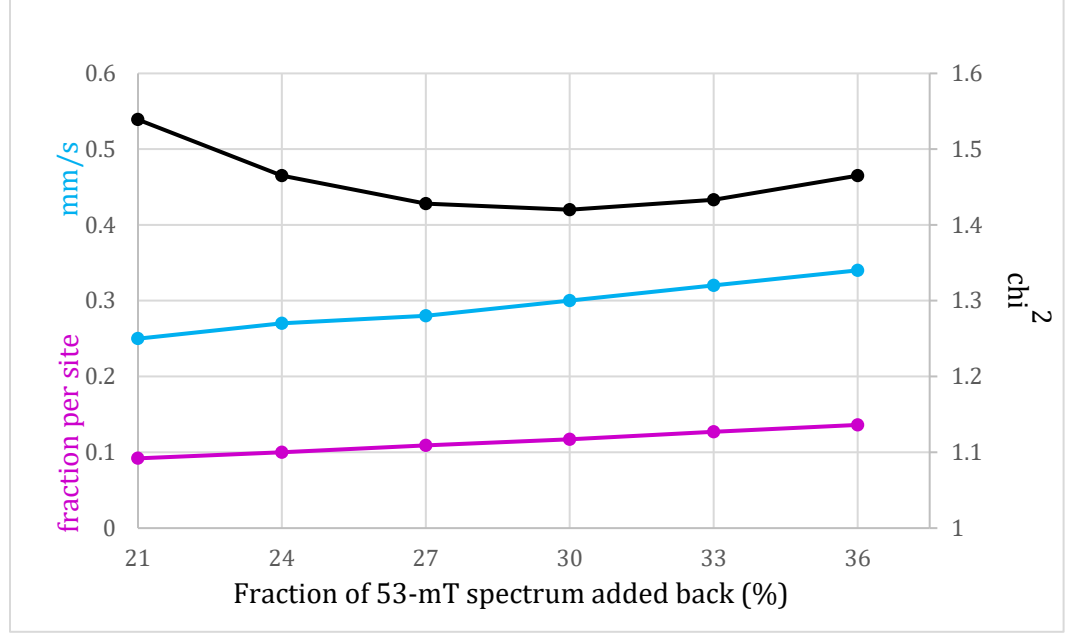


Figure S5. Variation of the Mössbauer parameters obtained from analysis of zero-field reference spectra [δ (top panel, solid lines), ΔE_Q (top panel, dashed lines), line width (bottom panel, cyan line), relative amount (bottom panel, magenta line), and quality of fit, χ^2 (bottom panel, black line) as a function of the relative amount of the simulation of the 53-mT spectrum of the [3Fe-4S]⁰-like cluster added back to the [0-53mT] difference spectrum.

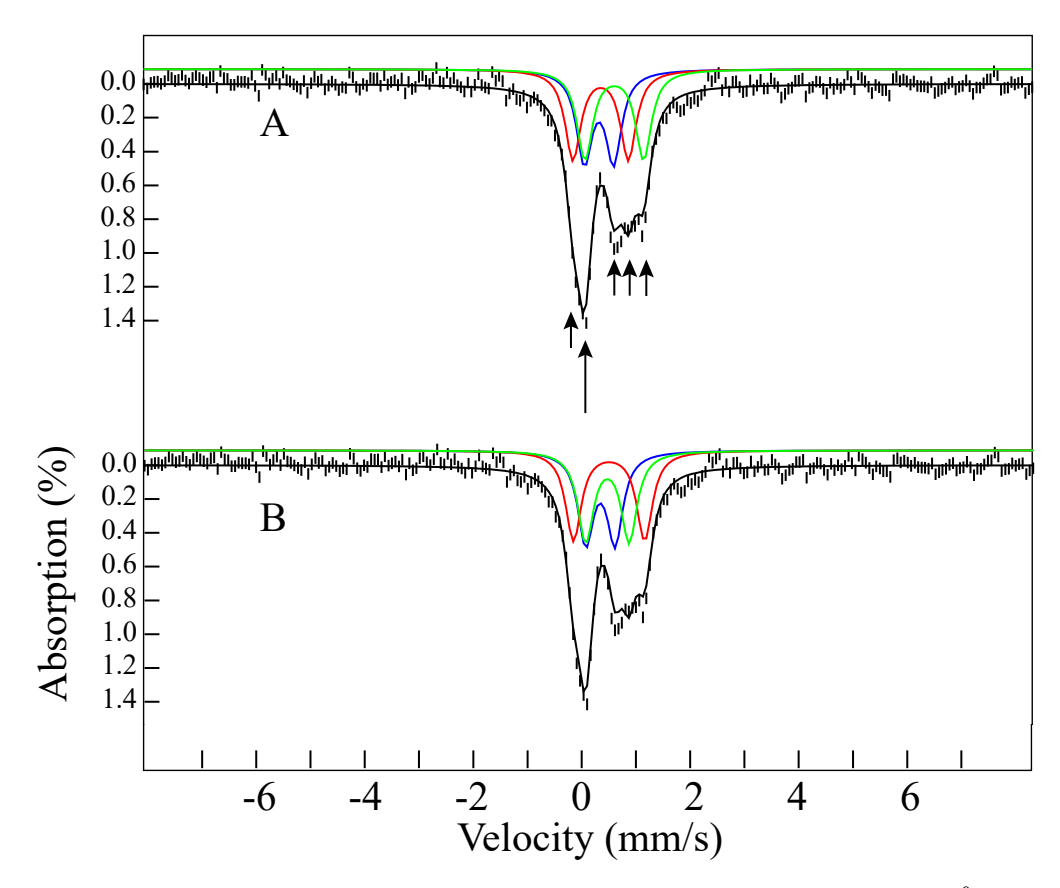


Figure S6. 4.2-K/zero-field Mössbauer reference spectrum of Bt MiaB [3Fe-4S]⁰-like auxiliary cluster (vertical bars). The spectrum was analyzed with the parameters of solution 1 (**A**) and solution 2 (**B**) from Table 1 of the main manuscript. The blue, red, and green lines are quadrupole doublet simulations associated with sites 1, 2, and 3, respectively. The solid black line overlaid with the experimental spectrum represents the added contribution from the three components.

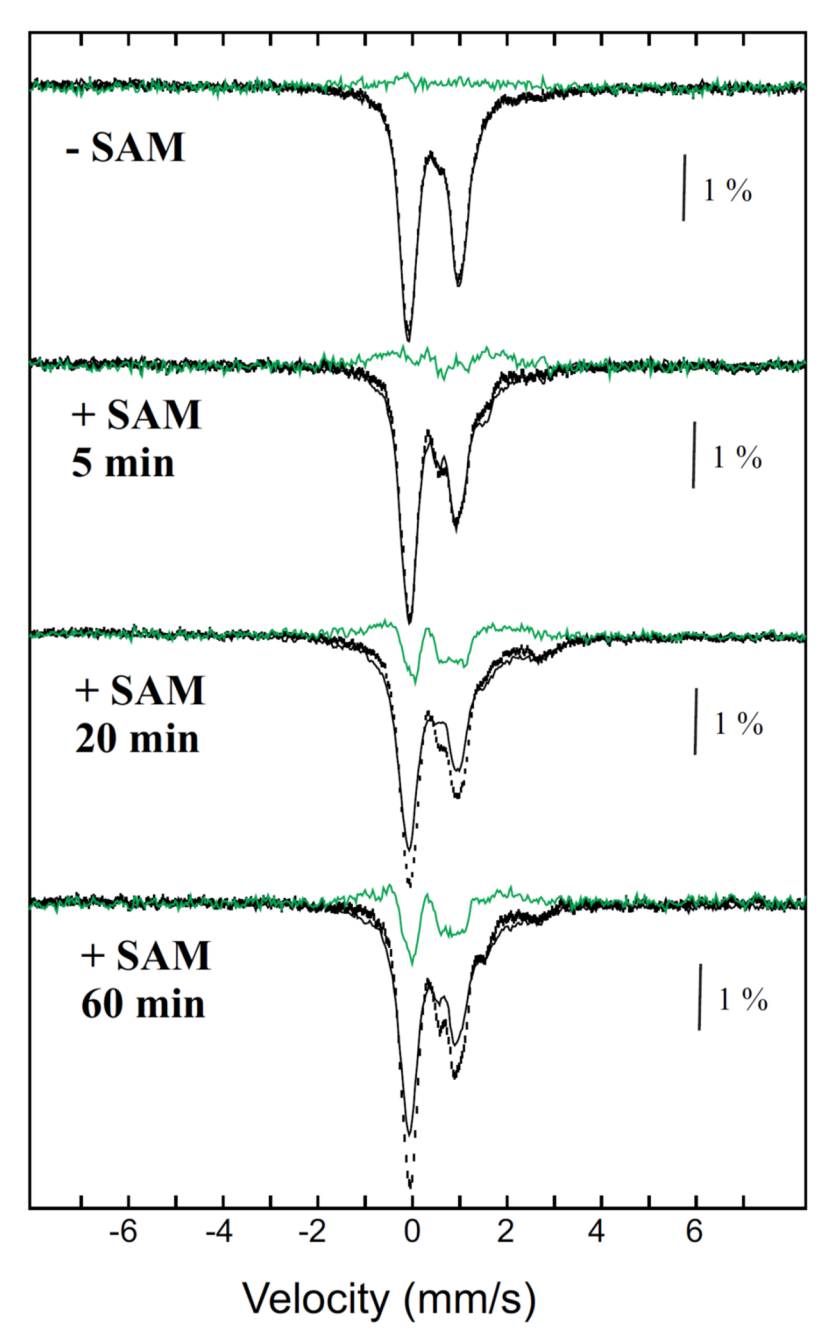


Figure S7. 4.2-K Mössbauer spectra collected in zero applied field (black vertical bars) or a 53-mT magnetic field applied parallel to the γ beam (black lines) of a sample reconstituted Bt MiaB WT (top spectra) or samples, where Bt MiaB was treated with tRNA substrate and SAM for 5 min, 20 min, or 60 min. The corresponding [0-53mT]-difference spectra are shown as green lines. The samples contain 200 μM Bt MiaB reconstituted with ⁵⁷Fe, 200 μM i⁶A tRNA ^{Phe} and 500 μM SAM.

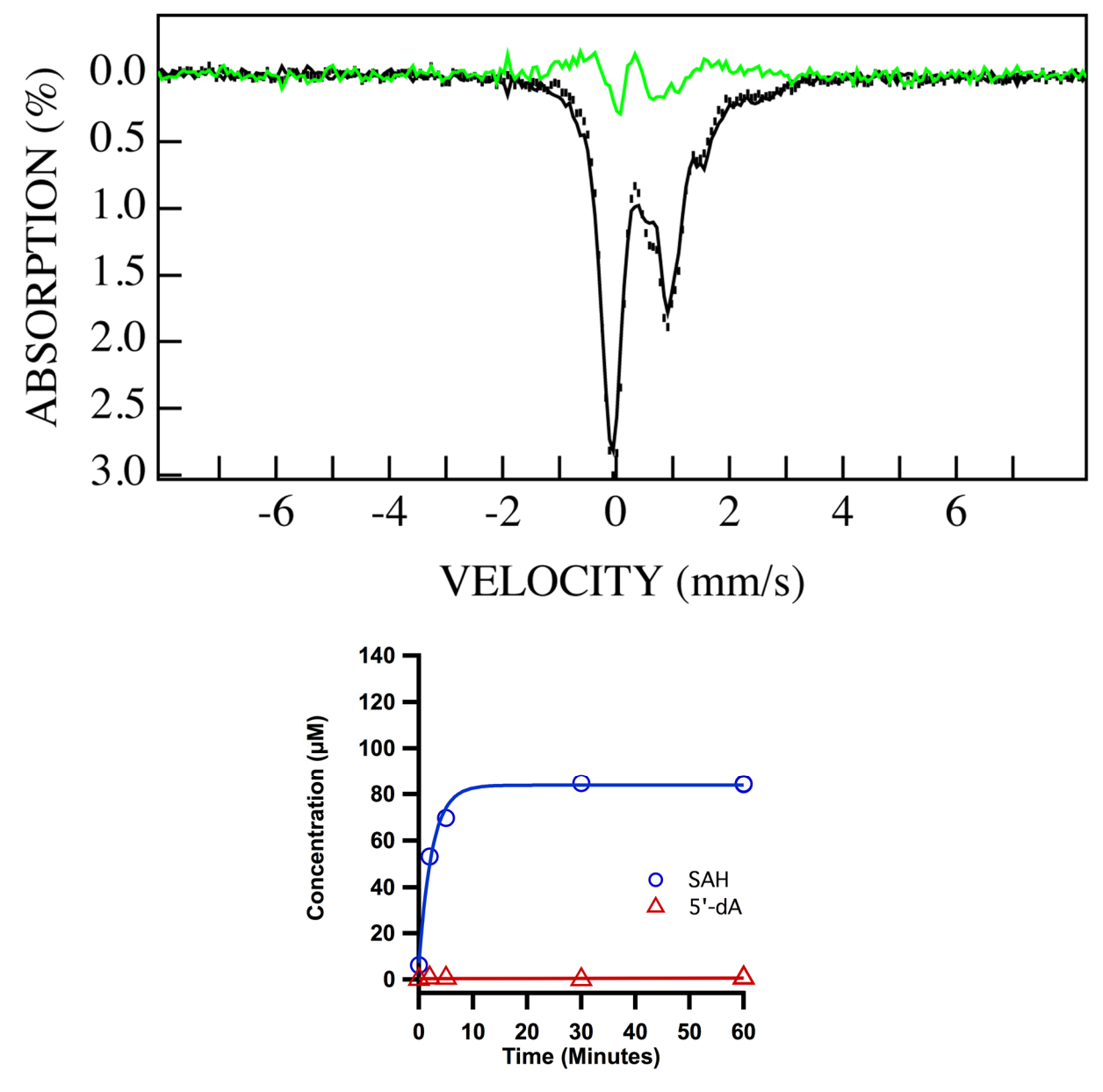


Figure S8. (Top panel) 4.2-K Mössbauer spectra of reconstituted *Bt* MiaB incubated with SAM for 60 min, in the absence of tRNA and low-potential reductant. The spectra recorded in zero-field and field strength of 53 mT are shown as vertical bars and black line, respectively. The [0-53mT] difference spectrum is shown as green line. The amplitude of the difference spectrum is approximately 70% of that of the 20-min sample in the presence of tRNA substrate and SAM. (Lower panel) LC/MS analysis monitoring the formation of SAH (blue circle) and 5′-dA-H (red triangle). The sample contains 200 μM *Bt* MiaB reconstituted with ⁵⁷Fe and 500 μM SAM.

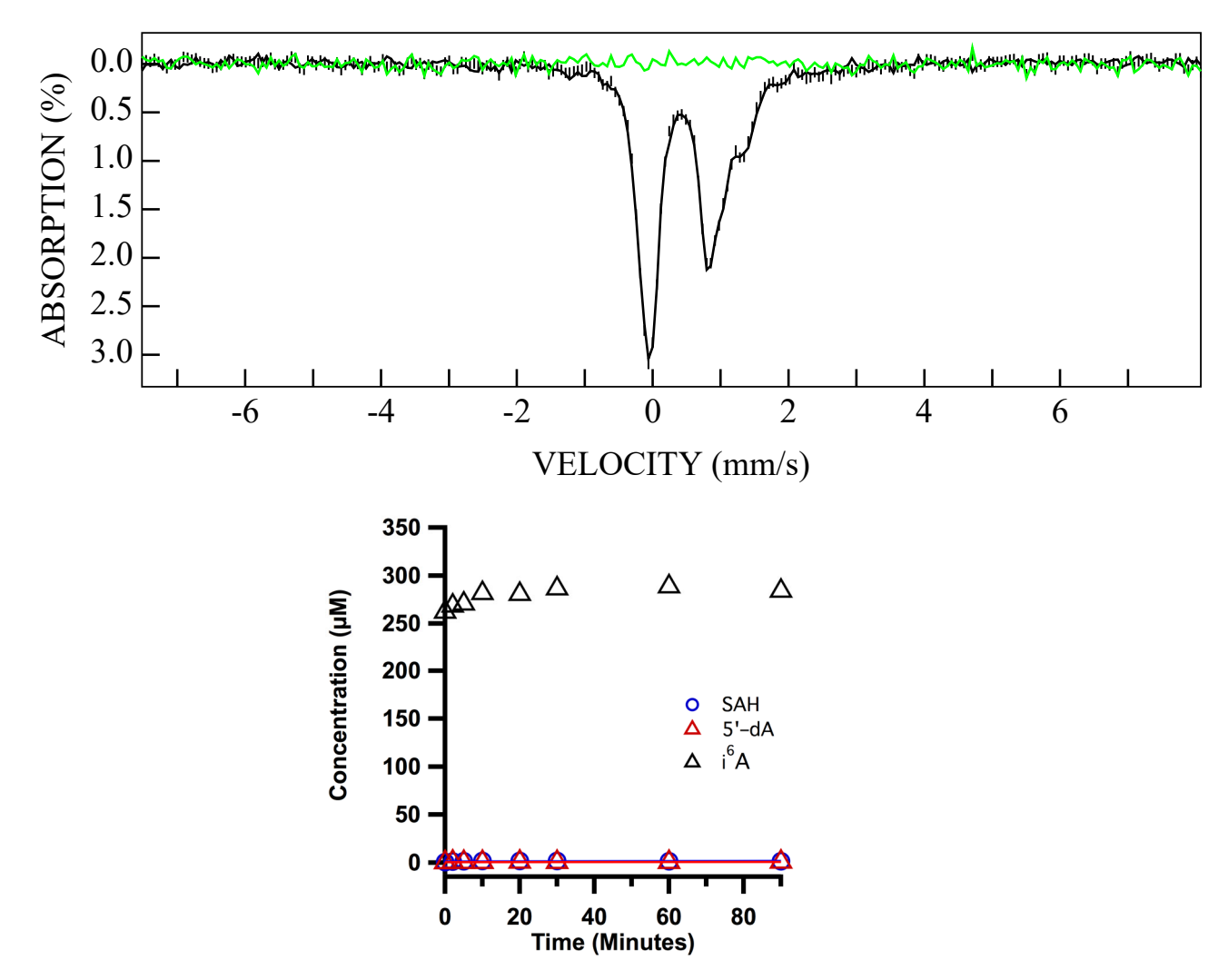


Figure S9. (Top panel) Comparison of zero-field (vertical bars) and 53mT (black line) Mössbauer spectra of reconstituted $^{\Delta Aux}$ MiaB (300 μM) incubated with SAM (600 μM) and 6 A tRNA (320 μM) for 60 min, in the absence of low-potential reductant. The [0-53mT] difference spectrum is shown as green line. (Lower panel) LC/MS analysis demonstrating that $^{\Delta Aux}$ MiaB is incapable of catalyzing the formation of SAH.

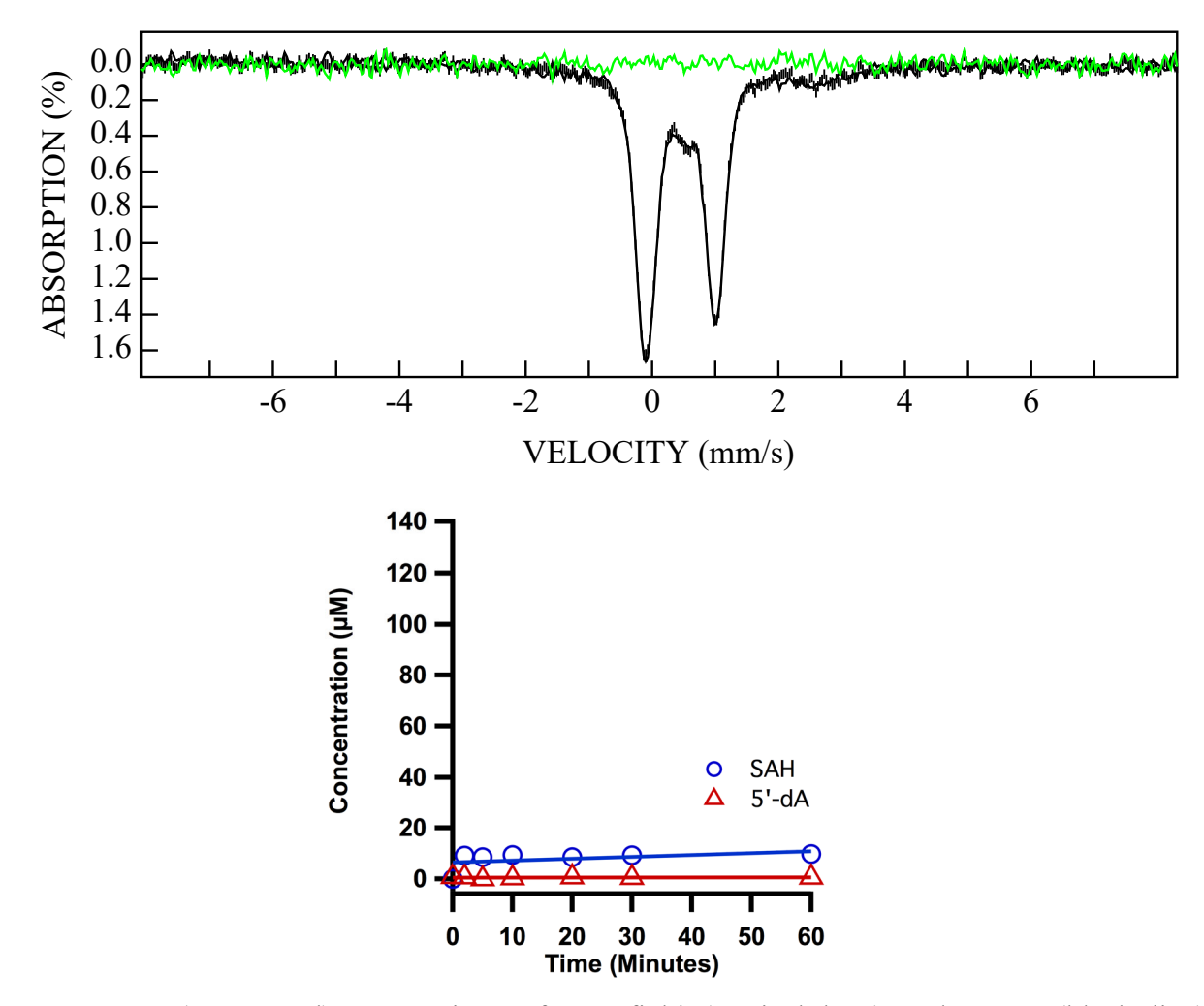


Figure S10. (Top panel) Comparison of zero-field (vertical bars) and 53mT (black line) Mössbauer spectra of reconstituted $^{\Delta RS}$ MiaB (300 μM) incubated with SAM (500 μM) and 6 A tRNA (200 μM) for 60 min, in the absence of low-potential reductant. The [0-53mT] difference spectrum is shown as green line. (Lower panel) LC/MS analysis demonstrating that $^{\Delta RS}$ MiaB is incapable of catalyzing the formation of SAH.

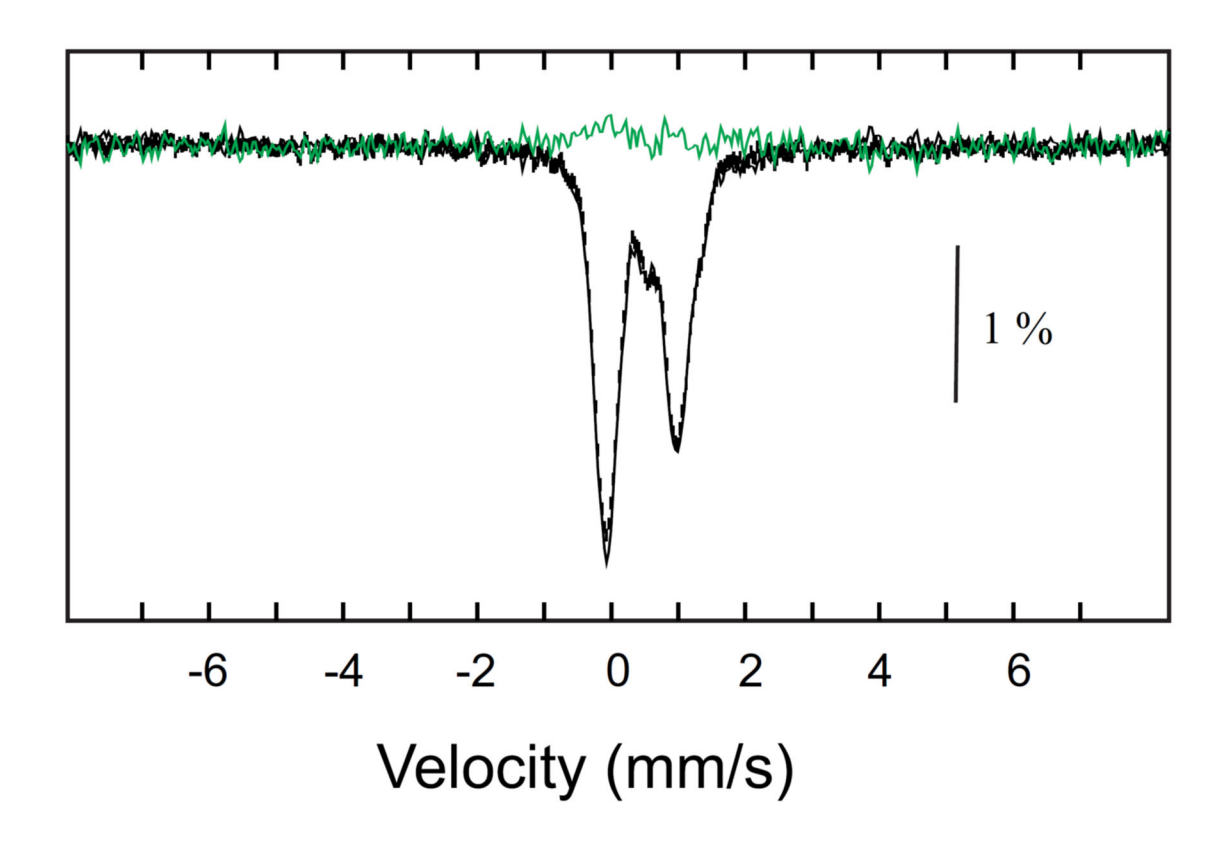


Figure S11. Comparison of 4.2-K/zero-field (vertical bars) and 4.2-K/53-mT (black line) Mössbauer spectra of reconstituted MiaB (300 μ M) incubated with i⁶A tRNA (200 μ M) for 15 min. The [0-53mT] difference spectrum is shown as green line.

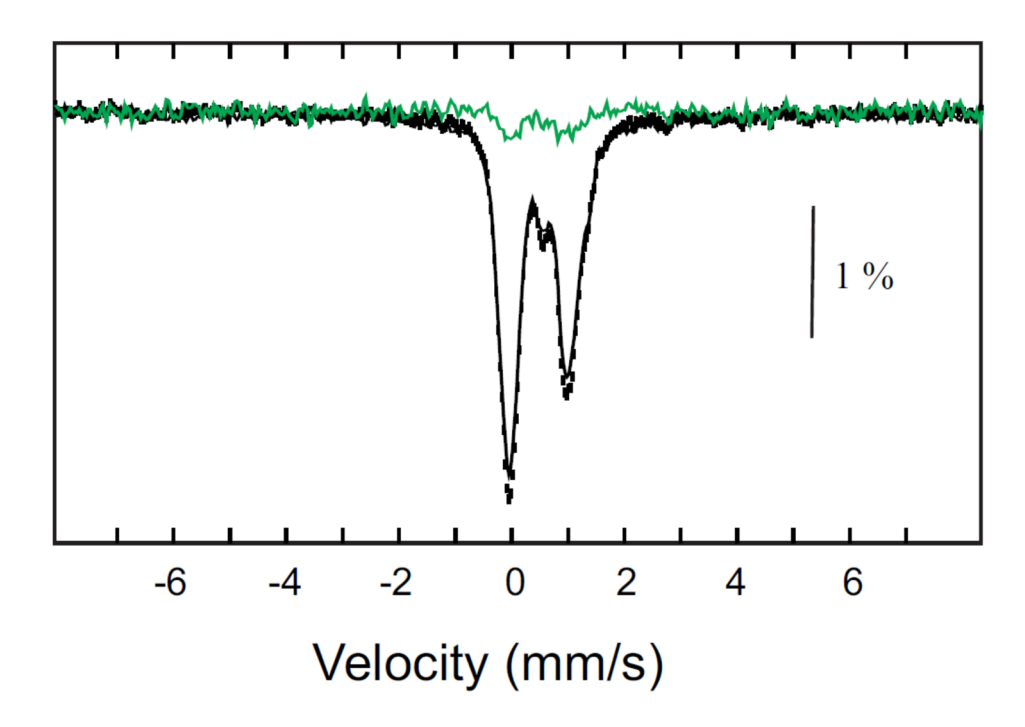


Figure S12. Comparison of 4.2-K/zero-field (vertical bars) and 4.2-K/53-mT (black line) Mössbauer spectra of reconstituted MiaB (200uM) incubated with CH₃SH (1 mM) for 30 min. The [0-53mT] difference spectrum is shown as green line.

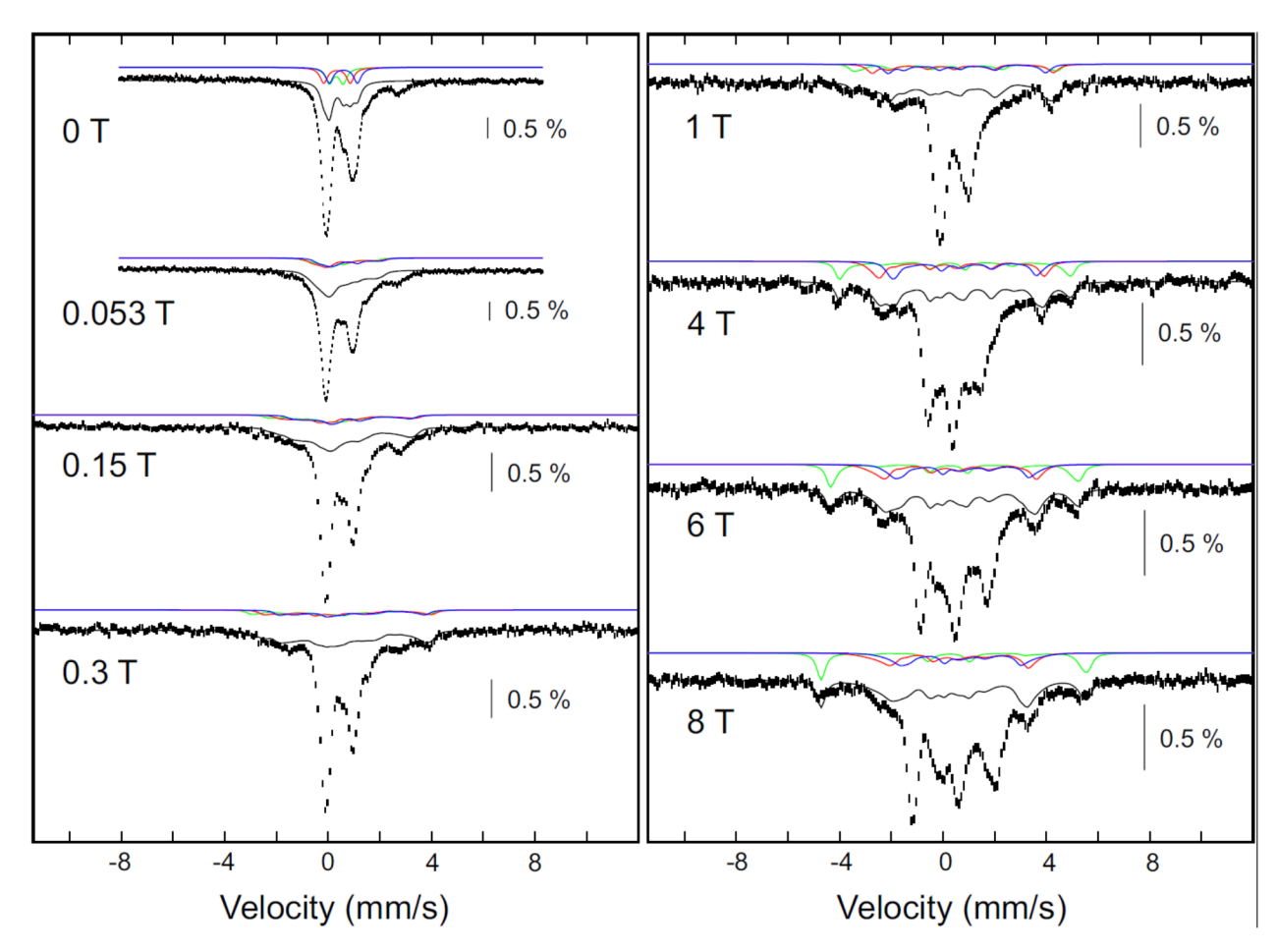


Figure S13A. 4.2-K/variable-field Mössbauer spectra of *Bt* MiaB after incubation with SAM for 20 min. Except for the spectrum recorded in the absence of applied field, all spectra were recorded in magnetic field applied parallel to the γ beam with field strength indicated in the spectra. In all spectra, the experimental data are shown as black vertical bars. The spectral features associated with the [3Fe-4S]⁰-like cluster are highlighted by the grey shade. The solid green, red, and blue lines are spin Hamiltonian simulations of the unique Fe^{III} site, the "Fe^{III}-like" site of the MV unit, and the "Fe^{II}-like" site of the MV unit, respectively. The parameters used for spin Hamiltonian simulations are listed in Table 1 of the main manuscript.

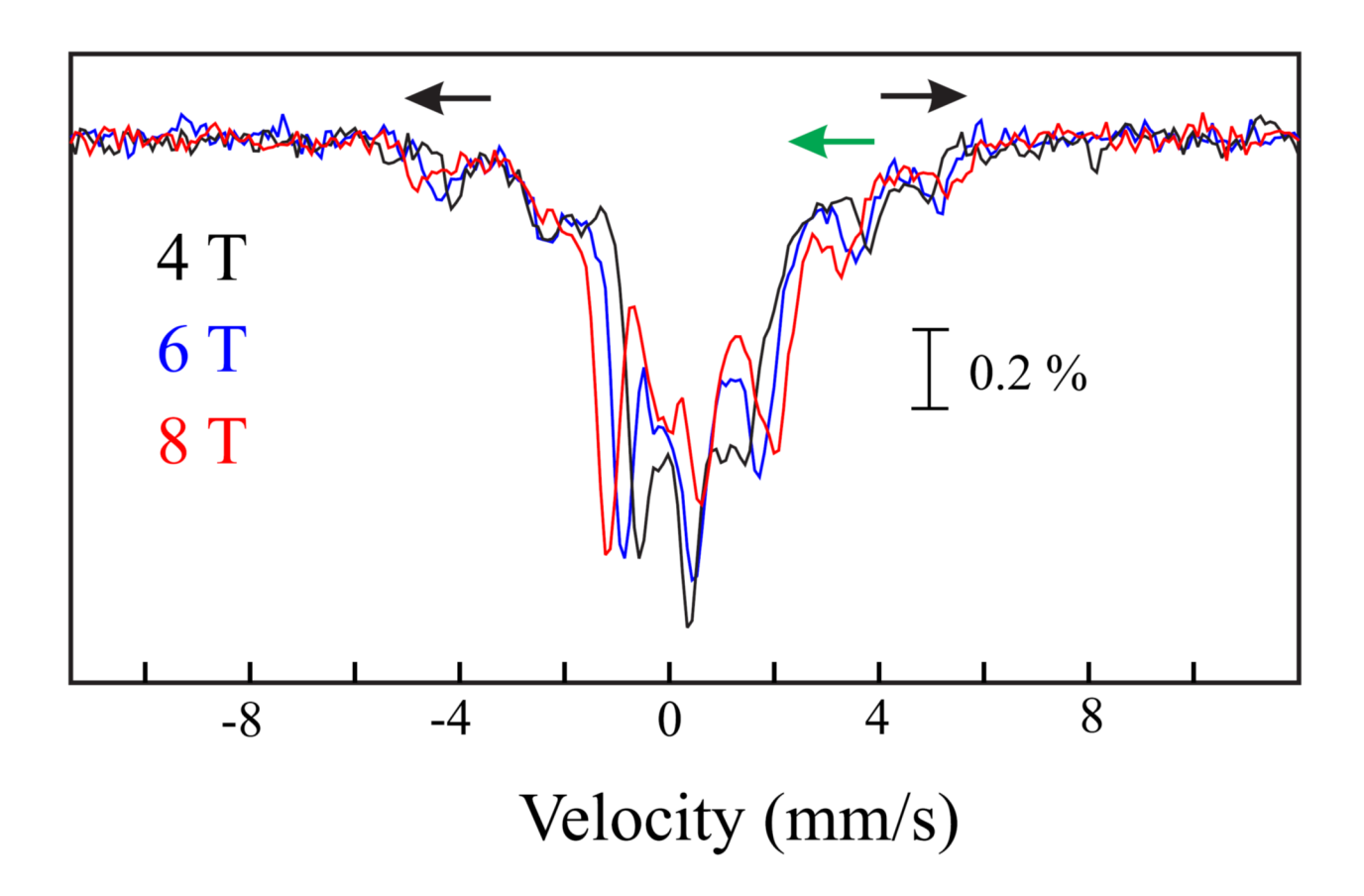


Figure S13B. Comparison of the 4.2-K Mössbauer spectra of *Bt* MiaB after incubation with SAM for 20 min collected in external fields of 4 T (black), 6 T (blue), and 8 T (red). The black arrows indicate the lines of the Fe^{III} site of which the lines move outward with increasing field, while the green arrow indicates the lines of the Fe sites of the MV unit, of which the lines move inward with increasing field.

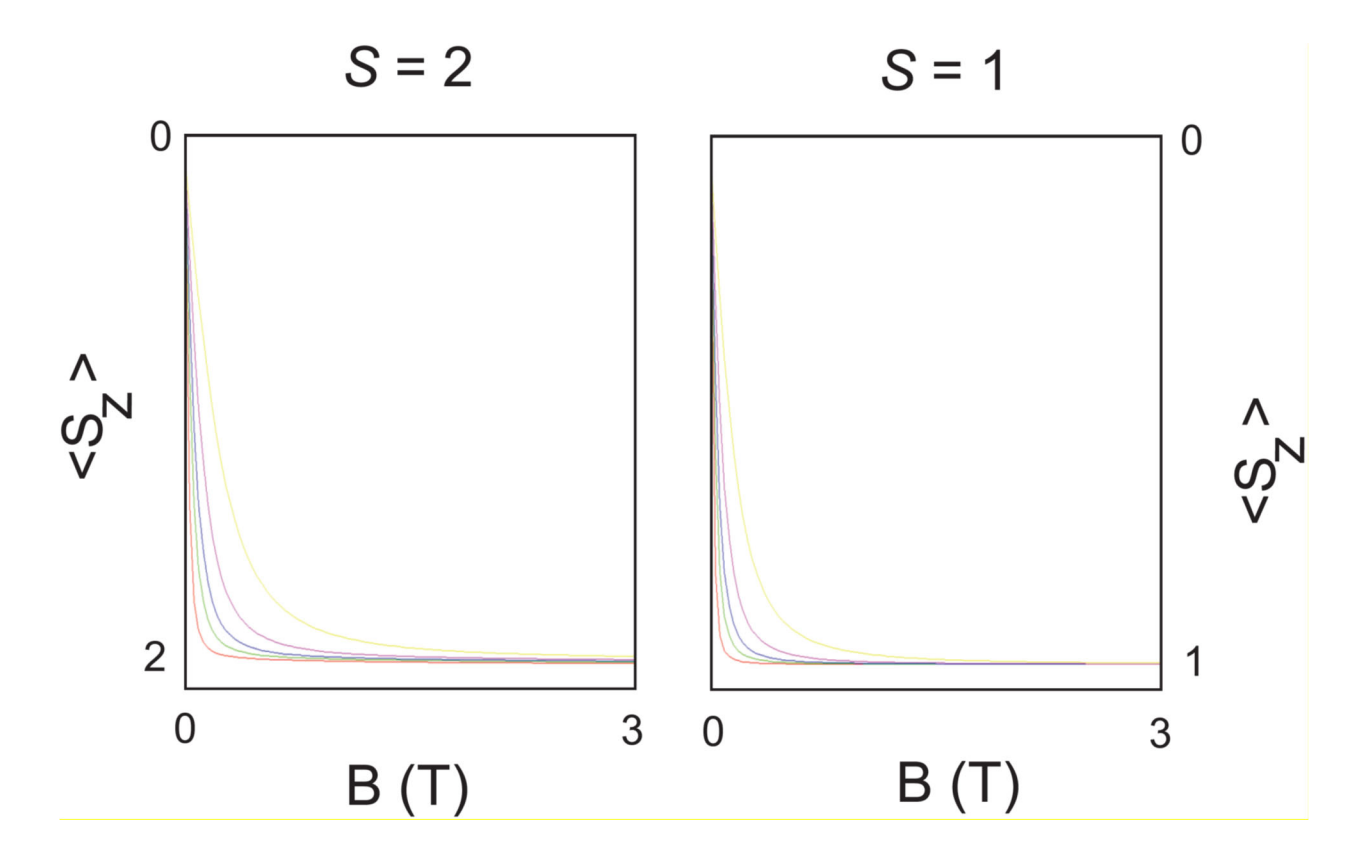


Figure S14 Spin expectation values for an electron spin system with S = 2 (left) and S = 1 (right), calculated for the electronic ground state with the assumption that the magnetic field is oriented along the z-direction of the zero-field splitting tensor. A rhombicity of E/D = 0.2 was assumed for all calculations. The calculations were carried out with values of D of -1 cm⁻¹ (red), -2 cm⁻¹ (green), -3 cm⁻¹ (blue), -5 cm⁻¹ (magenta), and -10 cm⁻¹ (yellow) for S = 2, and with values of D of -0.1 cm⁻¹ (red), -0.2 cm⁻¹ (green), -0.3 cm⁻¹ (blue), -0.5 cm⁻¹ (magenta), and -1 cm⁻¹ (yellow) for S = 1.

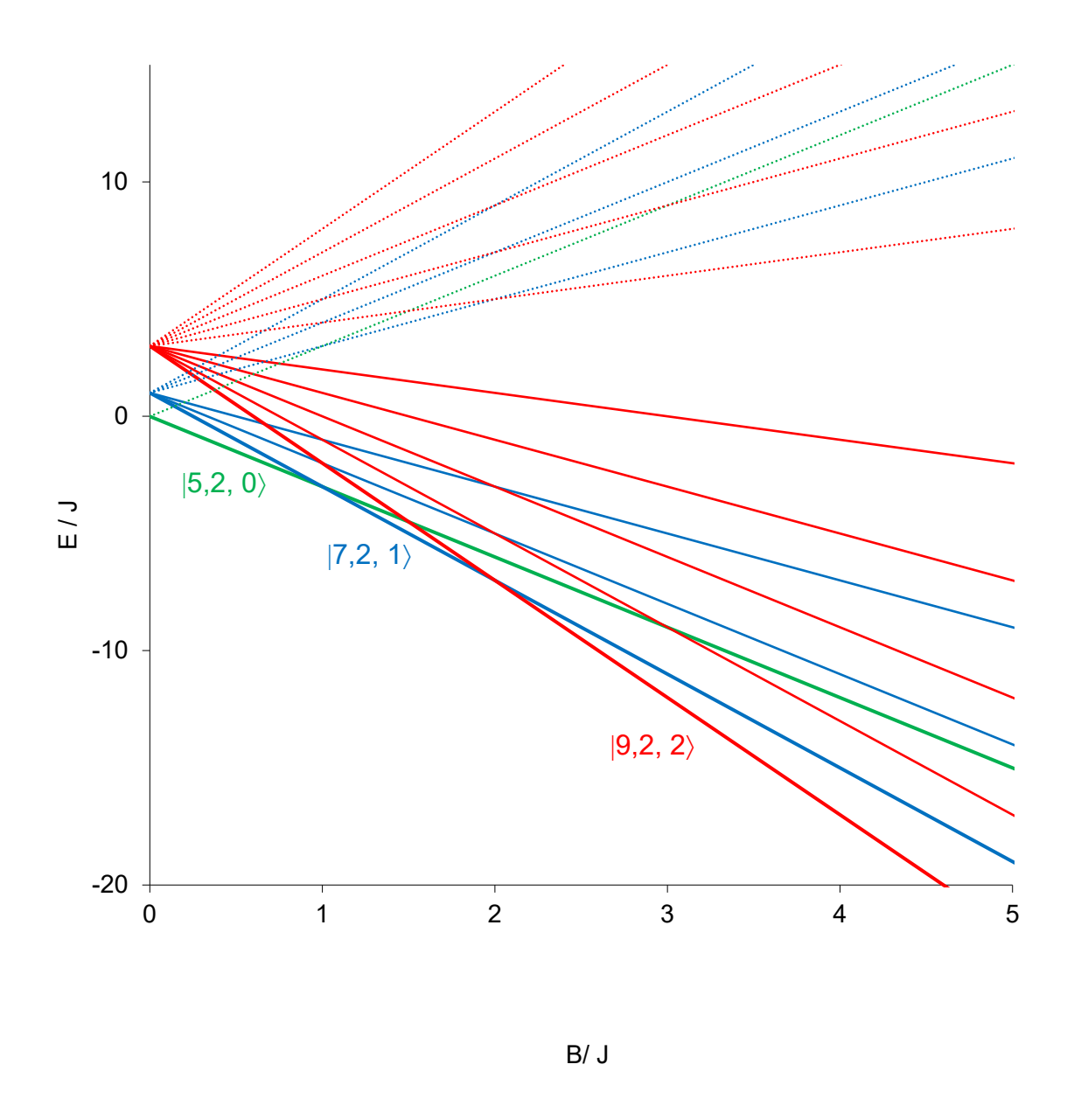


Figure S15A. Energy level diagram according to Equation S2 (or Equation S4 with $J_{mv}/J = 1$). States with $S_{tot} = 0$, $S_{tot} = 1$, and $S_{tot} = 2$ are shown in green, blue, and red. The three possible ground states are indicated with their spin quantum numbers and shown in bolder face.

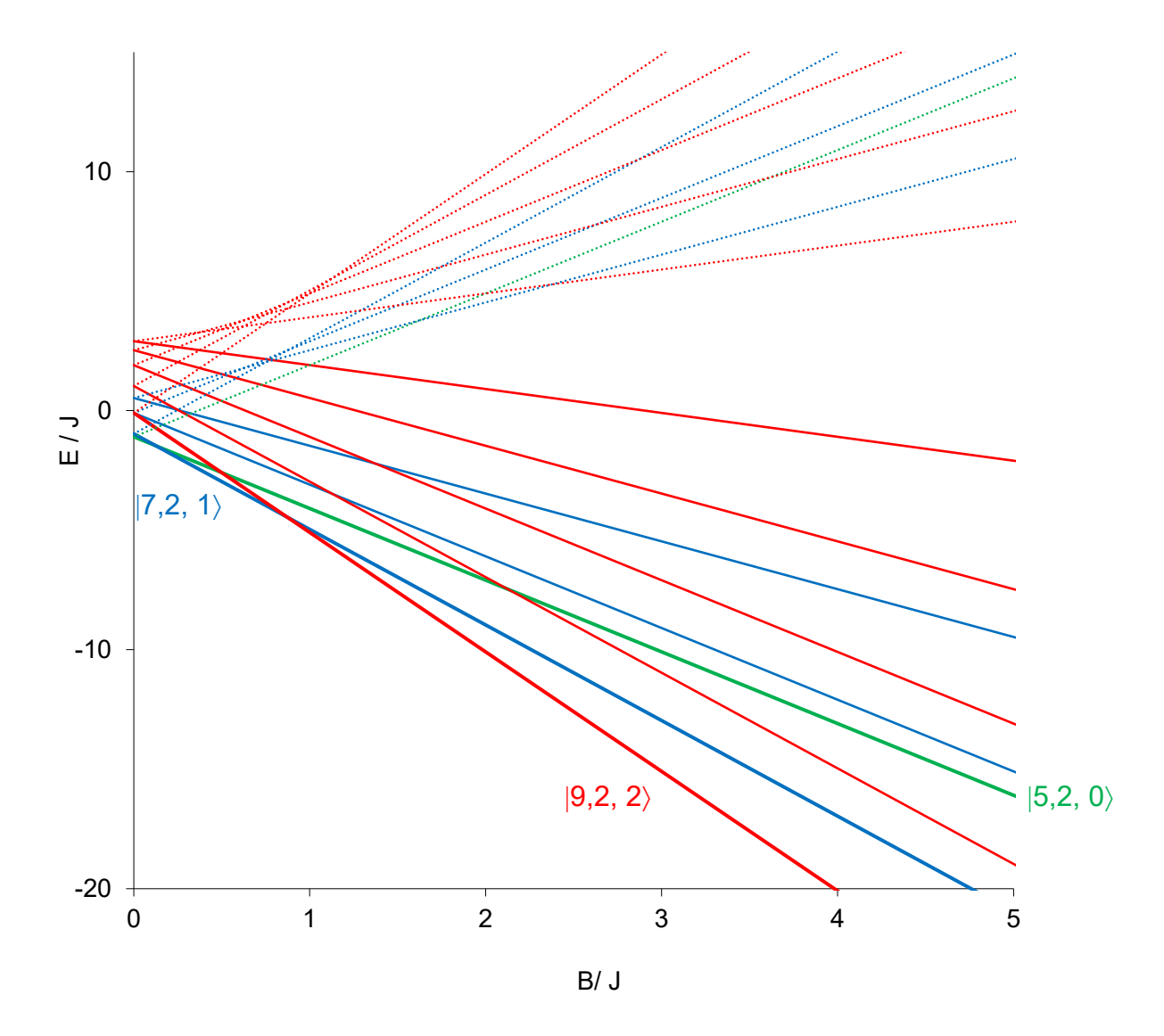


Figure S15B. Energy level diagram according to Equation S4 with $J_{mv}/J = 0.75$. States with $S_{tot} = 0$, $S_{tot} = 1$, and $S_{tot} = 2$ are shown in green, blue, and red. The three possible ground states are indicated with their spin quantum numbers and shown in bolder face.

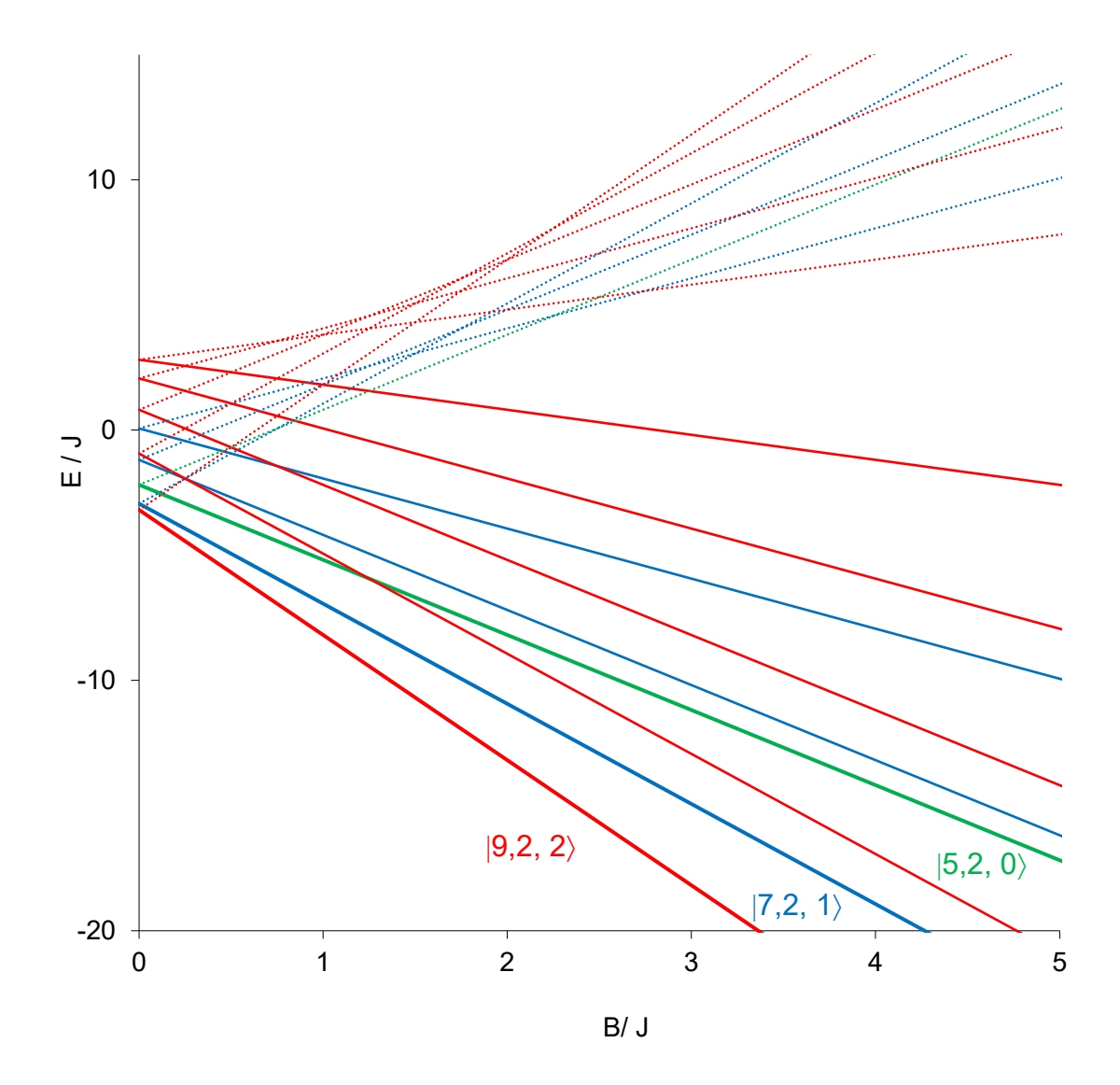


Figure S15C. Energy level diagram according to Equation S4 with $J_{\text{mv}}/J = 0.5$. States with $S_{\text{tot}} = 0$, $S_{\text{tot}} = 1$, and $S_{\text{tot}} = 2$ are shown in green, blue, and red. The three possible ground states are indicated with their spin quantum numbers and shown in bolder face.

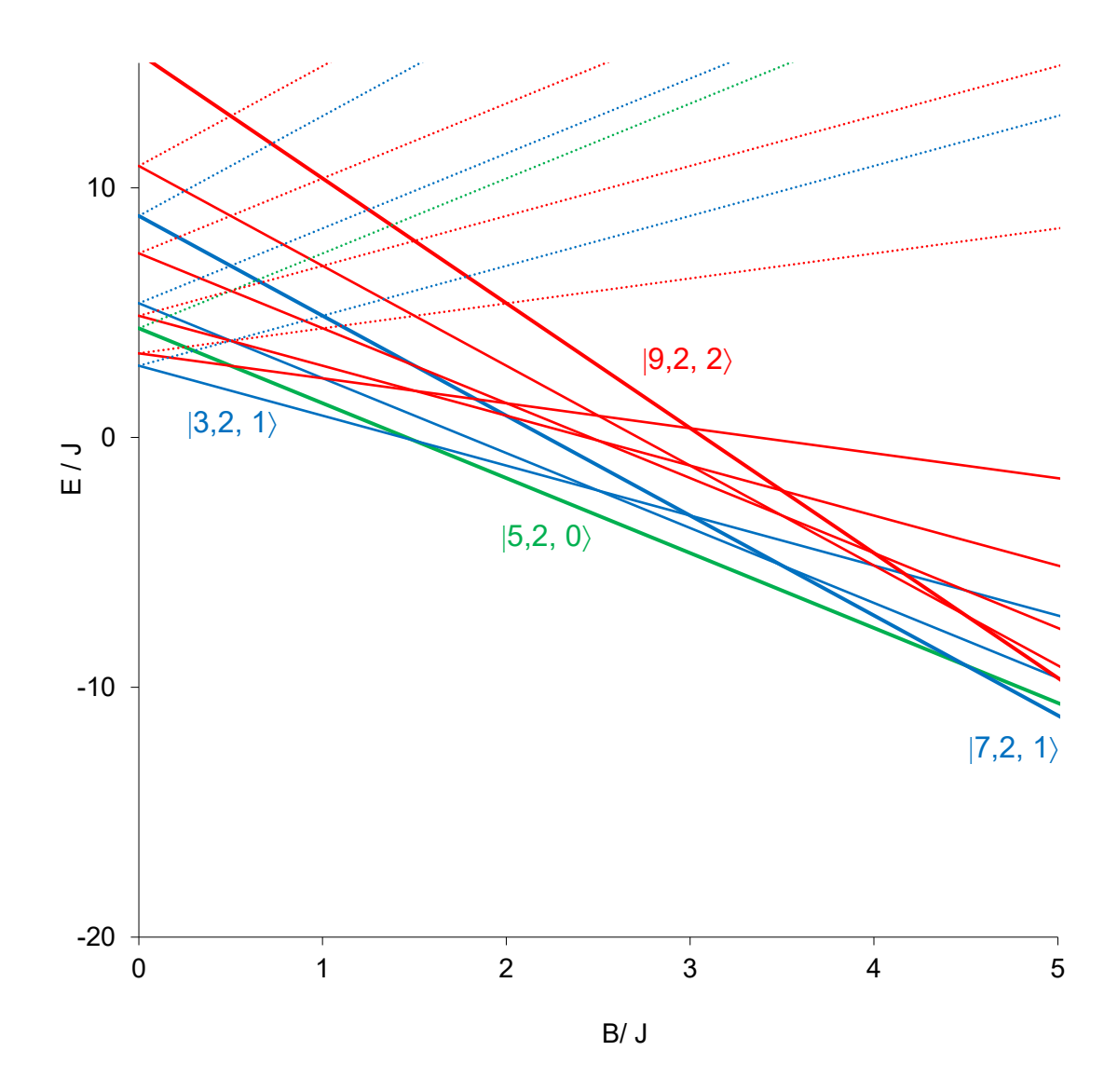


Figure S15D. Energy level diagram according to Equation S4 with $J_{mv}/J = 2$. States with $S_{tot} = 0$, $S_{tot} = 1$, and $S_{tot} = 2$ are shown in green, blue, and red. The three possible ground states are indicated with their spin quantum numbers and shown in bolder face.

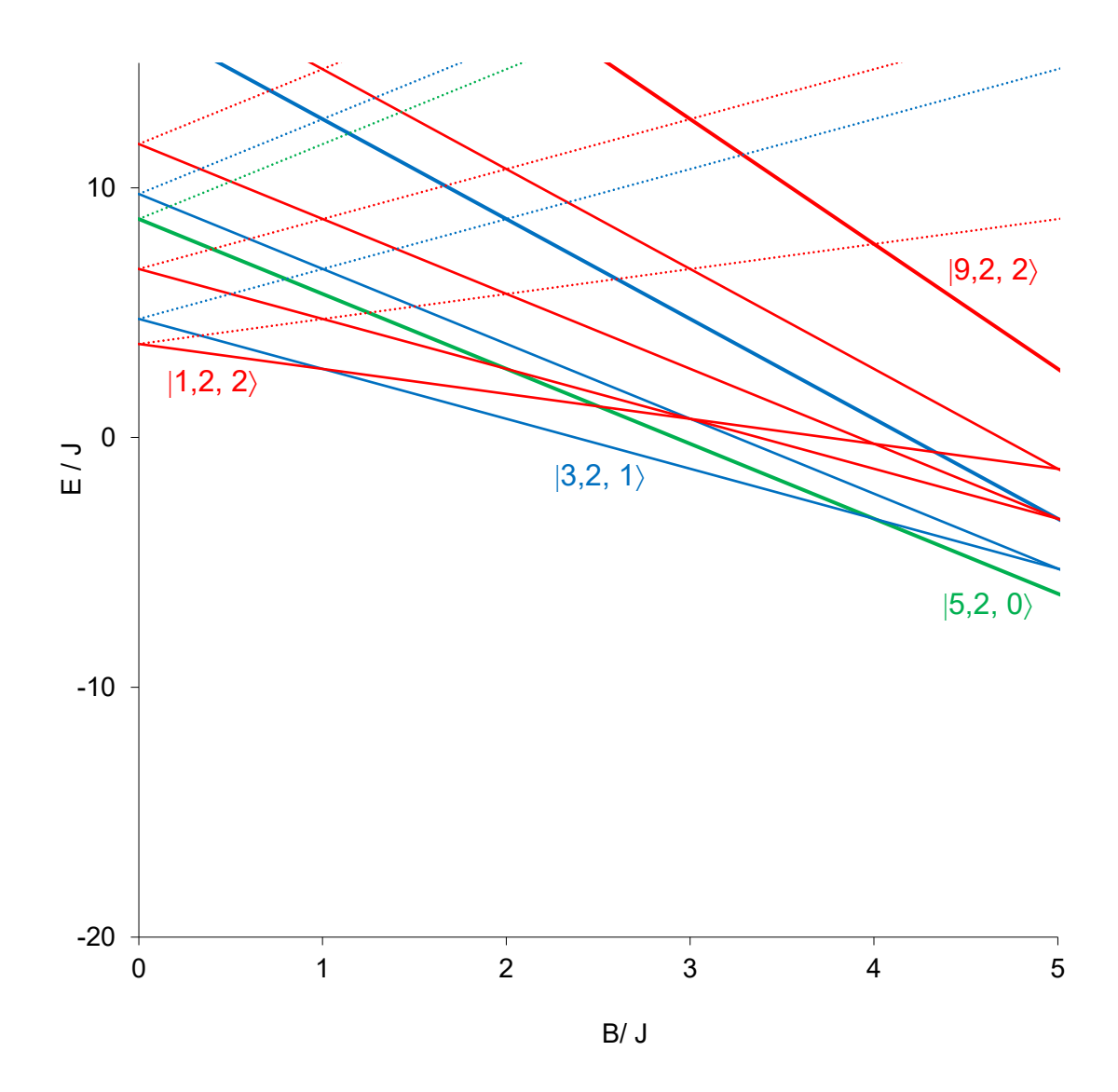


Figure S15E. Energy level diagram according to Equation S4 with $J_{mv}/J = 3$. States with $S_{tot} = 0$, $S_{tot} = 1$, and $S_{tot} = 2$ are shown in green, blue, and red. The three possible ground states are indicated with their spin quantum numbers and shown in bolder face.

References

- (1) Landgraf, B. J.; Arcinas, A. J.; Lee, K. H.; Booker, S. J. Identification of an Intermediate Methyl Carrier in the Radical S-Adenosylmethionine Methylthiotransferases RimO and MiaB, J. Am. Chem. Soc. 2013, 135, 15404.
- (2) Cicchillo, R. M.; Lee, K. H.; Baleanu-Gogonea, C.; Nesbitt, N. M.; Krebs, C.; Booker, S. J. *Escherichia coli* lipoyl synthase binds two distinct [4Fe-4S] clusters per polypeptide, *Biochemistry* **2004**, *43*, 11770.
- (3) Lanz, N. D.; Grove, T. L.; Gogonea, C. B.; Lee, K. H.; Krebs, C.; Booker, S. J.; Hopwood, D. A. RImN and AtsB as Models for the Overproduction and Characterization Radical SAM Proteins, *Natural Product Biosynthesis By Microorganisms and Plants, Pt B* **2012**, *516*, 125.
- (4) Lee, K. H.; Saleh, L.; Anton, B. P.; Madinger, C. L.; Benner, J. S.; Iwig, D. F.; Roberts, R. J.; Krebs, C.; Booker, S. J. Characterization of RimO, a New Member of the Methylthiotransferase Subclass of the Radical SAM Superfamily, *Biochemistry* **2009**, *48*, 10162.
- (5) Lanz, N. D.; Pandelia, M.-E.; Kakar, E. S.; Lee, K. H.; Krebs, C.; Booker, S. J. Evidence for a Catalytically and Kinetically Competent Enzyme-Substrate Cross-Linked Intermediate in Catalysis by Lipoyl Synthase, *Biochemistry* **2014**, *53*, 4557.
- (6) Molle, T.; Clémancey, M.; Latour, J. M.; Kathirvelu, V.; Sicoli, G.; Forouhar, F.; Mulliez, E.; Gambarelli, S.; Atta, M. Unanticipated coordination of tris buffer to the Radical SAM cluster of the RimO methylthiotransferase, *J. Biol. Inorg. Chem.* **2016**, *21*, 549.
- (7) Papaefthymiou, V.; Girerd, J. J.; Moura, I.; Moura, J. J. G.; Münck, E. Mössbauer study of *D. gigas* ferredoxin-II and spin-coupling model for the Fe₃S₄ cluster with valence delocalization, *J. Am. Chem. Soc.* **1987**, *109*, 4703.